The Role of PARylation in Skeletal Muscle During the Development of Cancer Cachexia

Abolfazl Nik-Akhtar

A thesis submitted in partial fulfilment of the requirements for the degree Master of Science of Biochemistry with Specialization in Human and Molecular Genetics

Department of Biochemistry, Microbiology, and Immunology

Faculty of Medicine

University of Ottawa

Table of Contents

List of Figures

List of Tables

List of abbreviations

OxPhos	Oxidative Phosphorylation
DMEM	Dulbecco's Modification of Eagle's Medium
CMMR	Canadian Mutant Mouse Repository
mTOR	Mammalian Target of Rapamycin
mTORC1	mTOR Complex 1
PGC-1a	Peroxisome Proliferator-Activated Receptor Gamma Coactivator 1- Alpha
ULK1	Serine/Threonine-Protein Kinase 1
SIRT1	Silent Mating Type Information Regulation 2 Homolog 1
LLC	Lewis Lung Carcinoma
ANOVA	Analysis of Variance
REDD1	Regulated in DNA Damage and Development 1
REDD2	Regulated in DNA Damage and Development 2
HAM'S F10	Ham's Formula 10
PARG	Poly (ADP-Ribose) Glycohydrolase
PARP1	Poly (ADP-Ribose) Polymerase 1
PARP2	Poly (ADP-Ribose) Polymerase 2
PARP4	Poly (ADP-Ribose) Polymerase 4
COPD	Chronic Obstructive Pulmonary Disease
AIDS	Acquired Immunodeficiency Syndrome
TNF-A	Tumor Necrosis Factor-Alpha
IL	Interleukin
PIF	Proteolysis Inducing Factor
STAT3	Signal Transducer and Activator of Transcription 3
NSAID	Non-Steroidal Anti-Inflammatory Drugs
C26	Colon-26
GLUT4	Glucose Transporter Type 4
IGF-1	Insulin-Like Growth Factor 1
TRIM63	Tripartite Motif Containing 63
FBOXO32	F-Box Protein 32
FOXO1	Forkhead Box Protein O1
ROS	Reactive Oxygen Species
NAD	Nicotinamide Adenine Dinucleotide
NAM	Nicotinamide
NA	Nicotinic Acid
NR	Nicotinamide Riboside
NMN	Nicotinamide Mononucleotide
SAM	Sterile Alpha Motif
PAR	Poly (ADP) Ribose
TNKS1	Tankyrase 1

TNKS2	Tankyrase 2
HAS	Huamn Skeletal Actin
Mer	Mutated Estrogen Receptor
PCR	Polymerase Chain Reaction
TA	Tibialis Anterior
GP	Gastrocnemius
QUAD	Quadricepses
GPS	Combined Mass of Gastrocnemius And Soleus
APS	Ammonium Persulafate
PBS	Phosphate Buffered Saline
HPA	Human Protein Atlas
GTEx	Genotype-Tissue Expression
iWAT	Inguinal White Adipose Tissue
gWAT	Gonadal White Adipose Tissue
BAT	Brown Adipose Tissue

Abstract

Cancer cachexia is a wasting syndrome causing involuntary weight loss and muscle atrophy. PARP1 is a nicotinamide dinucleotide-dependent enzyme that modifies target proteins by PARylation. The reversal process, dePARylation, is mediated by the PARG enzyme. PARP1 inhibitors are potent cancer agents, while PARG inhibitors are in clinical trials for similar cancers. Here we examine the role of PARylation on muscle homeostasis in cancer cachexia. We employed mouse models with inducible muscle specific knockouts of *Parp1 (Parp1*-IMKO) or *Parg (Parg*-IMKO) to investigate their implications on skeletal muscle in a cancer cachexia model. We assessed muscle loss, grip strength, and gene expression. Results show that *Parp1*-IMKO mice had increased muscle wasting, while *Parg*-IMKO had degradation rates similar to wild-type mice during cancer cachexia. This suggests reduced PARylation might worsen cancer cachexia, while an increase does not. This supports PARG inhibitor development as anticancer alternatives. Our study highlights challenges with PARP1 inhibitors and the need to study PARylation and dePARylation in muscle health during cancer cachexia, impacting clinical strategies using PARP1 or PARG inhibitors.

Acknowledgements

The field of biology offers a captivating glimpse into the intricacies of the natural world and the awe-inspiring complexity of life. The quest to understand the secrets of existence is a daunting challenge, but one that inspires us to push the limits of what we know and seek deeper insights into the mysteries of our universe. Exploring the interactions between molecules that underpin life itself is a humbling and inspiring experience. After all, the fact that we have evolved over billions of years to reach this point is a testament to life's power and resilience. We gain insights into the building blocks of existence and how they combine to create the magnificent organisms that surround us.

While the journey of discovery in biology is certainly challenging, the rewards are truly extraordinary. This quest requires tenacity, persistence, and an unwavering dedication to the pursuit of knowledge. However, the insights gained along the way have the power to transform our understanding of the world and our place within it.

The search for answers to life's most profound questions demands sacrifice and support from a vast array of individuals who dedicate their time and resources to support the minds that push the boundaries of science. Their unwavering commitment enables scientists to unlock the secrets of existence and to blaze a trail toward a brighter future.

Throughout my own journey, I have been blessed to have the support of a multitude of individuals. My family has always been my backbone, pushing me to be my best. Maman, Hamed, Darya and specifically Baba and Dash Ali thank you for believing in me. My supervisor, Dr. Menzies, I cannot thank you enough. Thank you for providing me with the tools and insights necessary to succeed, while my dear friends and colleagues, Alex and Yusmaris, taught me the importance meticulous attention to detail.

I would also like to express my gratitude the undergraduate students who have assisted me in the lab. I would also like to recognize the countless previous scientists whose tireless work and ground-breaking discoveries have paved the way for my own.

Thanks to the unwavering support of these individuals, I have made remarkable progress in unraveling the mysteries pushed me to where I am right now. However, the journey is far from over, and the road ahead is full of challenges. I am eager to explore new horizons, work with new colleagues, and delve deeper into the mysteries of the natural world. The pursuit of knowledge is an unending quest, and I am excited to continue along this path. As we continue to unearth the secrets of science and life, we are reminded of the infinite possibilities that await us in the years to come. I am honored to have such incredible support on this journey and look forward to what the future holds.

Abolfazl Nik-Akhtar, Ottawa, 2023

1 Introduction

1.1 Cachexia

Cachexia is a multifactorial and multisystemic syndrome, characterized by severe weight loss, muscle wasting, anorexia, and metabolic dysregulation[1]. Cachexia significantly compromises patients' quality of life, functional capacity, and survival outcomes[2]. This disorder is not an isolated entity but frequently develops as a secondary complication of chronic diseases such as chronic obstructive pulmonary disease (COPD), heart failure, renal failure, and acquired immunodeficiency syndrome (AIDS)[3,4]. The situation becomes critically complex, and the implications are significantly more severe when cachexia manifests in the context of cancer, leading to a condition termed cancer cachexia[1,3,5–8].

1.1.1 Cancer Cachexia

Cancer cachexia, recognized as a paraneoplastic syndrome, is distinct from cachexia resulting from other underlying causes[8–10]. The core manifestations of cancer cachexia overlap with cachexia, including weight loss of more than 5 percent over the preceding 6 months and muscle wasting, while the underlying pathophysiology, prognosis, and treatment considerations can be markedly different[1,3,7–10]. For example, 1) The tumor itself plays a crucial role in cancer cachexia, releasing various factors that trigger systemic inflammation and metabolic changes; 2) The presence of cancer can exacerbate the nutritional and metabolic challenges faced by patients, complicating the management of cachexia; and 3) Cancer treatments such as chemotherapy and radiation can themselves contribute to or exacerbate cachexia, adding another layer of complexity to the patient's clinical course[11].

1.1.1.1 Prevalence

This intricate interplay of systemic inflammation, metabolic abnormalities, and tumor-derived factors, affects an estimated 50-80% of cancer patients[12,13], thereby highlighting its substantial prevalence of cachexia. It is estimated that cachexia contributes to at least 30% of cancer deaths, underscoring the profound clinical implications of muscle wasting[11].

Over recent decades, an alarming trend has emerged, indicating an increase in the incidence of cachexia, particularly cancer cachexia. This rising prevalence can be attributed to several intersecting factors. Firstly, the global surge in cancer incidence, driven by aging populations and increased exposure to carcinogenic risk factors, has inevitably led to an escalation in cancer cachexia cases. Secondly, advancements in early cancer detection and treatment modalities have resulted in improved survival rates, thereby allowing patients to live long enough to potentially develop cachexia. Lastly, our expanding knowledge and recognition of this syndrome, coupled with more sophisticated diagnostic criteria and tools, have led to more accurate and timely diagnoses of cachexia.

1.1.1.2 Symptoms of Cancer Cachexia

Cancer cachexia, with its multifactorial and multisystemic impact, manifests with a variety of symptoms that extend beyond mere weight loss. Patients frequently present with anorexia or loss of appetite, which further compounds the weight loss and nutritional deficiencies. Fatigue is often reported and can be attributed to both general systemic illness and the specific loss of muscle mass, which leads to reduced physical stamina and functional capacity. Muscle

wasting or cachectic myopathy is another key symptom, characterized by progressive loss of skeletal muscle mass. This can lead to significant weakness and functional impairment, compromising the patients' mobility and independence. In advanced stages, cachexia can lead to respiratory muscle weakness, further exacerbating the fatigue and reducing the patient's exercise tolerance. Patients may also experience anemia and edema, further worsening their overall health status. Additionally, due to the systemic inflammatory response, patients may also suffer from low-grade fever[1,4,11,14,15]. The weight loss, muscle wasting, and general weakness can significantly impair a patient's functional capacity, compromising their ability to perform daily activities and reducing their quality of life[16].

The physical debility can also limit their tolerance to cancer treatments, including chemotherapy and radiation therapy, and may require dose reductions or treatment discontinuation. The altered metabolic state can affect drug metabolism and clearance, potentially reducing the efficacy of chemotherapeutic agents. Additionally, systemic inflammation and the related increase in cytokines can induce resistance to certain chemotherapy drugs[17].

1.1.1.3 Cachexia in Different Cancers and Sexes

Cancer cachexia manifests with varying degrees of prevalence, largely contingent upon the type of cancer, patient demographics, and the stage of the disease. It is important to note that this prevalence can vary significantly among different cancer types and patient populations[18].

A review of the available literature highlights intriguing disparities in the incidence of cancer cachexia based on gender. Generally, male cancer patients appear to have a higher

susceptibility to cachexia, though the reasons behind this tendency remain multifaceted and complex[19]. Hormonal differences, variations in body composition, and differing metabolic rates between the sexes are thought to be contributing factors[20] and this difference makes certain drug only effective in one sex[21] making it important to investigate both sexes in cancer cachexia studies.

Certain types of cancer are more commonly associated with the development of cachexia. Pancreatic and gastric cancers are notorious for their high incidence of cachexia, which can exceed 80% in advanced stages. Lung, colorectal, and esophageal cancers also have a significant association with cachexia. Cachexia can develop at any stage of cancer. However, it is often more prevalent and severe in advanced stages, where the systemic burden of the disease and the associated metabolic and inflammatory changes are typically most pronounced[1,18,22–24].

1.1.1.4 Mechanisms of Cancer Cachexia

Cancer cachexia is a complex, multifactorial syndrome whose genesis and progression are shaped by a constellation of interrelated factors. The development of cachexia is primarily driven by the cancer itself, but a variety of other influences, including certain drugs, can also contribute to its onset and progression. Indeed, some chemotherapeutic agents such as 5-fluorouracil (5-FU), cisplatin, and methotrexate and other medications used in the management of cancer and its associated symptoms can inadvertently promote the development of cachexia independent of their effect of tumor by exacerbating metabolic

dysregulation and inflammation, suppressing appetite, or causing nausea and other gastrointestinal side effects that interfere with nutritional intake[25–28].

At the molecular level, our understanding of cancer cachexia has been shaped by several key hypotheses that revolve around systemic inflammation, metabolic changes, and tumor-derived factors. This intricate interplay of factors creates a pathological environment that promotes muscle wasting through increased protein degradation and/or decreased protein synthesis, adipolysis[5], and overall metabolic dysfunction[29,30].

- Systemic inflammation is a cardinal feature of cancer cachexia. It is driven by proinflammatory cytokines such as tumor necrosis factor-alpha (TNF-α)[31], interleukin (IL)-1[32–35], and IL-6[36–38], which are released by the tumor and immune cells. These cytokines not only initiate and sustain the systemic inflammatory response but also directly induce muscle proteolysis and lipolysis, leading to muscle wasting and fat loss. They also interfere with the anabolic signals in muscle, inhibiting muscle regeneration and growth [25,29,31–34,36–39]. Notably, TNF-α has been implicated in the induction of the ubiquitin-proteasome pathway, a key mechanism responsible for protein degradation in muscles[31].
- Metabolic changes are another critical component of the cachexia syndrome. Cancer cells have an altered metabolic profile, often characterized by a shift towards aerobic glycolysis, known as the Warburg effect. This leads to an increase in glucose consumption by the tumor, potentially depriving the rest of the body of essential nutrients[40]. Additionally, the systemic inflammation[41] and hormonal changes

associated with cancer can induce insulin resistance[42], further exacerbating the metabolic dysregulation.

- Tumor-derived factors, including proteolysis-inducing factor (PIF)[43,44] and lipolysis-inducing factors (LIP)[43], have been identified as key players in the pathogenesis of cancer cachexia. PIF, produced by certain types of cancer, directly induces protein degradation in skeletal muscle through the activation of the ubiquitin-proteasome pathway[45]. LIP, on the other hand, promote the breakdown of adipose tissue, contributing to the loss of body fat observed in cachexia[46]. Several molecular pathways are implicated in the orchestration of these processes. The nuclear factor-kappa B (NF-κB) pathway, which is activated by proinflammatory cytokines, plays a significant role in muscle atrophy by upregulating the expression of ubiquitin ligases involved in protein degradation[27,47,48]. The activation of the signal transducer and activator of transcription 3 (STAT3) by IL-6 has also been associated with muscle wasting[36]. The myostatin/activin pathway is another critical pathway implicated in cachexia, as these factors inhibit muscle growth and promote muscle atrophy[49].

Collectively, these factors and pathways create a vicious cycle, where the tumor, systemic inflammation, and metabolic changes perpetuate each other, leading to progressive muscle wasting and metabolic dysfunction. The complex and multifactorial nature of cancer cachexia underscores the need for a comprehensive, multimodal approach to its management, targeting not just the tumor, but also the systemic inflammation and metabolic changes that fuel this debilitating syndrome.

1.1.1.5 Cancer Cachexia Management

The management of cachexia requires a comprehensive, multimodal approach that encompasses nutritional support, physical therapy, and pharmacological interventions, but the options are currently limited, and the effectiveness is often suboptimal. Currently, there are limited treatment options available, and these are primarily aimed at managing symptoms rather than addressing the underlying pathophysiology[3,6,15,29,39,50,51].

- Nutritional support remains a cornerstone of cachexia management, aiming to counteract weight loss and nutritional deficiencies. However, given the metabolic changes associated with cachexia, nutritional support alone often proves insufficient in reversing muscle wasting or halting disease progression[29].
- Pharmacological interventions have been pursued to augment the management of cancer cachexia.
    - Progestogens, such as megestrol acetate and medroxyprogesterone, are used to stimulate appetite and promote weight gain. However, their impact on muscle mass and function is negligible, and they are associated with potential side effects including thromboembolism and adrenal insufficiency[52].
    - Non-steroidal anti-inflammatory drugs (NSAIDs) like indomethacin have been examined for their potential to mitigate the systemic inflammation contributing to cachexia. While indomethacin can provide some symptom relief, it is often limited by gastrointestinal side effects[53–56].

- Anamorelin, a selective ghrelin receptor agonist, has shown promise in clinical trials, enhancing appetite, body weight, and lean body mass in patients with cancer cachexia[57–62].

Despite these options, the limitations of existing treatments underscore the necessity for more effective therapeutic strategies. Ongoing research is exploring targeted therapies, focusing on the molecular pathways implicated in cachexia, as well as combination therapies that address the condition from multiple angles.

The best strategy to manage cancer cachexia, however, may be prevention. Given the modest effectiveness and potential side effects of the currently available treatments, interventions that can prevent or delay the onset of cachexia may offer the greatest benefit. This emphasizes the need for early recognition of cachexia and the importance of ongoing research to unravel the complex pathophysiology and identify novel therapeutic targets.

1.1.1.6 Models in Cancer cachexia

Research models play a pivotal role in elucidating the complex pathophysiology of cancer cachexia. Both *in vivo* and *in vitro* models provide valuable insights, each with their distinct advantages and limitations.

- *In Vivo* Models: Mouse models are commonly employed in cancer cachexia research due to their genetic similarities with humans and well-characterized response to tumor growth. The use of specific mouse strains allows researchers to examine the influence of different genetic backgrounds on the development of cachexia. In addition to the

choice of mouse strain, the injection site of the tumor can also affect the manifestation of cachexia. Subcutaneous and orthotopic injections are often employed to mimic the disease's natural progression[63]. Among the mouse models, the Lewis Lung Carcinoma (LLC) model has been extensively used due to its consistent and reproducible induction of cachexia. Benefits of the LLC model include its reliability for studying the mechanisms underlying this condition. However, limitations may include its lack of complete genetic resemblance to human tumors, which can sometimes limit the translational relevance of the findings[64]. Another commonly used model is the Colon-26 (C26) carcinoma model. The C26 model is particularly useful for studying the metabolic aspects of cancer cachexia and is known for inducing severe muscle wasting. However, it may not be as effective for studying other systemic effects associated with cachexia, such as inflammation[65–67].

- In *Vitro* Models: Cell lines serve as a useful tool for studying the molecular mechanisms underlying cancer cachexia. They allow for controlled manipulation of variables and are essential for mechanistic studies for example by treating muscle cells with conditioned media from cachexia inducing cell lines. Several cell lines, both cancerous (e.g C26, LLC) and non-cancerous (e.g. C2C12), can be employed to study different aspects of cachexia, such as muscle wasting, adipose tissue atrophy, and systemic inflammation.

The LLC model, derived from a spontaneous lung tumor in a C57BL mouse, has been particularly valuable in both *in vivo* and in *vitro* cachexia research. In *vivo*, this model reliably induces robust weight loss, muscle wasting, and systemic inflammation, closely mimicking the

human condition. LLC-conditioned media has proven useful for investigating the cellular and molecular mechanisms underlying cachexia, such as muscle atrophy and metabolic alterations[64,68–71].

Despite the insights obtained from these models, it's crucial to acknowledge that they cannot fully recapitulate the complexity of cancer cachexia in humans. Therefore, findings from these models should always be validated in human studies, and continuous efforts should be made to improve the models' physiological relevance.

1.2 Skeletal muscle

Skeletal muscle, which constitutes about 40% of the total body mass in humans, is a highly adaptable tissue responsible for locomotion and whole-body metabolic health. It possesses a remarkable plasticity, enabling it to respond and adapt dynamically to various physiological and pathological stimuli, including physical exercise, aging, nutritional status, and disease states[72]. Satellite cells, the resident stem cells in skeletal muscle, are pivotal for the repair and regeneration of damaged muscle fibers. These cells spring into action upon muscle injury or stress, multiplying and maturing to replenish the muscle tissue and maintain its functional integrity[73]. Understanding the intricate biology of skeletal muscle is, therefore, not only fundamental to comprehending human physiology but also crucial in managing a wide range of health conditions. One such condition where skeletal muscle biology takes center stage is cachexia. Impairment of both muscle and muscle satellite cell function are key factors affected during cachexia that would otherwise help to maintain muscle mass[209]. However, despite its clear significance, the mechanisms underpinning muscle wasting in cachexia remain only

partially understood. To effectively address this gap, it is essential to dig in into the complexities of skeletal muscle biology, exploring the molecular and cellular processes that govern muscle mass maintenance and the factors that tip the balance towards muscle loss in disease states.

There are three main types of muscles in the human body: skeletal, smooth, and cardiac. Skeletal muscles are responsible for voluntary movements and are predominantly attached to the skeleton. Smooth muscles are involuntary and are found in various organs and structures, including the digestive tract, blood vessels, and airways. Cardiac muscle, also involuntary, is found exclusively in the heart, where it drives the heartbeat[74].

1.2.1 Muscle Energy Metabolism

Muscles are energy-demanding tissues, requiring a constant supply of ATP to support their contractile function. The energy metabolism of muscle is a complex and dynamic process, involving multiple metabolic pathways including glycolysis, oxidative phosphorylation, and fatty acid oxidation[72,75].

1.2.2 Muscle Plasticity

Muscle plasticity, the ability of skeletal muscle to alter its structural and functional properties in response to various stimuli, serves a pivotal role in maintaining muscle homeostasis. This remarkable adaptability is seen in the form of muscle hypertrophy (an increase in muscle size) or muscle atrophy (a decrease in muscle size), modulations in energy metabolism, and the transition of muscle fiber types[74–77].

Muscle hypertrophy, the process where muscle fibers increase in size due to an increase in myofibrillar protein content, is a result of chronic resistance exercise or mechanical overload[78]. This process is orchestrated by a complex network of signaling pathways, predominantly involving the Insulin-like Growth Factor 1 (IGF-1)/Akt/mechanistic target of rapamycin (mTOR) pathway. Upon mechanical stress, IGF-1 is secreted, which in turn activates Akt, a crucial protein kinase. Activated Akt then triggers mTOR, stimulating protein synthesis and suppressing protein degradation, thus leading to an overall increase in muscle mass[78–81]. Additionally, Akt promotes the translocation of glucose transporter type 4 (GLUT4) to the cell membrane, improving glucose uptake and enhancing glycogen synthesis, which fuels the high energy demand during hypertrophy[82–84]. Resistance training also stimulates mitochondrial biogenesis and shifts muscle metabolism towards oxidative phosphorylation, ensuring an efficient energy supply for enhanced protein synthesis[85–87].

Conversely, muscle atrophy is characterized by a decrease in muscle fiber size, primarily due to an increase in protein degradation or a decrease in protein synthesis. It can occur due to several conditions such as prolonged disuse, malnutrition, aging, or disease states, including cachexia[88–91]. At the molecular level, two major proteolytic systems, the ubiquitin-proteasome system (UPS) and the autophagy-lysosome system, are activated. UPS is regulated by two muscle-specific E3 ubiquitin ligases, Atrogin-1/MAFbx (*Fbxo32)* and MuRF1 (*Trim63*), which target myofibrillar proteins for degradation[92–94]. The autophagy-lysosome system degrades cellular components, including damaged organelles like mitochondria, through autophagosomes that fuse with lysosomes[92,95,96]. The forkhead box O (FOXO) family of transcription factors, particularly FOXO1 and FOXO3, are central regulators of muscle atrophy.

When activated, FOXO factors upregulate genes involved in proteolysis, including Atrogin-1 and MuRF1, and autophagy-related genes[97–101]. Metabolic changes in muscle atrophy involve a decrease in energy utilization, a shift towards a glycolytic phenotype, and impairment in mitochondrial function, leading to a reduction in ATP production and increased reactive oxygen species (ROS) generation[88].

1.2.3 Muscle mitochondrial changes in cachexia

Mitochondria experience significant alterations during cachexia[50]. There's a reduction in mitochondrial number, along with morphological changes, such as swelling and disorganization of cristae[11]. Mitochondrial biogenesis, regulated by PGC-1α, and mitochondrial dynamics, controlled by proteins such as Drp1 and Mfn2, are disrupted during cachexia[6,102–107].

Mitochondrial function also suffers, with compromised oxidative phosphorylation (OxPhos)[108,109]. This often occurs in unison with an increase in reactive oxygen species (ROS) generation, a sign of oxidative stress, which can further damage cellular structures and disrupt cellular functions[110,111].

1.2.4 Impact of tumor on muscles

Tumor-derived factors can also stimulate the upregulation of muscle-specific E3 ubiquitin ligases, such as MuRF1 and Atrogin-1/MAFbx, enhancing protein degradation and contributing to muscle wasting[92,94,112–115].

1.3 NAD^+ in health and disease

Nicotinamide adenine dinucleotide (NAD^+) is a vital pyridine nucleotide coenzyme ubiquitously present in all living cells, playing a critical role in numerous biological processes. As a key redox cofactor, NAD^+ participates in a multitude of redox reactions through its ability to oscillate between its oxidized (NAD^+) and reduced (NADH) forms. Given the diverse roles of NAD^+ in cellular metabolism and regulation, maintaining optimal NAD^+ levels is critical for cellular health and function. Disruptions in NAD^+ homeostasis has been implicated in various age-related diseases, cancer cachexia, metabolic disorders, and cellular senescence, highlighting the significance of understanding and modulating NAD^+ metabolism for therapeutic interventions[116–122].

1.3.1 NAD^+ Boosting

In recent years, the potential to boost NAD^+ levels has garnered significant attention as a possible strategy to combat cancer cachexia induced muscle loss[109], aging[123] and age-related diseases like sarcopenia[124]. This interest is rooted in numerous studies demonstrating that NAD^+ levels decline with age and in various disease states such as cachexia, potentially contributing to cellular dysfunction, tissue degeneration, and disease progression[109,116,117,123,124].

- NAD^+ precursors and supplementation: One approach to targeting NAD^+ metabolism in age-related diseases and cachexia is the use of NAD^+ precursors[109], such as nicotinamide (NAM), nicotinic acid (NA), nicotinamide riboside (NR), and nicotinamide mononucleotide (NMN). Supplementation with these precursors has been shown to

increase cellular and tissue NAD^+ levels, improving various physiological parameters in animal models of aging and age-related diseases[125,126], such as metabolic disorders, neurodegenerative diseases.

- Inhibiting NAD^+-consuming enzymes: Apart from its redox functions, NAD^+ is a substrate for several NAD^+ consuming enzymes that regulate essential cellular processes. Several enzymes consume NAD^+ during their catalytic processes, such as PARPs (poly(ADP-ribose) polymerases) and ADP-ribosyl cyclases (CD38/CD157). Inhibition of these enzymes can help preserve cellular NAD+ levels and improve cellular function[125–127]. For example, PARP inhibitors (described in detail in section 1.3.2.3.3) have shown promise in treating cancer, particularly in cases where the cancer cells have defects in DNA repair pathways[128–130]. CD38 inhibitors (described in detail in section 1.3.2.2) are being investigated for their potential to improve metabolic function and reduce inflammation in age-related diseases[131].

The modulation of NAD^+ levels can profoundly impact cellular function, enhancing the cell's ability to manage stress, repair DNA, regulate metabolism, and ultimately maintain overall cellular health. These interventions could have profound implications for combating cancer cachexia, age-related diseases. Nonetheless, more research is needed to fully understand the long-term effects of these interventions and their potential application in human health and disease.

1.3.2 NAD^+ Consumers

NAD^+ consumers are a diverse group of enzymes that participate in a wide array of cellular processes, highlighting the importance of NAD^+ in cellular metabolism, signaling, and overall cell function[125]. By modulating NAD^+ levels and activity, these enzymes contribute to the regulation of various physiological processes and the maintenance of cellular homeostasis[125]. These enzymes include PARPs, Sirtuins, SARM1, CD38/157 ADP-ribosyl cyclases, and DNA ligase[132]. Below we summarize several of these NAD+ consumers.

1.3.2.1 Sirtuins

Sirtuins are a family of NAD^+ dependent protein deacetylases and mono ADP-ribosyltransferases that play key roles in numerous cellular processes, such as DNA repair, gene silencing, cell survival, and aging. Sirtuins utilize NAD^+ as a substrate to remove acetyl groups from target proteins or to transfer ADP-ribose moieties to them. In doing so, sirtuins modulate the activity of various transcription factors and metabolic enzymes, affecting cellular responses to nutrient availability, oxidative stress, and DNA damage. In mammals, there are seven known sirtuins (SIRT1-SIRT7), each exhibiting distinct subcellular localization, substrate specificity, and functional roles[125].

1.3.2.2 ADP-ribosyl cyclase (CD38 and CD157)

ADP-ribosyl cyclases, such as CD38 and CD157, are NAD^+ consuming enzymes that catalyze the formation of cyclic ADP-ribose (cADPR) and nicotinic acid adenine dinucleotide phosphate (NAADP) from NAD^+ or $NADP^+$, respectively. These molecules function as intracellular calcium messengers, regulating calcium release from intracellular stores and modulating various

calcium-dependent cellular processes, such as proliferation, differentiation, and migration[133,134].

1.3.2.3 Poly (ADP-ribose) Polymerases (PARPs)

Poly (ADP-ribose) polymerases (PARPs) are evolutionarily conserved enzymes with crucial roles in many cellular processes. Their primary function involves catalyzing the transfer of ADP-ribose units from NAD+ onto target proteins. This action results in either mono-ADP ribosylation (MARylation) or poly-ADP ribosylation (PARylation), which in turn influences the function, localization, and stability of the target proteins. Consequently, this affects cellular activities such as DNA repair, gene transcription, chromatin remodeling, cellular stress responses, immune regulation, and signaling pathways[135–137].

1.3.2.3.1 Classification of PARP Family Members

The PARP family members are characterized by their conserved catalytic (CAT) domain responsible for their ADP-ribosylation activity. They are composed of different protein domains that determine their specific functional properties and target specificity. Accordingly, the PARP enzymes can be classified into four main groups:

- DNA-dependent PARPs: Comprising of PARP1, PARP2, and PARP3, these enzymes recognize and bind to damaged DNA structures due to their DNA-binding zinc finger motifs[138]. Specifically, PARP1 also contains a BRCA C-terminus domain which is primary involved in protein-protein interaction. Their primary role involves DNA damage recognition and repair and maintaining genomic stability[139].

- Tankyrases (PARP5a and PARP5b): These enzymes, also known as Tankyrase1 and Tankyrase2, possess ankyrin repeat domains and a sterile alpha motif (SAM) domain. They are involved in diverse cellular processes such as telomere maintenance, Wnt signaling, and mitotic spindle assembly[140].
- CCCH-type zinc finger PARPs: This group includes PARP7, PARP12, and PARP13, which contain CCCH-type zinc finger motifs. These enzymes are involved in gene expression regulation, RNA processing, antiviral response and cellular stress responses[141–149].
- Macrodomain-containing PARPs: Examples are PARP9, PARP14, and PARP15, characterized by a macrodomain that recognizes and binds to ADP-ribose moieties. These enzymes are involved in various aspects of immune regulation and cellular stress responses[150,151].

Given their diverse roles in cellular processes and their implication in various disease states, PARP enzymes have emerged as promising therapeutic targets. The development of PARP inhibitors has become a significant focus of research for the treatment of conditions such as cancer, neurodegenerative diseases, and inflammatory disorders.

1.3.2.3.2 Mono and Poly-ADP-ribosylation

Mono-ADP-ribosylation involves adding a single ADP-ribose unit to the target protein, while poly-ADP-ribosylation involves the addition of multiple ADP-ribose units to form a linear or branched poly(ADP-ribose) (PAR) chain on the target protein. The former often affects protein-protein interactions, enzymatic activities, or subcellular localization, modulating the function of the target protein. On the other hand, the latter can serve as a scaffold for the recruitment

of other proteins, leading to changes in protein complex assembly, chromatin structure, or transcriptional activity[152–154].

The PARP family enzymes, particularly PARP1, are the primary mediators of PARylation. PARPs use NAD+ as a substrate to catalyze the transfer of ADP-ribose units onto target proteins, generating long, branched chains of poly(ADP-ribose) (PAR). The process begins with the activation of PARP enzymes in response to specific cellular signals, most notably DNA damage. Once activated, PARP enzymes cleave NAD^+ into nicotinamide and ADP-ribose, and the latter is covalently attached to specific amino acid residues on target proteins. The process can be reversed by poly(ADP-ribose) glycohydrolase (PARG) (described in detail in 1.4) and other ADP-ribose hydrolases, which remove the PAR chains from proteins.

PARylation plays crucial roles in various cellular processes. The most well-studied role of PARylation is in the DNA damage response. PARylation at DNA damage sites leads to the recruitment and activation of DNA repair proteins, facilitating the repair process. Moreover, PARylation also plays roles in the regulation of gene transcription, chromatin structure, cell death pathways, and immune responses. The dysregulation of PARylation has been linked to a variety of human diseases, including cancer, neurodegenerative diseases, inflammation, and aging.

Given that NAD^+ is a substrate for PARylation, the process of PARylation has a significant impact on cellular NAD^+ levels and NAD^+ metabolism. Excessive activation of PARPs, such as during severe DNA damage, can lead to depletion of cellular NAD^+ and energetic crisis, a

condition termed "PARP-trapping". Therefore, the regulation of PARylation is crucial for maintaining NAD^+ homeostasis and cellular health.

Given the critical roles of PARylation in DNA repair and cell death, PARP inhibitors have been developed as cancer therapeutics, especially for cancers with defects in DNA repair pathways. Furthermore, the modulation of PARylation might also hold promise for neurodegenerative diseases, cardiovascular diseases, and age-related conditions, which are associated with dysregulation of NAD^+ metabolism and PARylation[152,154].

1.3.2.3.3 PARP inhibitors

The most well-known and clinically advanced group of PARP-targeting drugs are the PARP inhibitors, which are primarily used for the treatment of certain types of cancer. PARP inhibitors work by blocking the enzymatic activity of PARP enzymes, thus preventing them from certain functions such as repairing DNA damage. This is particularly effective in cancer cells with pre-existing defects in DNA repair pathways, such as BRCA1/2-mutated cancers, a strategy that can kill cancer cells in a process known as synthetic lethality. Several PARP inhibitors, including olaparib, rucaparib, and niraparib, have been approved for the treatment of ovarian, breast, and prostate cancers. Ongoing research is exploring the potential of PARP inhibitors in other cancer types and in combination with other therapeutic modalities, such as immunotherapy[155–158].

As outlined in table below, all the cancer drugs under consideration can inhibit PARP1, PARP2, or PARP3. It is noteworthy that Talazoparib exhibits a broader inhibitory profile, targeting not only PARP1, PARP2, and PARP3, but also tankyrase 1 (TNKS1) and tankyrase 2 (TNKS2).

Additionally, Olaparib demonstrates a similar inhibitory range, impacting PARP1, PARP2, PARP3, and TNKS1[155,156,158,159].

Table 1: List of prominent PARP1 inhibitors with FDA approval

Drug Name	Mechanism of action	Pharmacokinetics	Target	Indication	Year of first approval
Niraparib	PARP inhibition	Mean half-life=~36 h; median time to maximal concentration=3 h	PARP1, PARP2, PARP3	Ovarian	2017
Rucaparib	PARP inhibition	Mean half-life=17 h; median time to maximal concentration=1·9 h	PARP1, PARP2, PARP3	Ovarian	2016
Olaparib	PARP inhibition	Mean half-life=14·9 h (tablet) or 11·9 hours (capsule); median time to maximal concentration=1·5 h	PARP1, PARP2, PARP3, TNKS1	Ovarian, Breast, Pancreas, Prostate	2014
Talazoparib	PARP inhibition	Mean half-life = 90 hours; median time to maximal concentration = 1.0 to 2.0 hours.	PARP1, PARP2, PARP3, TNKS1, TNKS2	Breast	2018

1.4 PARG

Poly(ADP-ribose) Glycohydrolase (PARG) is an enzyme that plays a pivotal role in the regulation of PARylation as a post translational modification. PARG's role is to reverse this modification. It breaks the glycosidic bonds between ADP-ribose units in the PAR polymer, effectively removing PAR from proteins and thereby reversing the effects of PARylation. This action makes PARG crucial for maintaining the balance of PARylation in cells, which is important for normal cellular function[152,154].

Dysfunction or imbalance in the activities of PARP and PARG enzymes can lead to excessive or insufficient PARylation, both of which can have detrimental effects on cellular health. Overactive PARP activity or insufficient PARG activity can lead to excessive PARylation, depleting cellular NAD+ stores and leading to cell death. Conversely, underactive PARP activity or overactive PARG activity can result in insufficient DNA repair, potentially leading to genomic instability and cancer[152,153].

Therefore, understanding the balance and interplay between PARPs and PARG is crucial for understanding the cellular response to DNA damage, as well as the pathogenesis of diseases associated with DNA repair defects and NAD^+ metabolism dysregulation.

1.5 The Role of PARP1 and PARG in Cancer Cachexia

Recent advances in cancer cachexia research have illuminated a plethora of complex biological pathways, especially those implicated in muscle atrophy. Despite the growing comprehension of myriad proteins and genes, the precise functions of PARP1 and PARG remain somewhat nebulous. The potential therapeutic ramifications of modulating these molecules, particularly in the context of muscle wasting conditions like cancer cachexia, merit in-depth exploration.

Both genetic and pharmacological inhibition of PARP1 in murine models have rendered promising outcomes: improved muscular health attributed to improved mitochondrial function[126,127]. For example, mice treated with PARP1 inhibitors demonstrate increased endurance and mitochondrial function[127]. Concurrently, PARP1 deficient mice demonstrated augmented mitochondrial content, amplified energy expenditure in brown adipose and skeletal muscle, and resistance to metabolic disorders[160,161]. In the context of cancer cachexia,

where mitochondrial efficacy is often diminished[162–164], inhibiting PARP1 may offer a strategy to mitigate cachexia-induced mitochondrial impairments.

Notably, PARP inhibition also increases NAD^+ concentrations[161] - an imperative observation as skeletal muscle NAD^+ levels are notably reduced in cancer cachexia[109]. Augmenting NAD^+ levels might be a viable therapeutic modality. Moreover, PARP1 inhibition increases SIRT1 activity[161], thereby potentially enhancing skeletal muscle metabolism[161]. Such advantages are also evident in murine models with reperfusion injuries[165–167] and senescence[168], wherein PARP inhibitors protect skeletal muscle mitochondrial biogenesis and bioenergetics. Examining the wider implications, the ablation of PARP-1 prevents NF-kappaB activation[169,170], instrumental in muscle protein degradation and inflammation. Furthermore, muscle transcriptional responses to glucocorticoids, well-known muscle wasting agents, are contingent on PARP1-mediated PARylation. All supporting the idea that *Parp1* ablation might be beneficial in cancer cachexia.

However, contrasting these findings, certain data demand attention. It is correct that *Parp1* ablation might improve mitochondrial function and bioenergetics, but one should consider another biological role of PARP1 and PARylation. For example, a study by Doles and colleagues found that the adjunctive use of the PARP inhibitor veliparib with chemotherapy did not lead to improved muscle mass in patients with cancer and all the 60 patients in this study demonstrated significant weight loss[171]. Also, PARP1 mediated inhibition of the transcription factor FOXO1, observed in Ewing sarcoma RD-ES and SK-ES-1 cell lines, and CAPAN1 pancreatic cancer cells[172] requires attention as transcription factor FOXO1 regulates various proteins

involved in muscle atrophy[113]. Moreover, correlation between diminished PARP1 activity and increased energy consumption is important[127], particularly in the context of increased energy consumption in cancer cachexia[173]. Also, while the role of PARP1 in DNA repair is recognized, its basal activity and its influence on glycolysis necessitate a comprehensive analysis[173]. Additionally, PARP1 knockout mice exhibit a lower grip strength[174]. Overall, emerging data suggests that PARP1 has a protective role in muscle function and maintenance.

On the other hand, the role of PARG, the protein responsible for dePARylation, in muscle biology remains under-researched. Although, non-specific PARG inhibitors like Ellagitannin exhibit potential for muscle strength restoration[175], there is an urgent need for more targeted studies elucidating PARG's function. Given the clinical administration of PARP1 inhibitors and the dire prognostic implications of muscle depletion in cancer cachexia, grasping these molecular `interplays is imperative. As pharmaceutical companies focus on developing PARG inhibitors, deciphering their effects on muscle morphology is essential[176].

Considering the ambiguous and limited data regarding the role of PARP1 and PARG in skeletal muscle, and limited knowledge on their roles in cancer induced cachexia, we decided to answer these questions. Thus, we postulate that the dysregulation of skeletal muscle PARylation might exacerbate cancer cachexia. This proposition is not only clinically salient due to the prevalent application of PARP1 inhibitors in the clinic but also helps us determine the safety of therapeutic strategies centered on PARG inhibition. By elucidating these, we describe a more informed strategy for the management and remediation of cancer cachexia when considering pharmaceutical strategies that inhibit PARylation (PARPs) or dePARylation (PARG).

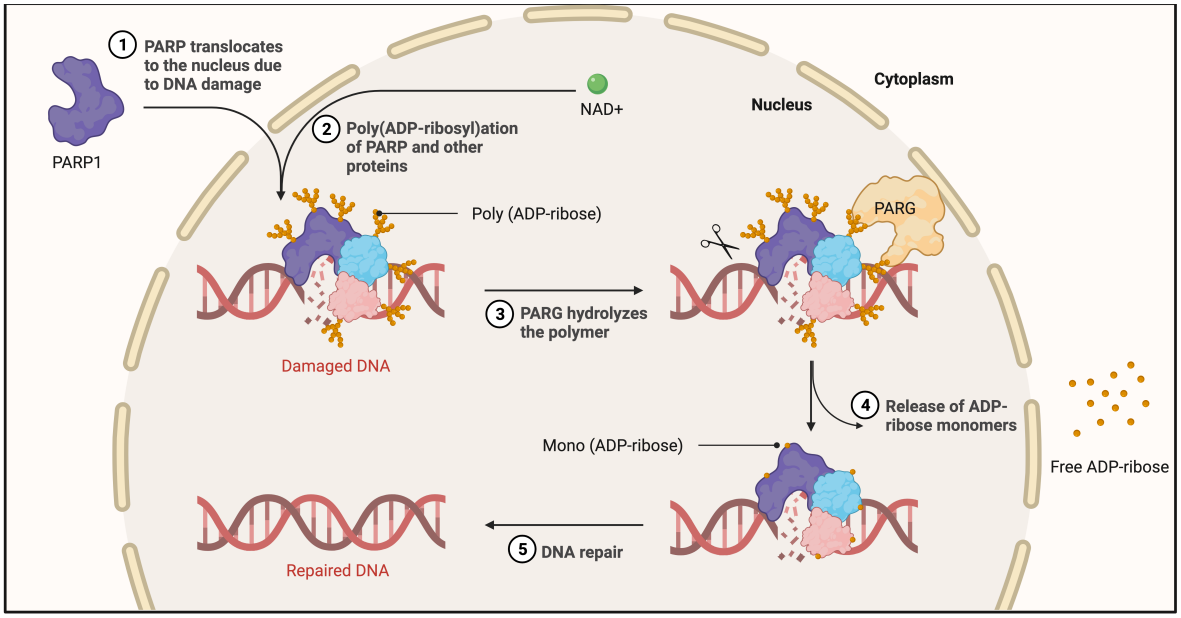

Figure 1: Metabolism of PARylation.
In a process called PARylation, PARP1 transfer the ADP moiety to target proteins including itself. This PAR chain can be later degraded by PARG. Illustration made by modifying a template in Biorender.com.

2 Hypothesis

Muscle deregulation of poly-ADP Ribosylation exacerbates Lewis Lung Carcinoma-induced muscle cachexia.

Aim 1: Describing the role of PARylation-related gene expression in the context of muscle physiology in cancer cachexia and exploring the therapeutic potential of targeting this pathway using *in vitro* models.

Aim 2: Validating the effects and role of (de)PARylation, by ablating *Parp1* or *Parg* expression in mouse skeletal muscle, in the development and progression of cancer cachexia in mice.

3 Materials and Methods

3.1 Generation of Inducible Skeletal Muscle Knockout Mice

To generate inducible muscle-specific ablation models of *Parp1* and *Parg*, a crossbreeding strategy was employed. The first line of mice utilized was the mature muscle-specific Human Skeletal actin promotor driven tamoxifen sensitive Cre-Recombinase mice (Human Skeletal Actin-Mutated estrogen receptor, Cre, Mutated estrogen receptor, HSA-MCM)[177]. In these mice, the Cre gene, which is responsible for mediating recombination at specific DNA locations, was driven by the Human Skeletal Actin (HSA) promoter, thus restricting its expression to mature muscle tissues. The HSA-MCM mice are tamoxifen-sensitive, allowing for the temporal control of the gene recombination process[178]. These HSA-MCM mice were then bred with two other mouse lines: *Parp1*-Floxed (B6(Cg)-Parp1 $^{tm1c(EUCOMM)Hmgu}$/WlkrJ) or *Parg*-Floxed (C57Bl/6N-Parg $^{tm2c(KOMP)Mbp)}$ /T_{cp}) mice. In these floxed mouse lines, LoxP sites, which are specific DNA sequences recognized by the Cre enzyme, flank the *Parp1* Exon 4 or *Parg* Exon 2-4 genes, respectively. This genetic arrangement permits the specific and inducible deletion of the *Parp1* or *Parg* genes in the presence of Cre and upon tamoxifen administration.

The HSA-MCM and *Parp1*-Floxed mice lines were procured from the Jackson Laboratory. *Parg*-Floxed mice were generated with collaboration with Canadian Mutant Mouse Repository (CMMR). Mating schemes and housing conditions adhered to institutional animal care guidelines. This breeding strategy allowed us to create mouse models wherein the *Parp1* and *Parg* genes could be conditionally deleted in mature muscle tissues upon tamoxifen administration.

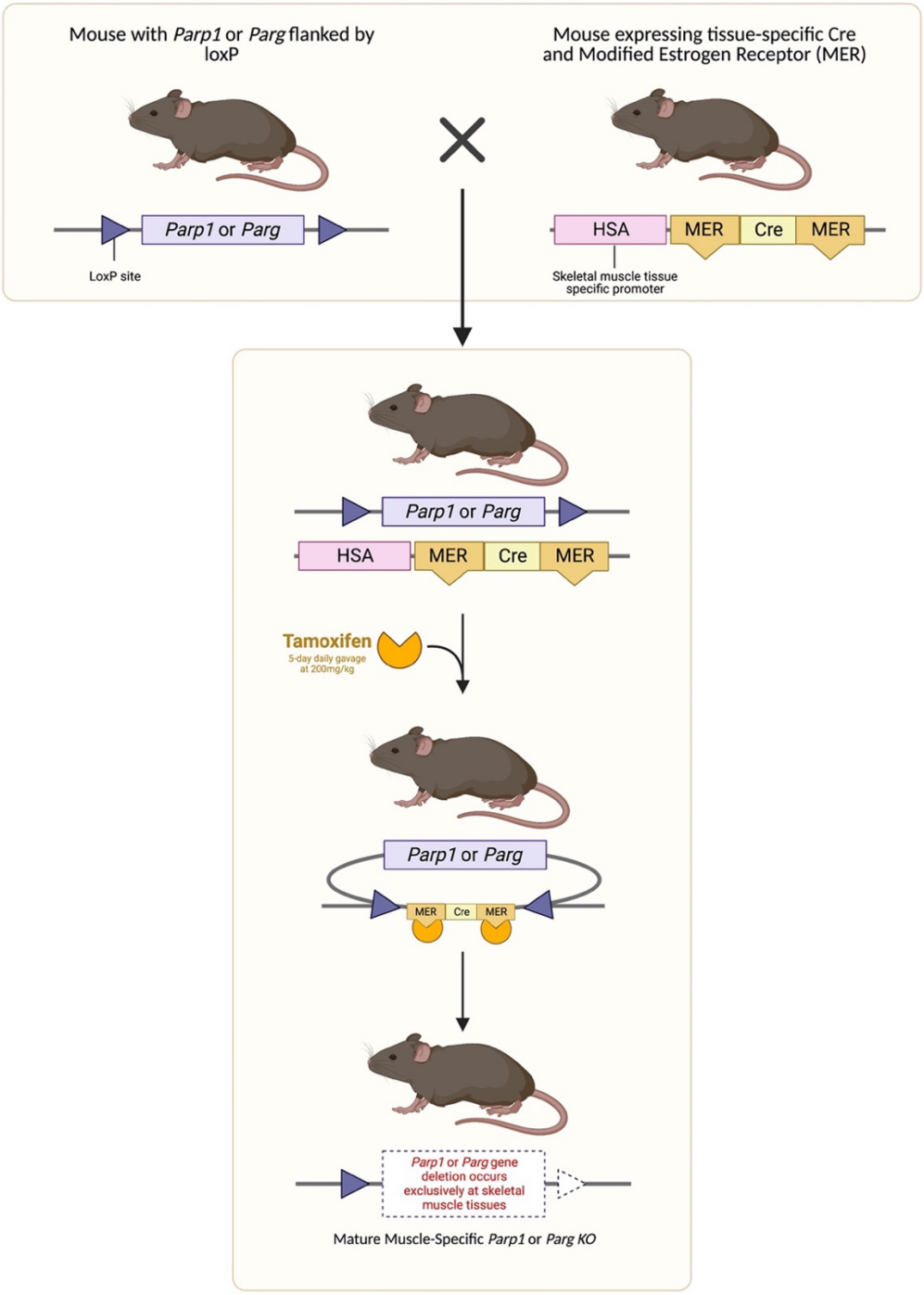

Figure 2: Generation of *Parp1*-IMKO and *Parg*-IMKO mice.
Parp1 or *Parg* mice were crossed with HSA-MCM mice. Upon tamoxifen administration, the activity of Cre enzyme in these mice led to targeted ablation of the floxed gene. Illustration made by modifying a template in Biorender.com.

3.1.1 Animal housing

A series of experiments were conducted using distinct groups of mice, selected randomly prior to each experiment. All animal studies received approval from the University of Ottawa Animal Care Committee (Protocols #: Hse-3236) and the ethics committee. The mice were maintained under a strict 12-hour light/dark cycle, had ad libitum access to food and water and were housed at room temperature. Tissues were collected from the mice during light period. The study involved groups of mice approximately 9 weeks old. Tamoxifen was administered to the mice via gavage for 5 consecutive days at 200mg/kg dose to activate the Cre-Lox recombination, this was followed by a 2-week rest period.

3.1.2 Mouse Genotyping

A small portion of ear tissue was collected from each mouse processed for DNA extraction. For DNA extraction, each sample underwent treatment with 50 mM NaOH and was incubated at 95°C for 30 minutes, which was followed by neutralization with 100 mM sodium acetate. After sacrificing the mice, a small sample of the tail was used to confirm the genotyping.

The extracted DNA was subsequently utilized for genotyping via polymerase chain reaction (PCR). Specifically, 200 ng of DNA was introduced into the Phire Tissue Direct PCR Master Mix (Thermo Scientific, Catalogue number F170S), along with primers targeting the HMG-CoA reductase (HMGR) and Cre recombinase genes, or LoxP *Parg* and wildtype *Parg*. The primer sequences are available in the table 2.

The mixture was then subjected to thermocycling conditions that included denaturation at 98°C for 3 minutes, followed by 40 cycles of denaturation at 98°C for 10 seconds, annealing at

65°C for 10 seconds, and extension at 72°C for 30 seconds, culminating with a final incubation at 72°C for 5 minutes. The resulting PCR products were preserved in a refrigerator for subsequent analysis.

PCR product separation was performed using 2% agarose gel electrophoresis supplemented with SYBR Safe dye (Catologue number S33102, Invitrogen™). The samples were loaded onto the gel in Tris base, acetic acid, and EDTA (TAE) buffer and subjected to a constant electrical charge of 90 volts for 30 minutes. The anticipated PCR product sizes for the HMGR and Cre genes were 800 bp and 350 bp, respectively, or for LoxP 813bp and 283bp, knockout 283bp and wildtype 648bp. The gel was subsequently imaged using a chemidoc under Syber-Safe option.

Table 2: List of primers used for genotyping.

Gene Target	Primer direction	Sequence
Hmgr	Forward	CAATCCTGGAGAAAACGCAC
Hmgr	Reverse	CAGAACACAGCACGGAAAGA
Cre	Forward	ATGTCCAATTTACTGACCG
Cre	Reverse	CGCCGCATAACCAGTGAAAC
Parg (wildtype)	Forward	CCTTGCATTCTGGGCTCATGGCTTG
Parg (wildtype)	Reverse	AAGCAGGAAGAACTAATGTGTCAGG
Parg (LoxP)	Forward	CTTAAGACCATCTGCAAGTCACAC
Parg (LoxP)	Reverse	GATGGCGAGCTCAGACCATAACTTC

3.2 Collagen Coating of Tissue Culture Dishes

A sterile 0.01% collagen solution was prepared using distilled autoclaved water. This solution was made with collagen (Sigma-Aldrich catalogue number C7661). Subsequently, a volume of 3 ml of this diluted solution was uniformly spread over the entire surface of a sterile 10 cm dish (Corning catalogue number 353003).

Once the solution was evenly applied, the dish was positioned in an incubator (HERAcell VIOS 160i, Thermo Fisher Scientific) programmed at a temperature of 37°C and an atmosphere of 5% CO^2. This setting was maintained for approximately 1 hour to facilitate collagen adherence to the dish surface.

Post incubation, the dish was then transferred under a biological safety cabinet, the surplus collagen solution was carefully aspirated using a sterile aspirator. The drying phase generally lasted between 1-2 hours. The resulting product was a dish layered with a fine coating of collagen. This collagen coating furnished a nurturing environment conducive to myoblast growth and adhesion in cell culture studies.

3.3 Isolation of Primary Myoblasts

Primary myoblasts were obtained from C57BI/6NTac mice. Hindlimb muscles of mice were procured and rinsed twice with Phosphate Buffered Saline (catalogue number 311-010-CL, Wisent Inc.). These muscles were subsequently minced using a sterile razor blade which was previously submerged in 70% ethanol. The muscle fragments were then exposed to a solution containing 10 g/L Collagenase B (catalogue number 11088831001, Roche Canada, Basel, Switzerland) and 4 g/L Dispase II (catalogue number D4693, Millipore Sigma, Burlington, Massachusetts, USA) in Ham's F10 media (catalogue number 318-050-CL, Wisent Inc.). The solution was incubated at 37°C for approximately 30 minutes, with intermittent agitation.

This mixture was then filtered using a 100µm cell strainer, yielding a cell suspension that was subsequently reconstituted in growth media. This growth media consisted of Ham's F10 media (catalogue number 318-050-CL, Wisent Inc.), supplemented with 20% Bovine Calf Serum (catalogue number SH3007203, Thermo Fisher Scientific), 1% penicillin-streptomycin (Gibco), and 0.005% (2.5 ng/mL) basic Fibroblast Growth Factor (catalogue number ab155734, Abcam, Cambridge UK)

This cell suspension was left to incubate on a non-collagen-coated plate for 1-2 hours to enable fibroblast adhesion while preventing myoblast adhesion. The supernatant, rich in myoblasts, was then transferred to a collagen-coated plate (catalogue number 353003, Corning) for 24 hours. Afterwards, cells were detached using a 0.05% trypsin-EDTA solution (catalogue number 325-043-CL, Wisent Inc.) and underwent a second pre-plating for 1-2 hours on non-collagen-coated plates. The resulting supernatant was transferred to collagen-coated plates and utilized in subsequent experiments.

The harvested cells were then expanded and cryopreserved. Briefly, cells were trypsinized using 0.05% trypsin-EDTA solution (catalogue number 325-043-CL, Wisent Inc.) and subsequently centrifuged at room temperature at 500 r.c.f. for 5 minutes. The supernatant was discarded and the cell pellet was resuspended in freezing media, consisting of 40% growth media (as defined earlier), 50% Bovine Serum Albumin (catalogue number SH3007203, Thermo Fisher Scientific), and 10% Dimethyl sulfoxide (catalogue number 85190, Thermo Fisher Scientific).

The cell suspension in the freezing media was then portioned into 1 ml aliquots in cryopreserving vials (catalogue number CLS430659, Millipore sigma) and relocated to a Mr. Frosty (catalogue number 5100-0001, Thermo Fisher Scientific) at room temperature, before being transferred to a -80°C freezer for long-term storage.

3.4 Collection of Lewis Lung Carcinoma-Conditioned Media

Lewis Lung Carcinoma (LLC) cells were induced at 50% confluency in their growth media. Post 24 hours, the media was gathered and transferred into a 50 mL tube. Subsequently, this tube was centrifuged at 4°C for 5 minutes at 500 r.c.f to eliminate any cell debris. The supernatant was carefully partitioned into aliquots, while the pellet was discarded. This conditioned media was subsequently stored at -80°C for future use.

Unconditioned LLC growth media was also generated as a control. The media was formulated by adding the identical supplements to DMEM as employed in the LLC growth media, with the exclusion of culturing any cells. This unconditioned media was then divided into aliquots and stored at -80°C for further use.

For experiments, the aliquoted conditioned media was thawed at 37°C, following which it was diluted at a 1:2 ratio with growth media. As a control, the unconditioned LLC media was also diluted at a 1:2 ratio with fresh growth media in a similar fashion. The resultant diluted media was then utilized in experiments.

3.5 Differentiation of Primary Myoblasts to Myotubes

Primary myoblasts' differentiation into myotubes was executed via the following protocol. Initially, the isolated primary myoblasts were propagated in growth media until they attained an approximate confluence of 70%. Following this, myoblasts were trypsinized using 0.05% Trypsin-EDTA buffer (catalogue number 325-043-CL, Wisent Inc.) and induced onto collagen-coated 6-well dishes at a density of 100,000 cells per square centimeter.

Post approximately 8 hours, myoblast adhesion to the plate was verified. The media was then switched from the growth media to a differentiation media. This differentiation media comprised of high glucose Dulbecco's Modification of Eagle Medium (catalogue number 319-005-CL, Wisent, Saint Jean Baptiste, QC, Canada), supplemented with 5% heat-inactivated horse serum (catalogue number 26050088, Gibco™ Fisher Scientific Company, Ottawa, ON, Canada) and 1% penicillin-streptomycin (catalogue number 15070063, Thermo Fisher Scientific). This differentiation media was replenished daily over a span of 3-4 days. To ensure the reliability of results, all experiments were replicated at least twice in triplicate.

3.6 Tumor Allograft

To establish the tumor allograft model, LLC cells were trypsinized and prepared for injection into the mice. The suspended cells were centrifuged at 500 r.c.f for 5 minutes at room temperature, then washed twice with PBS to remove serum from the media and limit the immune response in the mice. The cells were subsequently resuspended in PBS and their count was determined using the Countess II FL Automated Cell Counter (Catalogue number C10228, Invitrogen), following the trypan blue (Catalogue number T10282, Invitrogen) exclusion method. A solution comprising cells in PBS with a concentration of 5 × 10^6 cells was prepared, and 200 µL was loaded into a syringe with a 10 gauge needle which was kept on ice to ensure cell viability.

For the *in vivo* experiment, the mice were anesthetized two weeks after tamoxifen administration using 3.5% isoflurane vaporized in oxygen. Following this, LLC cells (1 × 10^6

cells in 200 µL of PBS) were subcutaneously injected into the mice's left flank. Control mice were administered a 200 µL injection of PBS in the left flank. Any mice displaying ulceration at the tumor site, a loss of 20% of their initial body weight, or a tumor size exceeding 17 mm × 17 mm were removed from the study before euthanasia, adhering to the stringent animal care standards. The animals were then humanely euthanized through cervical dislocation.

3.7 Grip Strength

A comprehensive approach to measure forelimb grip strength was systematically implemented on a weekly basis (day -1, 6, 13, 20) throughout the experiment. This procedure involved acclimatizing the mice to the testing room for 30 minutes, followed by each mouse grasping a wire mesh linked to a digital force transducer that recorded peak force. The mouse was then gently pulled horizontally away from the mesh by the base of its tail.

Both *Parp1*-IMKO and *Parg*-IMKO mice, as well as their control counterparts, were utilized as test subjects. The forelimb grip strength force was compared between nontumor control mice and those induced with LLC. The test comprised five consecutive pulls, each separated by an interval of approximately 5 seconds. The absolute grip strength, measured in gram-force, was calculated as the average of the peak forces from top three pulls. This process offered an accurate evaluation of muscle function and essential insights regarding the impacts of the experimental manipulations on muscle mass and function. Additionally, the body weight of each mouse was recorded before they were returned to their housing room.

3.8 Body Mass Measurement

Throughout the study period, body mass was measured for each mouse on days 0, 4, 7, 11, 14, 18, and 21 of the experiment. The measurement was performed using a digital scale that was calibrated before each use. The mice were weighed individually, with their weight recorded to the nearest 0.1 g.

3.9 Tissue collection

At the end of the study, which occurred on day 23 for *Parp1*-IMKO mice and day 21 for *Parg*-IMKO mice, all mice were humanely euthanized through cervical dislocation. Various tissues, including Tibialis Anterior (TA), Gastrocnemius (GP), Quadricepses (Quad), Spleen, liver, blood, soleus, and tumor were meticulously dissected from each mouse. The muscles were then weighed using a precise scale, and the data was contrasted between the control group (nontumor-PBS injected) and the experimental group (LLC induced).

Following dissection, some tissue samples were immediately flash-frozen in liquid nitrogen for subsequent biochemical analysis. Other samples were embedded in Optimal Cutting Temperature (OCT) compound (Catalogue number 23-730-571, Fisher Scientific) for histological examinations. The embedded samples were then immersed in liquid-nitrogen cooled isopentane for approximately 10 minutes before being placed in liquid nitrogen for long-term storage.

3.10 Total Protein Isolation and Quantification

3.10.1 Tissue Analysis

Flash-frozen quadriceps muscle tissue was first pulverized using a hammer on a liquid nitrogen-chilled aluminum block. The resulting powder was weighed, with amounts between 15-25 mg recorded for subsequent analysis.

A supplemented radioimmunoprecipitation (RIPA) buffer was prepared prior to homogenization. The buffer composition included 150 mM sodium chloride, 1% Triton X-100, 0.50% sodium deoxycholate, 0.10% sodium dodecyl sulfate, and 50 mM Tris. Protease and phosphatase inhibitors were added to the buffer, specifically, the Roche Complete Protease Inhibitor Cocktail (05892970001, Roche Canada, Basel, Switzerland) and Roche PHOStop Phosphatase Inhibitor Cocktail (4906837001 Roche Canada, Basel, Switzerland). Additional supplements in the buffer were 5 mM of sodium butyrate, 100 µM of fresh tannic acid, and 1 µM of olaparib. This buffer was added at a volume of 10 µl for each mg of tissue.

The tissue samples were homogenized using a Bead Mill 24 Homogenizer (Catalogue number 15340163, Fisherbrand) with two 2.8mm ceramic bead. The homogenization procedure involved three 40-second cycles at a speed of 2.09 m/s, interspersed with 22-second resting intervals.

Following homogenization, the homogenate was centrifuged at 16,000 rcf for 10 minutes at 4°C. The supernatant was then carefully transferred into a 1.5 mL microcentrifuge tube. The supernatant underwent another round of centrifugation, after which the resultant supernatant was moved to a new tube. This final supernatant sample was set aside for

downstream protein quantification processes. The pellet, consisting mainly of cell debris, was discarded.

3.10.2 Cell Culture Analysis:

Post-treatment, the media was drained from the Petri dishes and the dishes were washed twice using room temperature phosphate-buffered saline (PBS), which was then also removed. A volume of 150µl of ice-cold radioimmunoprecipitation assay (RIPA) lysis buffer was subsequently added to each dish. The cells were swiftly frozen in liquid nitrogen and the resulting frozen lysate was collected via scraping with a cell scraper (Thermo Scientific™). The lysate was then transferred into 1.5mL centrifuge tubes using a pipette.

Upon completion of homogenization and scraping, the tubes were instantly placed on ice and subjected to vigorous vortexing. The lysate was centrifuged at 16,000 relative centrifugal force (r.c.f.) at 4°C for 10 minutes, after which the supernatant was carefully collected. This procedure was executed twice, with the pellet being discarded each time. The resulting supernatant was transferred into fresh tubes and stored at -80°C for future use.

3.10.3 Total Protein Quantification:

The protein concentration in the samples was quantified using the DC protein assay (Bio-Rad Laboratories, Hercules, California, USA). Freshly prepared bovine serum albumin (BSA) standards were created in double distilled water (ddH2O) to span the linear range that the DC protein assay is designed to detect. Both standards and samples were analyzed in triplicate to enhance accuracy.

A colorimetric reaction was then performed, with the resulting absorbance measured using a POLARstar Omega plate reader (BMG Labtech). The protein concentration was calculated by dividing the measured protein quantity by the mass of tissue used for protein extraction, yielding the protein extraction efficiency.

3.10.4 Western Blotting

The samples were adjusted to a similar concentration by diluting in RIPA buffer and 4x Laemmli Buffer (Bio-Rad Laboratories, Hercules, California, USA Cat# 1610737), supplemented with 10% β-mercaptoethanol (Fisher Bioreagents, BP176-100). The diluted lysates were then heated for 5 minutes at 95 degrees Celsius, unless specified otherwise.

Subsequently, the diluted lysates were size-separated using 8%, 10%, or 12% SDS-PAGE gels, depending on the molecular weight of the target protein. The gels were made using the TGX Stain-free FastCast Acrylamide Kit (Bio-Rad Laboratories, Hercules, California, USA Cat# 1610183) with 10% Ammonium persulfate (APS) a day before the experiment and stored in a refrigerator. Each well of the gel was loaded with 15-25µg of protein, and the samples were separated using the Mini-PROTEAN system (Bio-Rad Cat# 1658006). The SDS-PAGE was run at a constant 35mA, 90 volts across the gel for 30 minutes, then at 120 volts for 50-60 minutes or until the ladder reached the end of the gel.

The StainFree gels were activated for 45 seconds using the stain-free setting on a ChemiDoc Touch Imaging System (Bio-Rad). Following activation, the proteins were transferred to a TransBlot Turbo Mini size 0.2µm nitrocellulose membrane (Bio-Rad) via the Trans-Blot

TurboTransfer System (Catalogue number 1704150EDU, Bio-Rad Laboratories, Hercules, California, USA on the midi-gel setting.

To visualize total protein per lane, the nitrocellulose membrane was imaged again under the stain-free blot setting with automatic exposure time, then blocked for an hour in a blocking buffer consisting of 5% w/v bovine serum albumin (Sigma, SKU A7906) in TBS-T buffer (50mM Tris-HCl, pH 7.6; 150mM NaCl; 0.1% Tween), while gently agitated at room temperature. The membranes were then incubated with primary antibodies diluted in TBS-T buffer overnight at 4°C, under gentle agitation. After being washed three times for 5 minutes each in TBS-T, the membranes were incubated for one hour with the corresponding IgG, horseradish peroxidase (HRP)-conjugated secondary antibody, with gentle agitation at room temperature.

Following three additional TBS-T washes, detection was carried out on a ChemiDoc system (Bio-Rad Laboratories, Hercules, California, USA) using 1 ml Clarity (Catalogue number 1705060, Bio-Rad Laboratories, Hercules, California, USA) or Clarity Max (Catalogue number 1705062, Bio-Rad Laboratories, Hercules, California, USA) enhanced chemiluminescent solutions on the chemiluminescence setting. The instrument automatically calculated an initial exposure time for imaging, which was then manually adjusted to capture multiple images and ensure the blot was not saturated. Images were processed and quantified using FIJI software on TIFF raw files after performing rolling ball background correction with a radius of 30.

In instances where membranes underwent a second round of immunoblotting, they were stripped of previous antibodies using Restore PLUS Western Blot Stripping Buffer (Catalogue number 46430 Thermo Scientific). The membranes were washed in the stripping buffer for 30

minutes in a shaking incubator at 100 relative centrifugal force at 37 degrees Celsius. After stripping, the membranes were reblotted with a secondary antibody and imaged to confirm no bands.

Table 3: List of antibodies and dilutions used for protein quantification.

Protein	Company	Product number	Total protein loaded	Primary dilution	Secondary dilution
Total OxPhos Rodent WB antibody cocktail	Abcam	Ab110413	10µg	1:1000	1:1000
M/PARylation	Cell signaling	E6F6A	10µg	1:1000	1:1000
FOXO1	Cell signaling	C29H4	10µg	1:1000	1:1000

3.11 RNA Isolation and Complementary DNA Synthesis

3.11.1 Tissue Analysis

The previously flash-frozen quadriceps muscle tissue was mechanically powdered using a hammer on a liquid nitrogen-cooled aluminum block. From the resultant crushed tissue, a segment weighing between 15-25 mg was accurately measured and transferred into reinforced tubes.

For each of these tubes, 1 ml of TRIzol reagent (catalog number 15596018, Fisher Scientific, Ottawa, ON, Canada) was added. This was followed by the addition of 200 µL of chloroform,

leading to gentle mixing through the inversion of the tube 10 times. Subsequently, the samples were subjected to centrifugation at 4°C with a force of 16,000 x g for a duration of 15 minutes.

The subsequent steps involved the extraction of the aqueous phase, which was then further refined using the EZ-10 DNAaway RNA Mini Prep Kit (catalog number BS881133, BioBasic, Markham, ON, Canada). This process adhered closely to the ma'ufacturer's guidelines, with the one exception being the replacement of ethanol with isopropanol. The RNA was then purified through elution in RNAase-free water.

Finally, the concentration of the RNA was determined using a NanoDrop 2000 Spectrophotometer (Fisher Scientific Company, Ottawa, ON, Canada).

3.11.2 Cell Culture Analysis

For the extraction of RNA from cell cultures, the cells were initially washed twice with room temperature phosphate-buffered saline (PBS). Following this, as much of the PBS as possible was aspirated and the plates were immediately flash-frozen in liquid nitrogen, before being transferred to a -80°C freezer for storage.

When required, the cells were scraped off the plates using a cell scraper. The RNA was then isolated employing the EZ-10 DNAaway RNA Mini Prep Kit (Catalogue number BS881133, BioBasic, Markham, ON, Canada), in accordance with the ma'ufacturer's instructions, except that isopropanol was used as a substitute for ethanol. Following the purification process, the RNA was eluted in RNAase-free water. Its concentration was then quantified using a NanoDrop 2000 Spectrophotometer (Fisher Scientific Company, Ottawa, ON, Canada).

3.11.3 cDNA Synthesis

After RNA extraction, the synthesis of complementary DNA (cDNA) was performed using the NEB First Strand cDNA synthesis kit (M0368; New England Biolabs Canada, Whitby, ON, Canada). In brief, each reaction involved the use of 1 µg of mRNA. This mRNA was then incubated with a mix containing ProtoScript Reverse Transcriptase, 62.5 µM Random Hexamers, 0.5 mM dNTPs, 10 mM DTT, and ProtoScript II Buffer. The reaction conditions were set at 25°C for 5 minutes, followed by 42°C for 60 minutes, and finally, 65°C for 20 minutes.

3.11.4 Quantitative Polymerase Chain Reaction (qPCR)

Quantitative PCR was conducted using the Luna Universal qPCR Master Mix (New England Biolabs Canada, Whitby, ON, Canada) utilizing the Syber Green method. Each reaction was assembled with 2.5 µL of Luna Universal qPCR Master Mix, 0.25 µM of both forward and reverse primers, 2 µL of RNAse/DNAse-free water, and 2.5 ng of cDNA. The reactions were carried out and the results were quantified with a CFX386 qPCR System (Bio-Rad Laboratories, Hercules, California, USA).

The PCR cycling parameters included an initial denaturation at 95°C for 1 minute, followed by 45 cycles of 15 seconds at 95°C and 30 seconds at 60°C. The resulting expression levels were normalized to the geometrical mean of at least 3 housekeeping genes, and relative gene expression was calculated using the $2^{-\Delta\Delta Ct}$ method. Statistical evaluations were carried out using GraphPad Prism 9, with a p-value of less than 0.05 deemed to represent statistical significance.

Table 4: Primer sequences for RNA quantification.

Gene Target	Primer direction	Sequence
Ppia	Forward	GAGCTGTTTGCAGACAAAGTTC
Ppia	Reverse	CCCTGGCACATGAATCCTGG
Tbp	Forward	ATGATGCCTTACGGCACAGG
Tbp	Reverse	GTTGCTGAGATGTTGATTGCTG
Actb	Forward	GGCTGTATTCCCCTCCATCG
Actb	Reverse	CCAGTTGGTAACAATGCCATGT
Gapdh	Forward	TGGCCTTCCGTGTTCCTAC
Gapdh	Reverse	GAGTTGCTGTTGAAGTCGCA
Parp1	Forward	AAAGCAGGCTGGCGCCGG
Parp1	Reverse	ACAGAGACACCTCTGCTGCG
Parp2	Forward	CACAGCTTGGTGACTTGTTCT
Parp2	Reverse	ACTCAGGCTTCAAAGTTTCCTC
Parp4	Forward	TCTTGCCAAATACCGTGCTTT
Parp4	Reverse	TGCTTAAAAACTCCGTAGCTTCA
Parg	Forward	GGGGACTCCGCTACCAAAG

Table 5: Cont. Primer sequences for RNA quantification.

Gene Target	Primer direction	Sequence
Sirt1	Forward	CAGCCGTCTCTGTGTCACAAA
Sirt1	Reverse	GCACCGAGGAACTACCTGAT
Trim63	Forward	CCAGGCTGCGAATCCCTAC
Trim63	Reverse	CCAGGCTGCGAATCCCTAC
Fbxo32	Forward	ACACATCCTTATGCACACTGG
Fbxo32	Reverse	TCTCCATCCGATACACCCACA
Ulk1	Forward	ACATCCGAGTCAAGATTGCTG
Ulk1	Reverse	GCTGGGACATAATGACCTCAGG
Pgc1a	Forward	AGACGGATTGCCCTCATTTGA
Pgc1a	Reverse	GGTCTTAACAATGGCAGGGTTT
Redd1	Forward	GGGATCGTTTCTCGTCCTCC
Redd1	Reverse	ATGAGGAGTCTTCCTCCGGC
Redd2	Forward	TCACCCTGGGAGTCTGCTAAGT
Redd2	Reverse	TTTGGTTTGCTTTGATCTGGAC

3.12 Bioinformatics Analysis

For conducting gene expression analysis, the publicly available RNA sequencing datasets GSE114820 and GSE133523 were employed. The data was processed using an assortment of bioinformatic tools. Initially, the datasets were downloaded into the Galaxy platform (version 22.05), followed by quality control checks using the FastQC toolkit. Subsequently, the data was refined and aligned to the genomes of either the mouse (Mus musculus, GRCm38.p5) or human (Homo Sapiens, GRCh38) utilizing the Hisat2 alignment tool. The HTSeq framework was employed to count the sequences, and the DESeq2 package was used to acquire normalized gene expression levels and differentially expressed genes. The resulting normalized counts were then log2 transformed, with a value of 1 added. For the Gene Set Enrichment Analysis (GSEA), the WebGestalt toolkit was used.

3.13 Statistical analysis

The software GraphPad Prism 9 was utilized for all statistical analyses. For scenarios where a single comparison was made between two groups at a single time point, Student's t-tests were applied. When comparisons involved two groups across multiple time points, 2-way repeated measures analysis of variance (ANOVA) was conducted. For situations where the comparison involved two groups and two conditions (for example, treatment and genotype) at a single time point, 2-way ANOVA was used. Post hoc tests using the Bonferroni correction were performed, specifically comparing differences between genotypes unless otherwise indicated. A threshold alpha value of 0.05 was established to determine statistical significance in all instances. Trends that failed to reach statistical significance but had p-values less than 0.1 were documented as such in graphs and explicitly reported in the text.

4 Results

4.1 Poly (ADP) Ribosylation is associated with skeletal muscle health in humans.

Data retrieved from the consensus dataset from Protein Atlas, comprised of normalized expression levels for 55 tissue types from merged Human Protein Atlas (HPA) and Genotype-Tissue Expression (GTEx) transcriptomic datasets, indicates a substantial expression of PARP1 in skeletal muscle (Figure 1A)[1]. The dataset reveals skeletal muscle as one of the tissues with the highest expression of PARP1, after tonsils, lymph nodes, and parathyroid glands. In parallel, PARG[2] is the most highly expressed in skeletal muscle, following kidney, in humans (Figure 1B).

Given the current use of PARP1 inhibitors, and the development of PARG inhibitors, in cancer we examined data from the United States Food and Drug Administration's (FDA) Adverse Event Reporting System (FAERS), which maintains comprehensive records of adverse clinical events associated with pharmaceutical products. In this database, we discovered that cancer treatments using inhibitors of PARP1 were associated with an increased incidence of musculoskeletal and connective tissue disorders when compared to platinum-based antineoplastic agents like Cisplatin (Figure 1C). Specifically, Niraparib, was associated with a higher proportion of musculoskeletal adverse events compared to Cisplatin, which are often used in association with PARP1 inhibitors. On the other hand, Talazoparib, had fewer reported

[1] https://www.proteinatlas.org/ENSG00000143799-PARP1/tissue, on June 20, 2023
[2] https://www.proteinatlas.org/ENSG00000227345-PARG/tissue, on June 20, 2023

adverse effects (Figure 1C). This variation may be attributable to several factors such as differences in bioavailability or drug distribution.

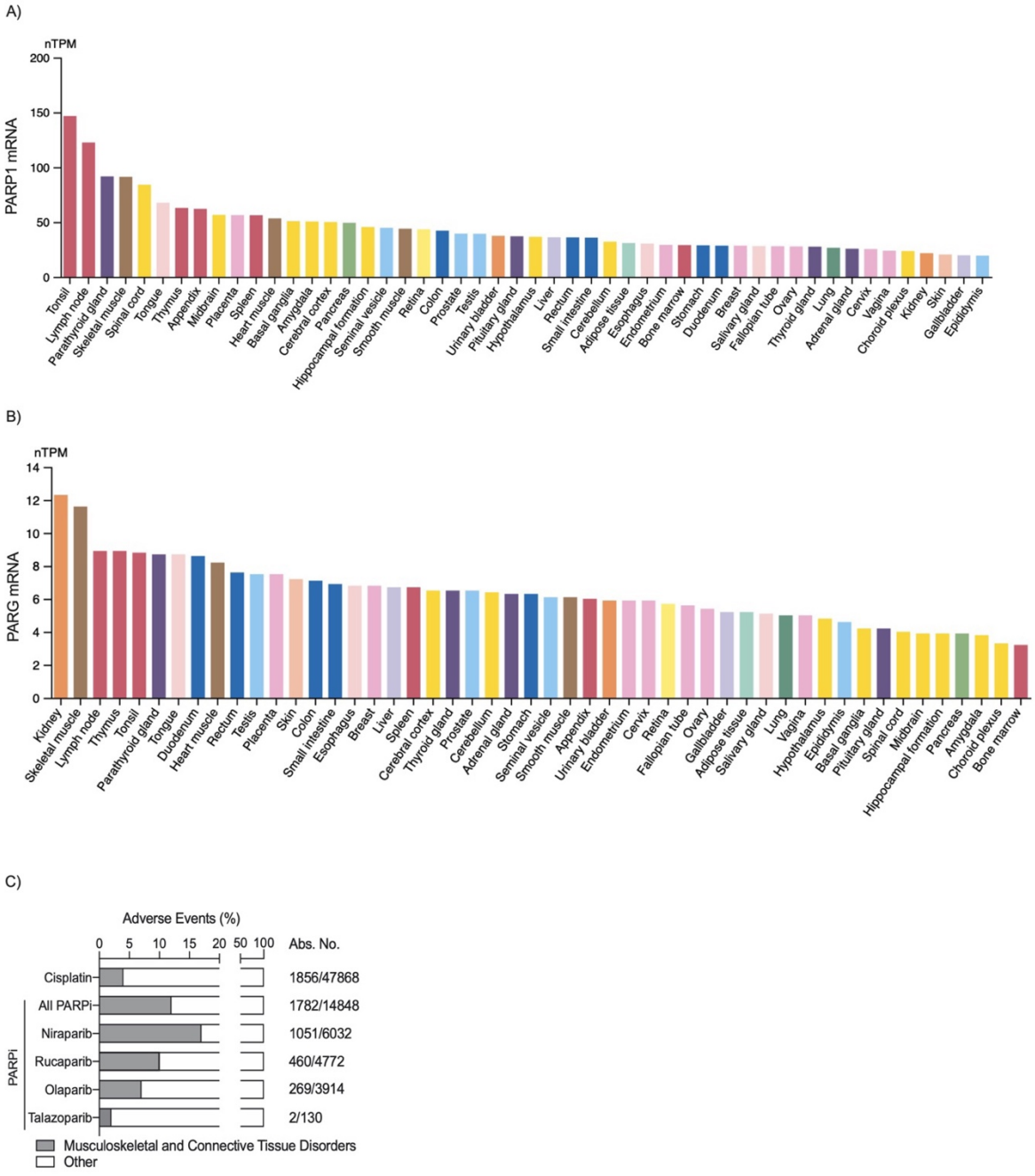

Figure 3. Inhibition of PARylation is associated with adverse musculoskeletal events.
Protein Atlas data showing high mRNA expression of A) *PARP1* and B) *PARG* in human skeletal muscle. Color-coded based on tissue groups with similar functional features, C) Reported

musculoskeletal adverse events for PARP inhibitors (PARPi) as percentage and absolute number of reported adverse events in relation to the total number of cases based on FAERS data. nTPM: Number of Transcript per Million.

4.2 Genes involved in PARylation homeostasis are altered in cachectic muscles of mice.

Given that PARP1 and PARG are highly expressed in human skeletal muscle, combined with observed musculoskeletal adverse effects of PARP inhibitors when treating cancer, we next examined the expression of genes and biological pathways linked to PARylation homeostasis in cachectic muscles. To do this we used a publicly available RNA-seq dataset (GSE114820) from mice that exhibited Lewis Lung Carcinoma (LLC)-induced cachexia. In this study, gastrocnemius muscle RNA was extracted for RNA sequencing (Figure 2A) from mice induced with LLC and compared to controls. Genes significantly altered 4 weeks after LLC induction revealed a pronounced upregulation of those involved in inflammation, indicating an integral role of inflammation in cachexia (Figure 2B). Importantly, enhanced PARylation activity has been linked to inflammatory responses in numerous tissues[179–181]. This was substantiated by a Gene Ontology analysis of differentially regulated genes, suggesting again the involvement of innate immunity, along with other processes known to involve PARylation signalling, such as DNA damage and repair processes[135,182,183], transcription[184–192], mRNA processing[193], apoptosis[194], and differentiation[195] (Figure 2C).

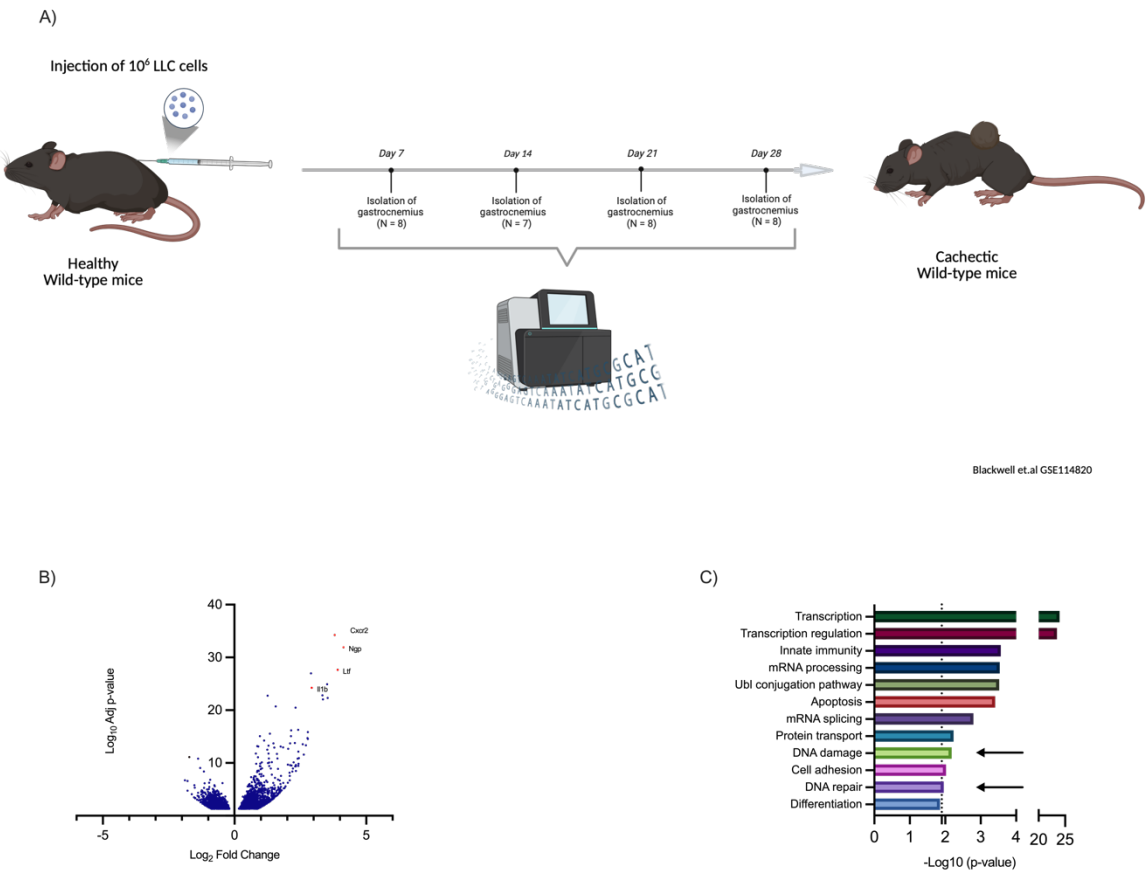

Figure 4: Analysis of differentially regulated genes in LLC-induced mouse muscle cachexia. A) Experimental design for GSE114820 B) Volcano plot highlighting a pronounced upregulation of inflammation-related genes, C) Gene Ontology analysis at week 4 reveals significant activation of processes like innate immunity, DNA damage, and DNA repair in cachectic muscles.

Further analysis of this dataset demonstrated that *Parp1*, *Parp2*, and ADP-ribose hydrolase 3 (*Arh3*) expression remained largely unchanged in the muscle of cachectic mice during the progression of cancer cachexia (Figure 3A, B, C, I). *Parp4*, *Tnks1*, *Neurl4*, and *Parg* were upregulated (Figure 3A, D, E,G,H), and *Tnks2* was downregulated (Figure 2F) 4 weeks after LLC induction indicating potential roles for these genes in cancer cachexia. These data do not however examine changes in PARylation dynamics, through changes in enzymatic activity, yet still emphasize the potential importance of PARylation in LLC-induced cancer cachexia.

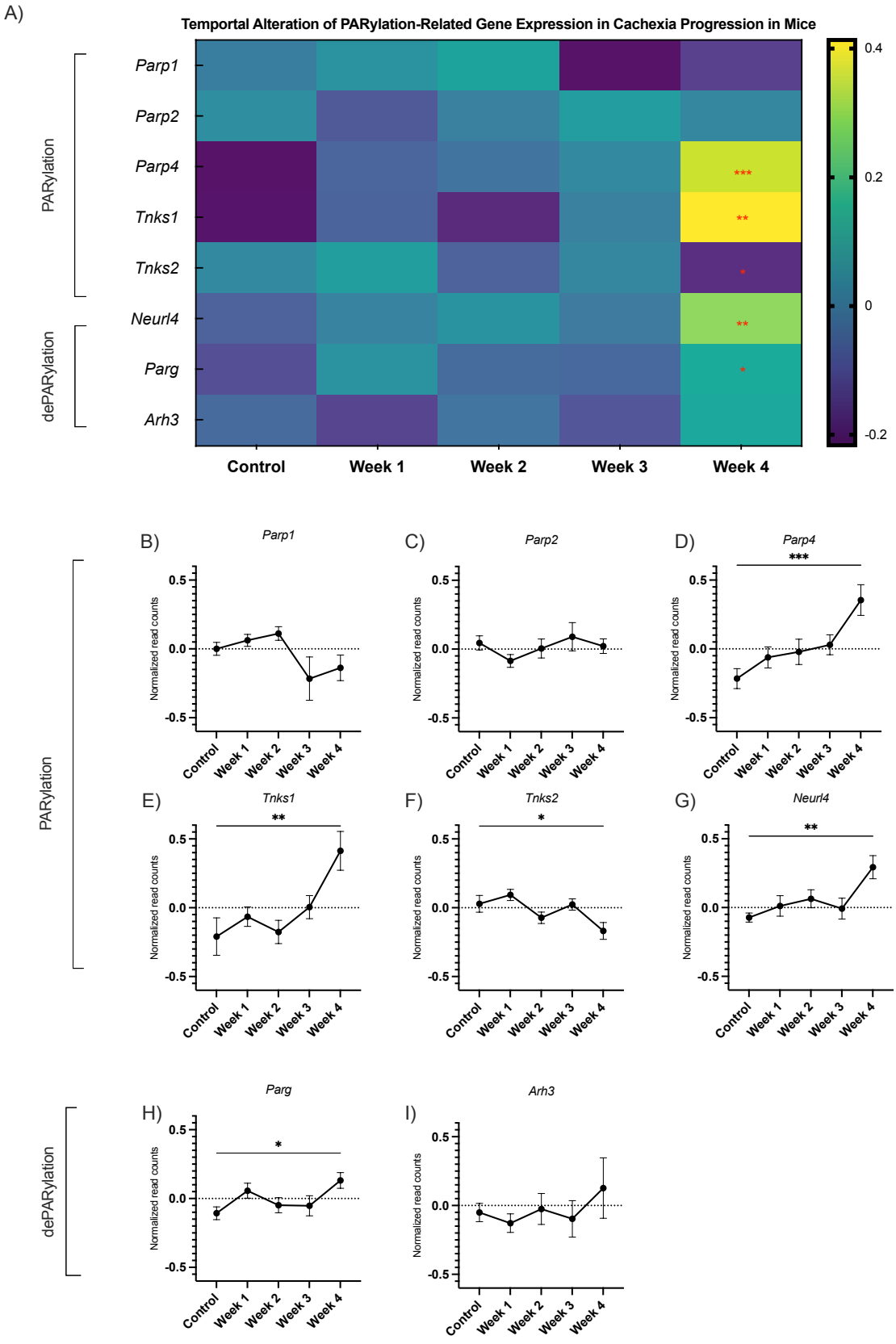
A)
Temporal Alteration of PARylation-Related Gene Expression in Cachexia Progression in Mice
PARylation
dePARylation
Parp1
Parp2
Parp4
Tnks1
Tnks2
Neurl4
Parg
Arh3
***
**
*
**
*
Control
Week 1
Week 2
Week 3
Week 4
0.4
0.2
0
-0.2
B)
Parp1
C)
Parp2
D)
Parp4
***
E)
Tnks1
**
F)
Tnks2
*
G)
Neurl4
**
H)
Parg
*
I)
Arh3
Normalized read counts
0.5
0.0
-0.5

Figure 5: Dynamic changes in PARylation-related gene expression during cancer cachexia progression in mice.
A) Heatmap showcasing the normalized gene expression four weeks post-LLC-induction. The figure further illustrates gene expression of B) *Parp1*, C) *Parp2*, D) *Parp4*, E) *Tnks1*, F) *Tnks2*, G) *Neurl4*, H) *Parg*, and I) *Arh3*. Normalized gene counts were log2 transformed after division by the median. N=7-8. Significance is indicated by *: $p < 0.05$, **: $p < 0.01$, ***: $p < 0.001$, and ****: $p < 0.0001$, using one-way ANOVA with Bonferroni post-hoc correction.

4.3 PARG inhibition protects primary myotubes from atrophy-related gene expression.

We then turned our focus to the possible impact of LLC-Conditioned Media (LLC-CM) on gene expression of myotubes as a cell culture model of cancer cachexia. Our qPCR analysis on primary myotubes demonstrated that LLC-CM can increase *Trim63* (also known as *MurF1)* gene expression, a gene involved in muscle protein degradation via the ubiquitin-proteasome system[92,94] (Figure 5C). Moreover, in accordance with previous research LLC-CM treatment increases *Redd1* expression but not *Redd2*[196], genes involved in cellular stress response capable of inhibiting mechanistic Target of Rapamycin Complex 1[197]. However, while LLC-CM increased the expression of *Trim63*, it did not increase the *Fboxo32* (also known as *Atrogin1*) a gene shown to increase in LLC-CM treated myotubes and involved in muscle atrophy through the regulation of protein synthesis and degradation. (Figure 6A). Atrogin-1 and MuRF1 operate within the ubiquitin-proteasome pathway for muscle protein degradation but target different substrates and may be regulated differently. Interestingly, inhibition of PARG using PDD rescued the LLC-CM-mediated expression of *Trim63* and *Redd1* and had no effect on *Fboxo32* and *Redd2* (Figure 6B). Moreover, since previous studies demonstrated that *Redd1* inhibition halts muscle mass loss in cancer induced cachexia[196], and *Trim63* is a major protein in the ubiquitin proteasome system that degrades myosin heavy chain[92,112], increased PARylation due to PARG inhibition appears to be beneficial.

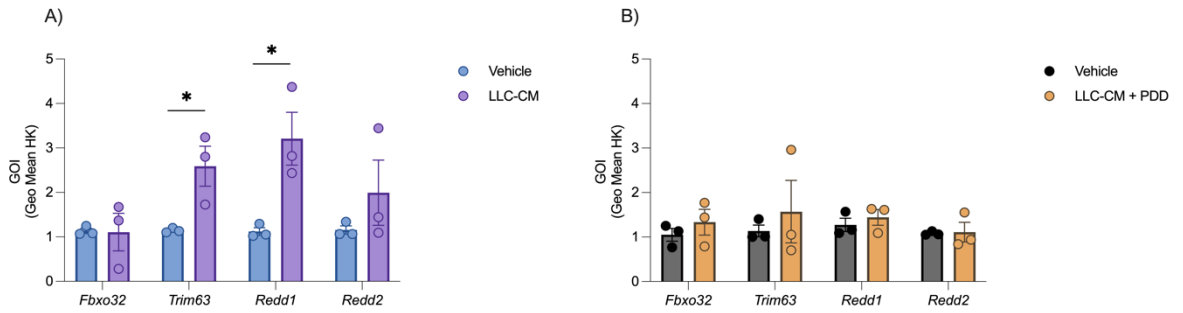

Figure 6: PARG inhibition reduces LLC-CM-induced atrophy-related gene expression in mouse primary myotubes.

A)qPCR analysis on myotubes revealed increased expression of *Trim63* and *Redd1* after 24-hours LLC-CM treatment, while *Fbxo32* and *Redd2* remained unchanged. B) PARG inhibition halted the LLC-CM-induced overexpression of *Trim63* and *Redd1*. Genes were normalized based on geometrical mean of *Tbp*, *Actb*, *Gapdh*, *Ppia* using $2^{\wedge\Delta Ct}$. Bars in graphs represent mean values and error bars are s.e.m. Statistical significance is denoted by *: $p < 0.05$, **: $p < 0.01$, ***: $p < 0.001$, and ****: $p < 0.0001$, determined using student t-test (N=3)

4.4 Optimization of LLC-Induced cancer cachexia in mice.

We then sought to further elucidate the impact of PARylation on cancer cachexia in *vivo* using a tumor allograft model. Firstly, we optimized an LLC tumor allograft model for the evaluation of onset and progression of cachexia over the course of 21-24 days. Female mice subcutaneously injected with 1×10^6 LLC cells showed no differences in body mass post-injection (Figure 7A), however, we noted a significant decrement in the tumor-free body mass at sacrifice (Figure 7B). Tumor mass at sacrifice averaged 1.6 grams (Figure 7C). Splenomegaly a symptom frequently associated with systemic inflammatory conditions such as cancer, was observed at sacrifice (Figure 7D). Prominent declines in both the inguinal white adipose tissues (iWAT) (Figure 7E) and gonadal white adipose tissues (gWAT) was recorded (Figure 7F), with no change in brown adipose tissue (BAT) mass (Figure 7G). A trend towards a 16% reduction in the mass of the Tibialis Anterior (TA) was observed (Figure 7H), accompanied by a reduction in the combined mass of the gastrocnemius and soleus muscles (GPS) (Figure 7I). The Quadricep (Quad) mass also demonstrated a trend towards reduction (Figure 7J). These trends, collectively, imply the onset of cachexia-induced muscle wasting. Mice injected with 5×10^6 cells cells displayed rapid subcutaneous tumor growth reaching an ethical endpoint by day 18 (Figure S1A). Despite a reduction in overall body mass (Figure S1B), no reduction was noted in the mass of the TA muscle (Figure S1C), suggesting that the swift tumor progression might have overshadowed the cachexia-induced muscle wasting typically observed.

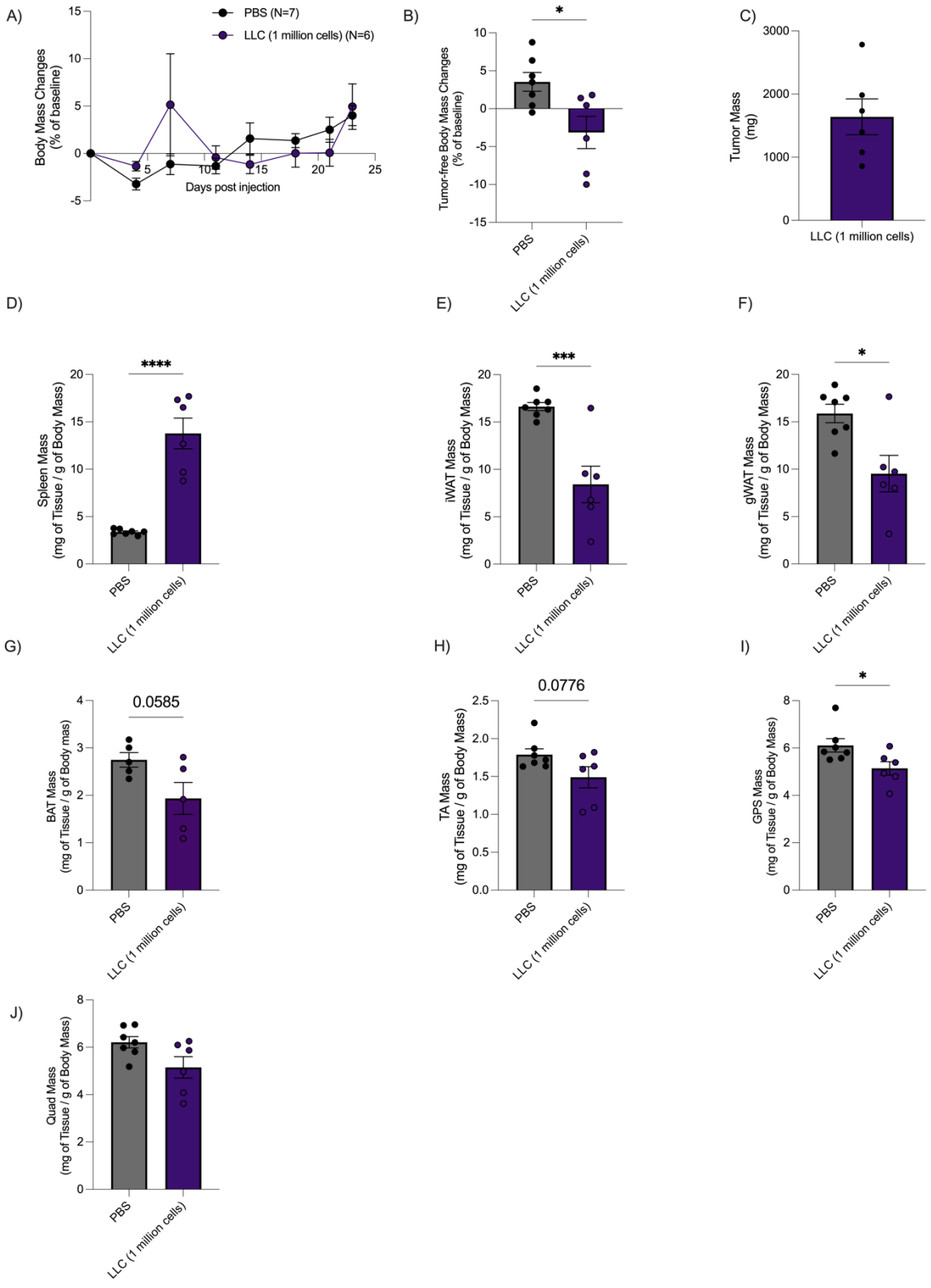
A)
PBS (N=7)
LLC (1 million cells) (N=6)
Body Mass Changes (% of baseline)
Days post injection
B)
*
Tumor-free Body Mass Changes (% of baseline)
PBS
LLC (1 million cells)
C)
Tumor Mass (mg)
LLC (1 million cells)
D)
****
Spleen Mass (mg of Tissue / g of Body Mass)
E)
***
iWAT Mass (mg of Tissue / g of Body Mass)
F)
*
gWAT Mass (mg of Tissue / g of Body Mass)
G)
0.0585
BAT Mass (mg of Tissue / g of Body mas)
H)
0.0776
TA Mass (mg of Tissue / g of Body Mass)
I)
*
GPS Mass (mg of Tissue / g of Body Mass)
J)
Quad Mass (mg of Tissue / g of Body Mass)

Figure 7: Validating the 1×10^6 LLC cells induction model for cancer cachexia.
A) Body mass changes between groups injected with 1×10^6 cells. B) Tumor-free body mass, C) tumor mass. D) Spleen mass E) iWAT mass, F) gWAT mass and G) BAT mass. H) TA mass I) GPS mass loss J) Quad mass. Bars represent means, and error bars indicate s.e.m. Statistical significance denoted by *: $p < 0.05$, **: $p < 0.01$, ***: $p < 0.001$, and ****: $p < 0.0001$ using student t-test or two-way ANOVA with Bonferroni post-hoc correction. (N=6-7).

4.5 Skeletal muscle ablation of *Parp1* exacerbates muscle mass loss in LLC-induced cancer cachexia of male mice.

To examine the role of PARylation during cancer cachexia we developed an inducible *Parp1* muscle-specific knockout mouse (*Parp1*-IMKO) using Cre technology (Figure 8A). Due to the breeding limitations all tests ere performed in male mice. Based on our optimization experiments we used 1×10^6 LLC cells to induced cachexia in these mice and monitored them for 24 days. Despite no difference in the percentage change of body mass (Figure 8B), a substantial reduction was noted in the post-sacrifice tumor-free body mass of LLC-induced mice of both genotypes when compared to their PBS-injected controls (Figure 8C). There was no difference in LLC tumor mass or growth rates between *Parp1*-IMKO and WT mice (Figure 8D, E). Splenomegaly presented similarly in both LLC-induced WT and *Parp1*-IMKO mice at sacrifice (Figure 8F). The liver exhibited no significant change in mass in both LLC-induced WT and *Parp1*-IMKO mice (Figure 8G). However, as expected LLC-induced reductions were observed across adipose tissue depots and were similar in both wild-type and *Parp1*-IMKO mice (Figure 8H, I, J). Importantly, progressive decrements in forelimb grip strength became evident in WT but not *Parp1*-IMKO mice by day 20 post-LLC induction (Figure 8K, L). The mass of the quadriceps, and combined mass of gastrocnemius and soleus muscles remained stable in tumor-bearing WT mice but showed a significant decrease in *Parp1*-IMKO mice (Figure 8M,

N). Both cohorts presented reduced tibialis anterior mass (Figure 8O) with *Parp1*-IMKO mice demonstrating a greater loss (24.8%) than WT mice (14.2%) when compared to their respective control groups. This suggests that muscle specific *Parp1* activity may provide a protective effect against muscle wasting in male mice in the context of cancer cachexia. Consequently, the absence of *Parp1* renders male mice more susceptible to muscle loss during cancer cachexia. Collectively, these observations align with data from the FDA's adverse effect reporting system on PARP1 inhibitors, reinforcing the notion that PARP1 may serve a protective role against muscle mass loss.

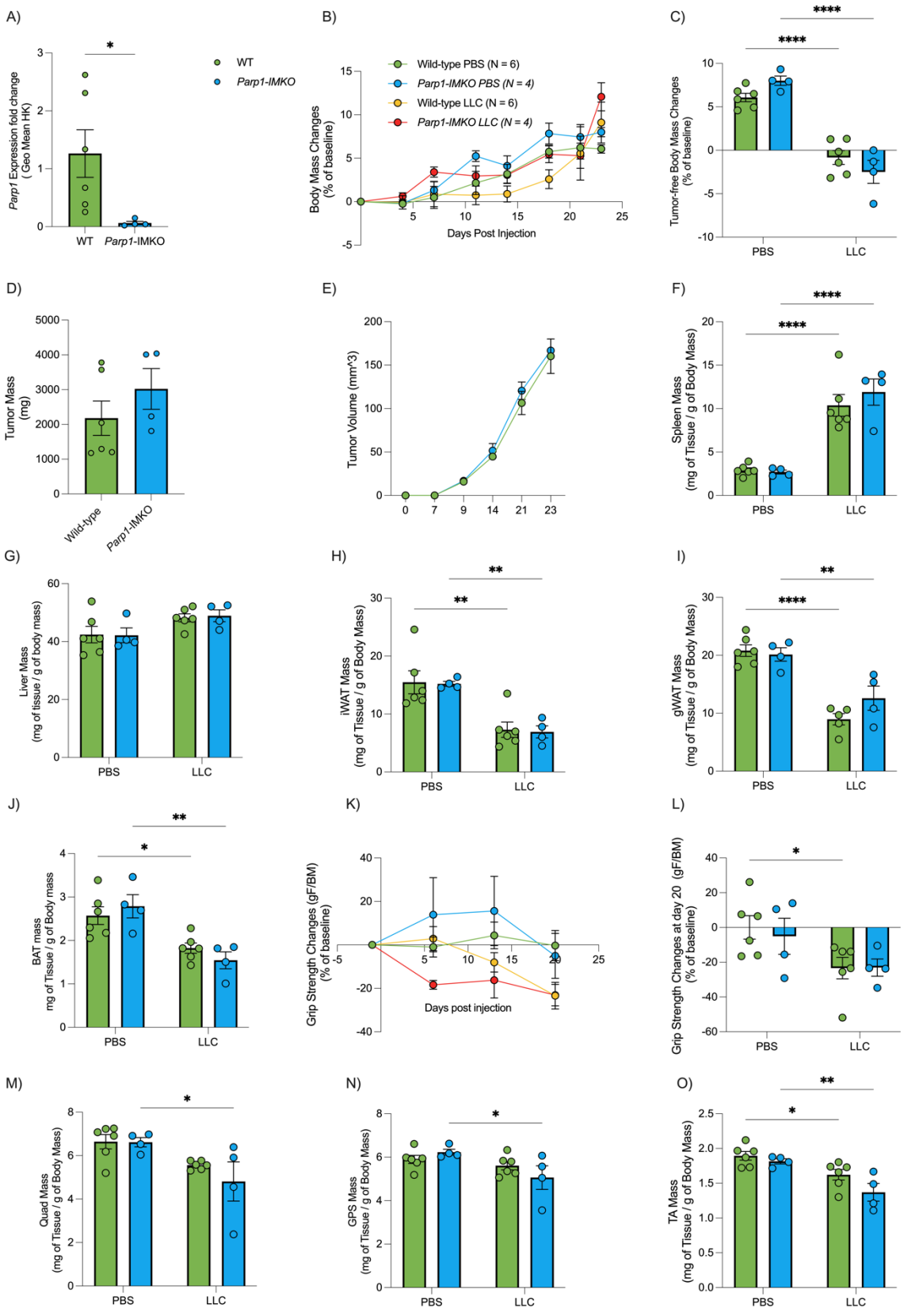
A)
Parp1 Expression fold change (Geo Mean HK)
WT
Parp1-IMKO
B)
Wild-type PBS (N = 6)
Parp1-IMKO PBS (N = 4)
Wild-type LLC (N = 6)
Parp1-IMKO LLC (N = 4)
Body Mass Changes (% of baseline)
Days Post Injection
C)
Tumor-free Body Mass Changes (% of baseline)
PBS
LLC
D)
Tumor Mass (mg)
Wild-type
Parp1-IMKO
E)
Tumor Volume (mm^3)
F)
Spleen Mass (mg of Tissue / g of Body Mass)
G)
Liver Mass (mg of tissue / g of body mass)
H)
iWAT Mass (mg of Tissue / g of Body Mass)
I)
gWAT Mass (mg of Tissue / g of Body Mass)
J)
BAT mass mg of Tissue / g of Body mass
K)
Grip Strength Changes (gF/BM) (% of baseline)
Days post injection
L)
Grip Strength Changes at day 20 (gF/BM) (% of baseline)
M)
Quad Mass (mg of Tissue / g of Body Mass)
N)
GPS Mass (mg of Tissue / g of Body Mass)
O)
TA Mass (mg of Tissue / g of Body Mass)

Figure 8: Muscle mass loss in cancer cachexia with *Parp1* ablation in male mice.
Parp1 knockout was confirmed in the quad muscle of animals, with gene expression normalized based on geometrical mean of *Tbp*, *Actb*, *Gapdh*, *Ppia* using $2^{\wedge\Delta Ct}$. B) Changes in body mass percentage, C) tumor-free body mass, D) Tumor mass and E) tumor growth. F) splenomegaly was observed. G) Liver mass did not change. H) iWAT, I), gWAT, J) BAT mass, K) Grip strength post LLC-induction and at L) day 20. M) Quad mass and N) GPS mass, O) TA mass. Bars in graphs represent mean values and error bars are s.e.m. Statistical significance is denoted by *: $p < 0.05$, **: $p < 0.01$, ***: $p < 0.001$, and ****: $p < 0.0001$, determined using t-test or two-way ANOVA with a Bonferroni post-hoc correction. (N=4-6).

4.6 *Parp1* ablation increases expression of genes linked to muscle degradation.

Next, we examined the role of PARP1 in regulating PARylation and signalling pathways associated with muscle atrophy during cancer cachexia. We first examined the changes in Mono/Poly ADP Ribosylation (M/PARylation) and found a reduction in *Parp1*-IMKO in comparison to WT quadriceps. However, no alteration was observed between PBS-treated mice and cachectic mice in both WT and *Parp1*-IMKO muscle, suggesting that cachexia does not change the total M/PARylation in quadriceps (Figure 9A, B). Interestingly, in line with a reduction in M/PARylation, FOXO1, a transcription factor that regulates genes involved in muscle atrophy, was upregulated in PBS-treated *Parp1*-IMKO when compared to WT muscle. Despite no further change of total M/PARylation in LLC-induced *Parp1*-IMKO mice, FOXO1 was further elevated, an effect not observed in the WT group (Figure 9C). One of the genes regulated by FOXO1 is *Trim63.* In line with an increase in FOXO1 protein expression, PBS-treated *Parp1*-IMKO mice show an upregulation of *Trim63* transcript expression in muscle when compared to WT mice. *Trim63* gene expression in cachectic mice was similarly elevated in both WT and *Parp1*-IMKO mice (Figure 9D). From this we conclude that despite observing an increase in FOXO1 and *Trim63* there was no change in muscle mass in PBS-treated *Parp1*-IMKO mice compared to WT. However, we predict that it is the activation of this signalling

pathway during normal physiological conditions that increases the susceptibility of *Parp1*-IMKO mice to accelerated muscle protein degradation during cachexia when compared to WT animals. Our investigation did not show an upregulation of *Redd1* (Figure 9E), a previously identified marker of muscle cachexia[196]that increased when myotubes were treated with LLC-CM (Figure 4A). Moreover, *Ulk1*, a gene integral to autophagy, was reduced in *Parp1*-IMKO but not WT mice following LLC induction (Figure 9F). The reduction of *Ulk1* in *Parp1*-IMKO mice during cachexia may exacerbate muscle atrophy and contribute to greater muscle mass loss compared to WT mice.

Elevated *Pgc1-a* expression was observed in *Parp1*-IMKO mice when compared to WT animals, which was completely attenuated in mice induced with LLC (Figure 9G). Prior studies have elucidated the activation of *Pgc1a* via *Parp1* inhibition due to increased intracellular NAD^+ pools, further facilitating NAD^+-dependent Sirt1-induced PGC1α deacetylation. PGC1α is considered to be a master regulator of mitochondrial biogenesis. Consistent with this, we observed an upregulation of subunits of the oxidative phosphorylation chain, specifically in complex II and V in PBS-treated *Parp1*-IMKO muscle when compared to WT muscle. Cachexia, however, reduced all the complexes in both WT and *Parp1*-IMKO, suggesting that the beneficial effects of *Parp1* ablation on mitochondria cannot be maintained in cachexia (Figure 9H).

To check for compensation by other PARP enzymes we examined *Parp2* and *Parp4* genes which did not differ between PBS- and LLC-treated groups for WT mice but was reduced for both genes in *Parp1*-IMKO mice. This might suggest a potential influence of the cachectic state

on the regulation of *Parp2* and *Parp4* in the absence of *Parp1* (Figure 9I, J). In contrast, *Parg* expression remained stable across WT and *Parp1*-IMKO mice (Figure 9K).

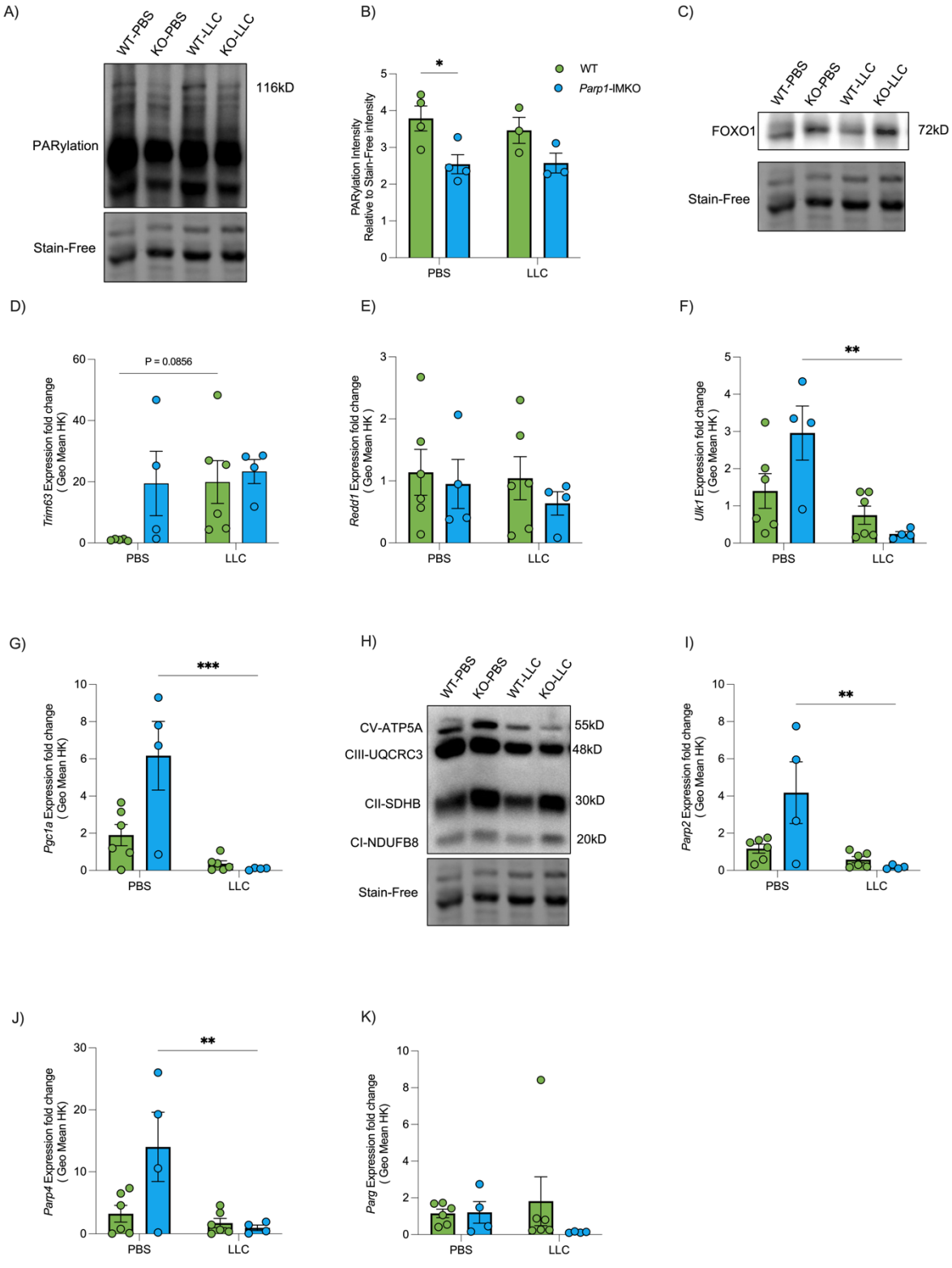
A)
WT-PBS
KO-PBS
WT-LLC
KO-LLC
116kD
PARylation
Stain-Free
B)
*
WT
Parp1-IMKO
PARylation Intensity
Relative to Stain-Free intensity
PBS
LLC
C)
WT-PBS
KO-PBS
WT-LLC
KO-LLC
FOXO1
72kD
Stain-Free
D)
P = 0.0856
Trim63 Expression fold change
(Geo Mean HK)
PBS
LLC
E)
Redd1 Expression fold change
(Geo Mean HK)
PBS
LLC
F)
**
Ulk1 Expression fold change
(Geo Mean HK)
PBS
LLC
G)
***
Pgc1a Expression fold change
(Geo Mean HK)
PBS
LLC
H)
WT-PBS
KO-PBS
WT-LLC
KO-LLC
CV-ATP5A
CIII-UQCRC3
CII-SDHB
CI-NDUFB8
55kD
48kD
30kD
20kD
Stain-Free
I)
**
Parp2 Expression fold change
(Geo Mean HK)
PBS
LLC
J)
**
Parp4 Expression fold change
(Geo Mean HK)
PBS
LLC
K)
Parg Expression fold change
(Geo Mean HK)
PBS
LLC

Figure 9: Gene Expression in *Parp1*-IMKO Mice in male mice.
A) Western Blotting (WB) for PARylation, quantified in B), C) WB for FOXO1. D) *Trim63* expression, E) *Redd1*, F) *Ulk1*,G) *Pgc1a*, H) WB for OxPhos complexes, I) *Parp2* J) *Parp4* K) *Parg* expression in both WT and *Parp1*-IMKO groups. Genes were normalized based on geometrical mean of *Tbp*, *Actb*, *Gapdh*, *Ppia* using $2^{\wedge\Delta Ct}$. Bars in graphs represent mean values and error bars are s.e.m. Statistical significance is denoted by *: $p < 0.05$, **: $p < 0.01$, ***: $p < 0.001$, and ****: $p < 0.0001$, determined using two-way ANOVA with a Bonferroni post-hoc correction. (N=4-6)

4.7 Skeletal muscle ablation of *Parg* does not exacerbate muscle mass loss.

Given that PARG inhibition reduces LLC-CM-induced *Trim63* and *Redd1* expression in primary myotubes (Figure 6A), we aimed to determine the role of PARG in mouse muscle during cachexia. To do this we created a skeletal muscle-specific inducible *Parg KO* mouse model that showed a significant reduction in *Parg* expression (*Parg*-IMKO; Figure 10A). These mice and their WT controls then received an LLC allograft and were monitored for 21 days. In line with the findings from the *Parp1*-IMKO cohort, our data did not indicate a significant difference in body mass change for either male or female *Parg*-IMKO or WT mice (Figure 10B,C). However, tumor-free body mass demonstrated a discernible reduction in both wild-type and *Parg*-IMKO mice for males (Figure 10D) but not females (Figure 10E). Tumor mass did not show any differences between the male or female animal groups (Figure 10F,G). Concurrent with observations in the *Parp1*-IMKO cohort, we noted the occurrence of splenomegaly in our male and female mice (Figure 10H, I) without changes in liver mass (Figure 10J, K). The induction of cachexia significantly impacted gWAT in all groups, while BAT remained unaffected in both male and female mice (Figure 10L, M, N, O). iWAT demonstrated a reduction in both groups of the male mice following LLC-induction (Figure 10P), while only the *Parg*-IMKO female mice remained unchanged (Figure 10Q).

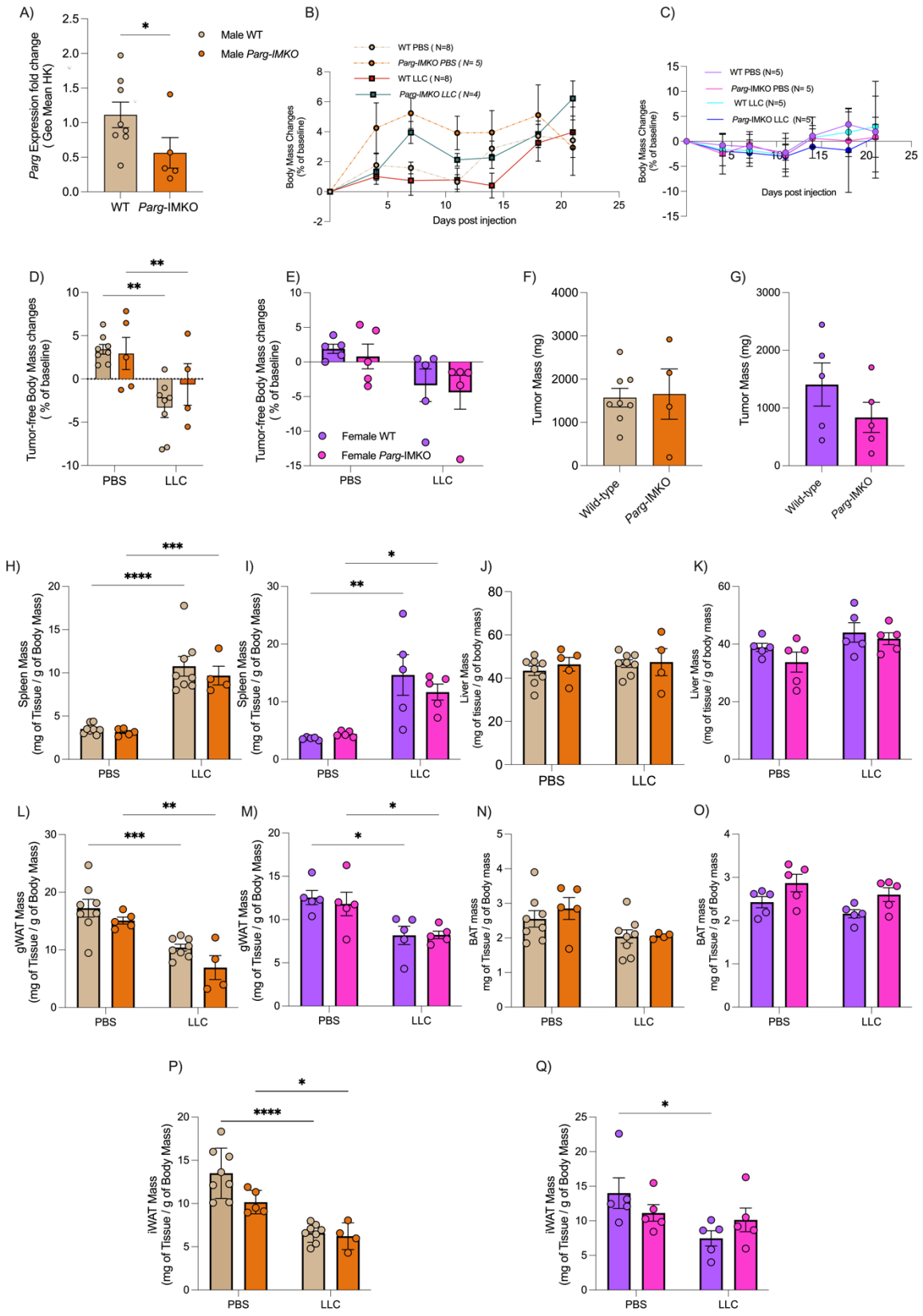
A)
Parg Expression fold change (Geo Mean HK)
Male WT
Male Parg-IMKO
WT
Parg-IMKO
B)
WT PBS (N=8)
Parg-IMKO PBS (N= 5)
WT LLC (N=8)
Parg-IMKO LLC (N=4)
Body Mass Changes (% of baseline)
Days post injection
C)
WT PBS (N=5)
Parg-IMKO PBS (N= 5)
WT LLC (N=5)
Parg-IMKO LLC (N=5)
Body Mass Changes (% of baseline)
Days post injection
D)
Tumor-free Body Mass changes (% of baseline)
PBS
LLC
E)
Tumor-free Body Mass changes (% of baseline)
Female WT
Female Parg-IMKO
PBS
LLC
F)
Tumor Mass (mg)
Wild-type
Parg-IMKO
G)
Tumor Mass (mg)
Wild-type
Parg-IMKO
H)
Spleen Mass (mg of Tissue / g of Body Mass)
PBS
LLC
I)
Spleen Mass (mg of Tissue / g of Body Mass)
PBS
LLC
J)
Liver Mass (mg of tissue / g of body mass)
PBS
LLC
K)
Liver Mass (mg of tissue / g of body mass)
PBS
LLC
L)
gWAT Mass (mg of Tissue / g of Body Mass)
PBS
LLC
M)
gWAT Mass (mg of Tissue / g of Body Mass)
PBS
LLC
N)
BAT mass mg of Tissue / g of Body mass
PBS
LLC
O)
BAT mass mg of Tissue / g of Body mass
PBS
LLC
P)
iWAT Mass (mg of Tissue / g of Body Mass)
PBS
LLC
Q)
iWAT Mass (mg of Tissue / g of Body Mass)
PBS
LLC

Figure 10: Effect of skeletal muscle *Parg* ablation on cancer cachexia in male and female mice. A) qPCR analysis confirms the ablation of *Parg* in quadriceps muscles, with gene normalized based on geometrical mean of *Tbp*, *Actb*, *Gapdh*, *Ppia* using $2^{\wedge\Delta Ct}$. B) Male and C) Female Body mass changes, D) Tumor-free body mass in males E) and females. F) Tumor mass in males and G) females. H) Male spleen mass I) Female spleen mass J) Male liver mass K) Female liver mass L) Male gWAT and M) Female gWAT, N) Male BAT O) Female BAT, P) Male iWAT and Q) Female iWAT. Bars in graphs represent mean values and error bars are s.e.m. Statistical significance is denoted by *: $p < 0.05$, **: $p < 0.01$, ***: $p < 0.001$, and ****: $p < 0.0001$, determined using student t-test and two-way ANOVA with a Bonferroni post-hoc correction. (N=4-8)

Forelimb grip strength was not reduced for either *Parg*-IMKO or WT mice, even at the 20-day mark in both sexes (Figure 11A, B, C, D). This divergence from the effect on WT mice in the earlier Parp1-IMKO cohort set of experiments (Figure 8L) might be attributable to minor variations in the execution of grip strength tests. A similar decline in TA mass was observed in both groups WT and *Parg*-IMKO male mice following LLC-induction (Figure 11E). Although when comparing to the *Parp1*-IMKO cohort of mice, the cachectic animals from the male *Parp1*-IMKO cohort exhibited an average 24.8% reduction while the cachectic male mice from the *Parg*-IMKO cohort only demonstrated an average 13% reduction. Female *Parg*-IMKO TA mass was not significantly altered and therefore appeared protected against cachexia (Figure 11F). Altogether, *Parg* ablation in skeletal muscle does not augment the loss of TA mass under the influence of LLC-induced cachexia in male mice and rather attenuates muscle loss in female mice. No reduction was observed in GPS, Soleus, and Quad mass for either *Parg*-IMKO or WT female or male mice (Figure 11 G, H, I, J, K, L). This result is similar to those found in the WT mice from the *Parp1-IMKO* cohorts, however rather than causing a loss in muscle mass, as was found in the *Parp1*-IMKO mice, Parg-IMKO mice did not show any exasperation of muscle loss. These findings suggest that unlike in the absence of *Parp1*, there is no additional loss in

muscle mass or strength following *Parg* ablation in males and in females there appears to be an attenuation of TA muscle loss.

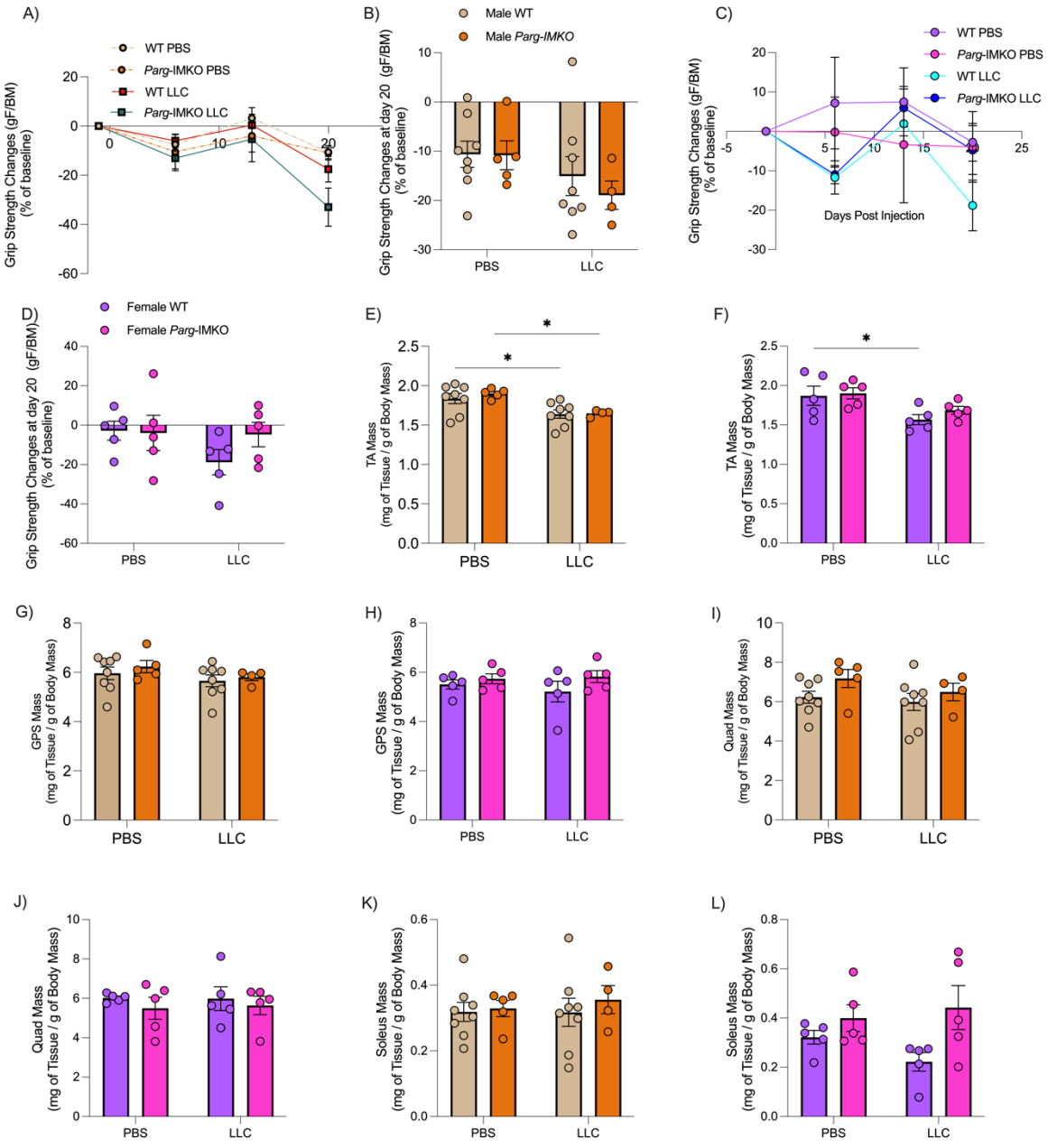

Figure 11: Effect of skeletal muscle *Parg* ablation on cancer cachexia induced muscle mass loss in male and female mice.

A) Forelimb grip strength changes over the course of 20 days following LLC-induced in males B) Forelimb grip strength at day 20 after LLC induction in males and C) D) in females

respectively. E) TA mass in males F) and females. G) GPS mass in males and H) females. I) Quad mass in males and J) females. K) Soleus mass in males and L) females. Bars in graphs represent mean values and error bars are s.e.m. Statistical significance is denoted by *: $p < 0.05$, **: $p < 0.01$, ***: $p < 0.001$, and ****: $p < 0.0001$, determined using student t-test and two or three-way ANOVA with a Bonferroni post-hoc correction. (N=4-8)

4.8 *Parg* ablation decreases the expression of genes involved in muscle atrophy in cancer cachexia.

We next set out to investigate the impact of skeletal muscle *Parg* ablation on *gene* expression in muscle isolated from male mice. In opposition to *Parp1*-IMKO mice, PBS-treated *Parg*-IMKO mice showed no change in *Trim63* expression and exhibited reduced expression in cachexia, when compared to WT controls (Figure 12A). Interestingly, when comparing PBS- to LLC-treatments *Fbxo32* expression did not change in *Parg*-IMKO mice while the WT controls trended higher (p=0.0668; Figure 12B). *Redd1* expression did not change across any of the mouse groups (Figure 12C). *Ulk1*, a gene that was elevated only in PBS-treated *Parp1*-IMKO compared to LLC-induced mice, was not altered in this cohort (Figure 12D) suggesting that *Parg* ablation does not influence the autophagy processes.

Finally, our data showed no significant impact of either cancer cachexia or *Parg* absence on the expression levels of *Sirt1*, *Pgc1a*, *Parp1*, *Parp2*, or *Parp4* (Figure 12E, F, G). Thus, the transcriptional regulation of SIRT1 or known PARylating PARP family members remained unaltered. Our results present compelling evidence of the potential interplay between skeletal muscle *Parg* ablation, and *Trim63* and *Fbxo32* expression, which may be responsible for the lack of change, or attenuation in certain cases, of *in vivo* markers of muscle loss seen in male or female *Parg*-IMKO mice.

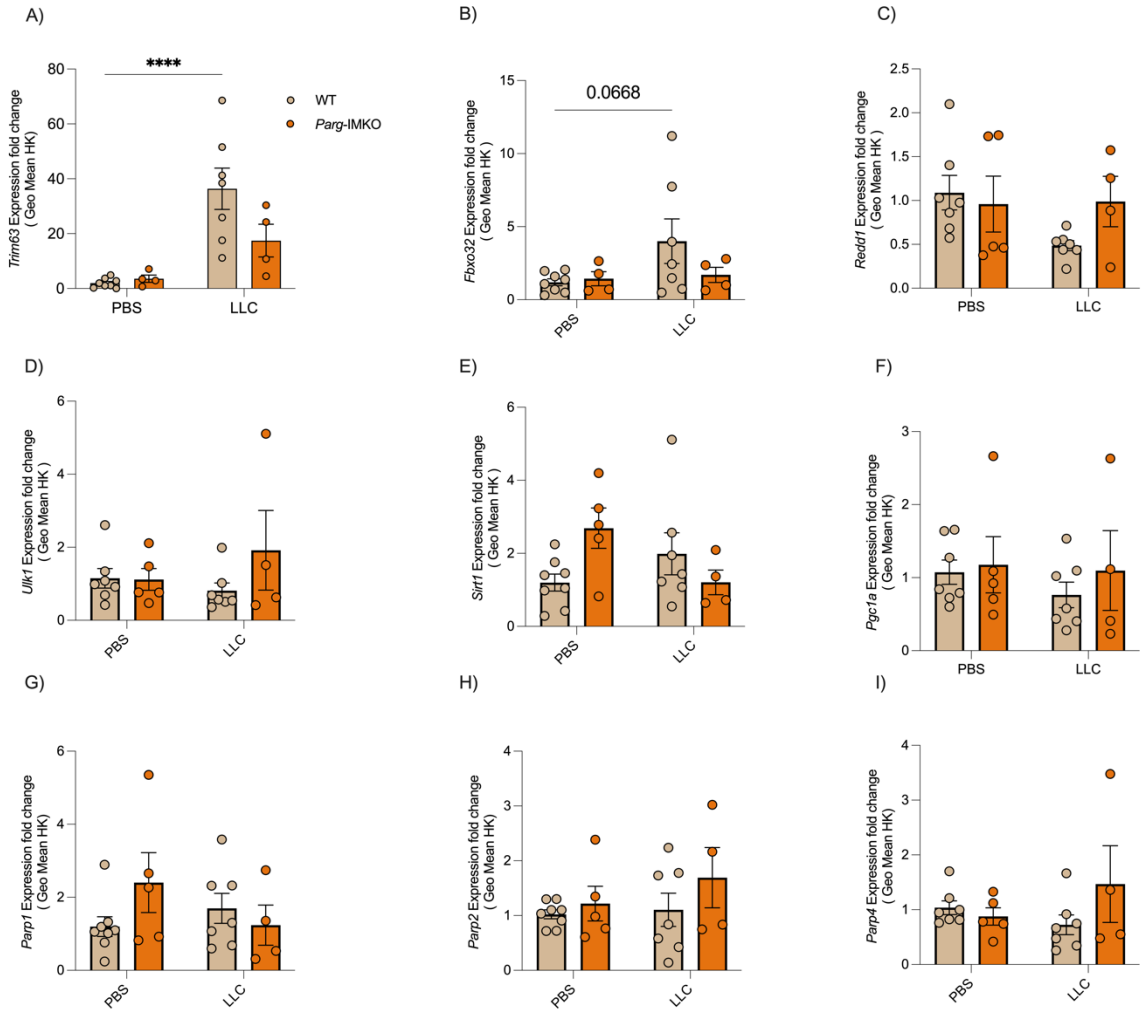

Figure 12: Attenuation of cachexia induced *Trim63* and *Fboxo32* responses with skeletal muscle *Parg* ablation in male mice.
A) *Trim63*, B) *Fbxo32*, C) *Redd1* D) *Ulk1* E) *Sirt1*, *F) Pgc1a,* G) *Parp1* H) *Parp2* I) *Parp4.* Genes were normalized based on geometrical mean of *Tbp*, *Actb*, *Gapdh*, *Ppia* using $2^{\wedge\Delta Ct}$. Bars represent means, and error bars indicate s.e.m. Statistical significance denoted by *: $p < 0.05$, **: $p < 0.01$, ***: $p < 0.001$, and ****: $p < 0.0001$, determined using one-way ANOVA with Bonferroni post-hoc correction. (N=4-8)

5 Discussion

Cancer cachexia represents a multifaceted paraneoplastic syndrome, predominantly characterized by profound muscle wasting, which is observed in approximately 80% of individuals diagnosed with cancer. The onset and progression of cancer cachexia are influenced by a myriad of factors, including the specific tumor type, concurrent comorbidities, and the spectrum of anticancer agents administered to the patient. Given the current absence of efficacious pharmacological interventions specifically targeting cancer cachexia[1,22], it becomes imperative to critically evaluate the safety profiles of administered anticancer agents in the context of cachexia development. Of note, a novel class of drugs designed to inhibit PARP1 has been introduced to induce synthetic lethality with their applications continually expanding. Through PARylation, PARP1 utilizes NAD^+ molecules to transfer ADP-Ribose moieties to target proteins, consequently modulating their functional and structural attributes. The counteractive process of dePARylation, is facilitated by PARG[128–130,183,198]. Emerging evidence posits that inhibiting dePARylation mirrors the effects of PARylation inhibition when considering processes such as DNA damage repair[130] and may therefore pose as equally effective anticancer treatments. Nevertheless, the many potential biological ramifications of perturbing muscle specific (de)PARylation in the setting of cancer cachexia remain inadequately explored. This study pioneers the examination of the consequences of skeletal muscle-specific perturbation of PARylation, employing two inducible models of either *Parg* or *Parp1* muscle specific knockouts.

Analyzing public RNA-seq datasets focused on cancer cachexia induced by LLC revealed notable alterations in genes related to PARylation homeostasis, such as *Parp4*, *Tnks1*, and

Parg. These changes in gene expression highlight the potential intricate relationship between PARylation and the pathophysiology of cancer cachexia, setting the stage for our subsequent mouse studies. Numerous murine models of cancer cachexia demonstrate a decrease of both lean and adipose tissue mass, including those using the LLC-allograft model[5,199,200 198]. In our experimental paradigm, both *Parp1*-IMKO and *Parg*-IMKO mice manifested reductions in iWAT and gWAT which was align with previous reports[5,199]. We found no difference between our skeletal muscle-specific *Parp1* or *Parg* ablation models following LLC induction, indicating that there is no strong influence of skeletal muscle PARP1 or PARG on systemic processes or energy metabolism in cancer cachexia. Similarly, splenomegaly, a surrogate marker of systemic inflammation[201], often concomitant with cancer cachexia-induced systemic inflammation, was analogous in both *Parg*-IMKO and *Parp1*-IMKO mice relative to their WT counterparts. This observation suggests that the spleen's inflammatory response remains largely unaltered by muscle-specific ablation of *Parp1* or *Parg*.

When assessing the role of PARylation on muscle cachexia we first observed distinct phenotypic alterations following the skeletal muscle-specific ablation of *Parp1* in mature male mice. Specifically, muscle mass in the quadriceps, the TA, as well as the combined mass of the gastrocnemius and soleus was exasperated when compared with the WT cohort. In contrast, mature male and female mice with inducible muscle-specific knockout of *Parg* exhibited no discernible muscle mass loss in the quadriceps and gastrocnemius, similar to their WT controls. Interestingly, female *Parg*-IMKO mice, in particular, showed no loss in TA muscle mass in comparison to the loss observed in WT mice.

The pronounced muscle mass loss observed in *Parp1*-IMKO mice can potentially be ascribed to the regulatory role that Parp*1* plays in the inhibition of *Foxo1* gene expression, which was first demonstrated in Ewing sarcoma RD-ES and SK-ES-1 cell lines, and CAPAN1 pancreatic cancer cells[172]. It is noteworthy that FOXO1 functions as a transcription factor, capable of augmenting the expression of genes that are intrinsically linked to muscle atrophy, such as *Trim63*[112–114,172]. *Trim63*, in particular, is upregulated in various forms of muscle atrophy and plays a pivotal role in the ubiquitination then degradation of proteins, including myosin heavy chain[114]. Related to this process, our analyses revealed an elevated expression of the *Trim63* gene in the quadriceps of PBS-treated *Parp1*-IMKO mice which was maintained following LLC-inductino. We predict that the elevated *Trim63* levels in PBS-treated *Parp1*-IMKO may have led to a susceptibility to muscle cachexia in these mice and exaggerated reduction of muscle mass following LLC induction. We therefore propose that the persistent elevation of *Trim63* gene expression might predispose the muscle to exacerbated protein degradation, especially under stressors such as those induced by cancer cachexia[112,113]. Intriguingly, *Parg*-IMKO mice did not show significant changes in expression of *Trim63* under PBS- or LLC-treated conditions.

Interestingly, previous research has demonstrated the potential beneficial effects of *Parp1* ablation, or its pharmacological inhibition, on the improvement of mitochondrial metabolism controlled by an NAD^+ surplus that drives NAD+-dependent SIRT1 activity [125–127,202]. Our findings corroborate this particular mechanism by showing that the ablation of *Parp1* in skeletal muscle leads to an enhancement of OxPhos protein levels in muscles. This is particularly relevant to cancer cachexia as seminal work by Brown et al., along with contributions from other researchers, posits that mitochondrial degeneration is an integral

facet of the pathogenesis of cancer cachexia[164,203]. Our data not only confirms the notion of mitochondrial degeneration in the context of cancer cachexia but also uniquely underscores that while PARP1-mediated mitochondrial improvements are evident they do not counteract the deleterious effects of cancer cachexia on muscle strength or mass.

In contrast to *Parp1*-IMKO mice, PBS-treated *Parg*-IMKO mice showed no increase in *Trim63* gene expression. Further to this, upon LLC-induction of cachexia *Parg*-IMKO mice did not exhibit a significant increase in *Trim63*, unlike the LLC-induced WT mice. *In vitro* analyses further demonstrated the capacity of PARG to modulate *Trim63* expression. Myotubes exposed to LLC-conditioned media exhibited amplified *Trim63* expression which was attenuated with PARG inhibition via PDD treatment. Future investigative endeavors should be channeled towards elucidating the mechanisms through which PARG and PARP1 regulates *Trim63* gene expression. To further examine the robustness of PARG's influence on atrophy related gene expression we examined another related gene named *Fbxo32*. A similar trend was found where there was no difference between PBS-treated *Parg*-IMKO mice and WT *Fbxo32* expression, then following LLC-induction *Parg*-IMKO mice showed no increase while WT mice trended upward (p=0.0668). Ultimately, under cachectic conditions *Parg*-IMKO mice do now show upregulation of the atrophy genes tested and therefore may offer a protective buffer against muscle atrophy in some cases.

The paradoxical observation that male *Parg*-IMKO mice, despite exhibiting diminished levels of atrogenic markers like *Trim63* and *Fbxo32*, sustain a similar rate of muscle mass loss to their wild-type counterparts is intriguing. Muscle atrophy is a complex interplay of myriad molecular

pathways. While *Trim63* and *Fbxo32* are established markers of muscle atrophy in the context of cancer cachexia[112,114,115], their diminished expression does not necessarily negate the activation of alternative atrophy-inducing pathways. The equilibrium between protein synthesis and degradation is pivotal for muscle mass maintenance in healthy adults. In muscle atrophy, there's either an increase in protein degradation, a decline in protein synthesis, or a combination of both. It's conceivable that in *Parg*-IMKO mice, other mechanisms or pathways might be compensating for the attenuated atrogenic activity, culminating in a similar rate of muscle mass loss, at least in male mice. One caveat is that in female *Parg*-IMKO mice there appeared to be a protective effect on TA muscle mass when comparing to the observed loss of TA mass in the WT animals following LLC-induction.

Nonetheless, we have not yet fully characterized either *Parg*-IMKO or *Parp1*-IMKO mice, and despite wet muscle mass and grip strength providing invaluable insights, it is conceivable that further testing will provide more accurate phenotyping of their muscle. For example, quantitative metrics of the muscle phenotype should include an assessment of both fiber-type and minimum ferret diameter. Additional in *vivo* tests could also inspect changes in protein synthesis via puromycin integration to elucidate whether altered muscle mass equates to a decreased rate of protein synthesis or measuring protein degradation with pulse-chase method[204]. Consequently, our data propound that heightened PARylation levels, via *Parg* ablation, can counteract the cancer cachexia-induced upregulation of *Fbxo32* and *Trim63*. However, the precise mechanisms governing why this modulation did not change the overall phenotype of male mice compared to controls and yet exhibited some improvement in female mice remains enigmatic. Future work that will examine differences in gene and protein

expression in both male and female mice for all cohorts (beyond the scope of this study) will help define mechanistic differences that lead to altered phenotypes.

Metabolic differences between male and female organisms present a unique basis for the inclusion of sex analysis in metabolic syndromes like cachexia. Variations in body composition, insulin sensitivity, muscle fiber types, and hormonal regulation contribute to differential cachexia responses between the sexes[19,20]. Some treatments may exhibit sex-specific efficacy, underscoring the imperative necessity for inclusive research. Recognizing these differences, our study adopted a comprehensive approach, encompassing both sexes. However, mechanisms governing any sex differences noted, particularly in *Parg*-IMKO mice, have not yet been explored. Avenues for exploration are diverse and may hinge on systemic differences. For example, given that the androgen receptor can directly induce *Parg* expression in prostate cancer cell lines[205], there might be a differential response to cancer cachexia in skeletal muscle *Parg* ablation between the sexes. This inclusivity might pave the way for tailored therapeutic strategies in the future.

6 Limitations and future work

Our study was not without limitations. Firstly, targeted gene expression analysis by qPCR provides a snapshot but doesn't necessarily capture the entire narrative. A gene might exhibit elevated expression, yet its protein levels might remain unchanged. As for the protein level, changes in protein expression may not give insight into the activity of a protein which often relies on protein-protein interactions and post-translational modifications. Although not included in this thesis, we have prepared samples for unbiased RNA-seq that have been sent

for analysis and for future proteomics analysis that will be combined with current and future targeted quantification of gene and protein expression. Secondly, our study leveraged the LLC-induced cachexia mouse model, derived from a spontaneous lung tumor in a C57BL mouse. While invaluable for cancer cachexia research, this model cannot wholly emulate the intricacies of human cancer cachexia. Consequently, findings from this model warrant validation in human studies. Continuous endeavors should be made to enhance the model's physiological relevance and thus exploration of alternative cachexia models such as patient-derived xenograft models that could serve to corroborate our findings. Thirdly, another limitation was the relatively modest sample size. There are several results that are inherently susceptible to technical variation, such as when assessing muscle grip strength or muscle mass. While our findings are enlightening, they should be interpreted with care. Increasing the sample size in future studies for both sexes would increase the robustness of the results, offering a better understanding of the roles of PARP1 and PARG in muscle homeostasis during cancer cachexia. Moreover, advanced imaging techniques or molecular assays could provide deeper insights into these aspects. For instance, ex *vivo* contraction experiments could offer another layer of validation for muscle function. Another limitation of our investigation is that we used unconditioned LLC growth as media as control for our *In vitro* studies. A better control could be to use conditioned media from a non-cachexia-inducing cell line such as T-cell lymphoblastoma cell line (EL4). Future work should also consider evaluating mitochondrial function by isolating fresh mitochondria from muscle in each cohort and measuring their respiration rates. This would complement our existing observations and provide a more comprehensive view of muscle cell health. Lastly, it's worth noting that our study did not

assess the role of PARG and PARP1 in muscle stem cells. This is worth further investigation, as (de)PARylation could influence muscle regeneration in cancer cachexia. Prior investigations have highlighted the exacerbation of membrane-level muscle damage in the of C26-induced cancer cachexia mouse model. While damage in this model instigates the activation of muscle progenitor cells, myogenesis is prematurely arrested, precluding full differentiation[48]. Given recent data about the role of PARP1 in myogenesis[206], the administration of PARP1 inhibitors necessitates circumspection. Primarily, PARP1 is indispensable for the complete differentiation of myoblasts[206]. Additionally, the expression dynamics of PARP1 undergoes fluctuations during differentiation[195,206]. Matteini et al. have elucidated that PARP1 reduces the expression of myogenin and other MyoD targets, potentially through modulating H3K4me3 levels or influencing MyoD binding[195]. Furthermore, the myogenetic transcriptional activator, Yin Yang1, undergoes direct PARylation by PARP1.[207] Another pivotal player in myogenic progression is the transcription factor CCAAT/enhancer binding protein beta (C/EBPb)[208,209], which was initially identified to undergo PARylation during adipogenesis[210]. Given its role in myogenesis, C/EBPb might also be subjected to an influence from PARylation. To address this, we have already developed inducible mouse models lacking *Parp1* or *Parg* in resident muscle stem cells (satellite cells; *Parp1*-iMSKO, *Parg*-IMKSO) and our future investigation will examine the role of (de)PARylation on muscle stem cell fate and function. Collectively, these insights underscore the importance of preserving robust myogenesis in both health and disease, thereby suggesting that pharmacological interventions altering PARP1 or PARG be approached with caution.

7 Conclusion

Our findings underscore that skeletal muscle-specific ablation of *Parp1* exacerbates muscle wasting in cancer cachexia. This has profound clinical implications, especially as patients are increasingly receiving PARP1 inhibitors. Given the correlation between cancer rates and age, and the heightened susceptibility of the elderly to muscle wasting disorders like sarcopenia, the development of safe cancer therapeutic agents is of paramount importance. To further this endeavor, we probed the impact of *Parg* ablation in muscles during cachexia. Given that the development of *Parg* inhibitors are underway and are being assessed in clinical trials to induces synthetic lethality in cancer cells, akin to *Parp1* ablation, our data might offer a proof of concept that *Parg* ablation does not exacerbate muscle wasting in cancer cachexia and may offer a better alternative to PARP1 inhibition.

8 References

1. Baracos, V.E., Martin, L., Korc, M., Guttridge, D.C., and Fearon, K.C.H. (2018). Cancer-associated cachexia. Nature Reviews Disease Primers 2018 4:1 *4*, 1–18. 10.1038/nrdp.2017.105.
2. Bachmann, J., Heiligensetzer, M., Krakowski-Roosen, H., Büchler, M.W., Friess, H., and Martignoni, M.E. (2008). Cachexia worsens prognosis in patients with resectable pancreatic cancer. Journal of Gastrointestinal Surgery *12*, 1193–1201. 10.1007/S11605-008-0505-Z/TABLES/6.
3. Fearon, K.C.H., Glass, D.J., and Guttridge, D.C. (2012). Cell Metabolism Review Cancer Cachexia: Mediators, Signaling, and Metabolic Pathways. Cell Metab *16*, 153–166. 10.1016/j.cmet.2012.06.011.
4. Wagner, P.D. (2008). Possible mechanisms underlying the development of cachexia in COPD. European Respiratory Journal *31*, 492–501. 10.1183/09031936.00074807.
5. Kir, S., and Spiegelman, B.M. (2016). CACHEXIA & BROWN FAT: A BURNING ISSUE IN CANCER. Trends Cancer *2*, 461–463. 10.1016/J.TRECAN.2016.07.005.
6. Sun, R., Zhang, S., Lu, X., Hu, W., Lou, N., Zhao, Y., Zhou, J., Zhang, X., and Yang, H. (2016). Comparative molecular analysis of early and late cancer cachexia-induced muscle wasting in mouse models. Oncol Rep *36*, 3291–3302. 10.3892/OR.2016.5165.
7. Bruera, E., and Sweeney, C. (2000). Cachexia and asthenia in cancer patients. Lancet Oncology *1*, 138–147. 10.1016/S1470-2045(00)00033-4.
8. von Haehling, S., and Anker, S.D. (2010). Cachexia as a major underestimated and unmet medical need: facts and numbers. J Cachexia Sarcopenia Muscle *1*, 1–5. 10.1007/S13539-010-0002-6.
9. Deans, C., and Wigmore, S.J. (2005). Systemic inflammation, cachexia and prognosis in patients with cancer. Curr Opin Clin Nutr Metab Care *8*, 265–269. 10.1097/01.MCO.0000165004.93707.88.
10. Eys, J. van (2003). Nutrition and Cancer: Physiological Interrelationships. https://doi.org/10.1146/annurev.nu.05.070185.002251 *5*, 435–461. 10.1146/ANNUREV.NU.05.070185.002251.
11. Tisdale, M.J. (2009). Mechanisms of cancer cachexia. Physiol Rev *89*, 381–410. 10.1152/physrev.00016.2008.
12. von Haehling, S., and Anker, S.D. (2014). Prevalence, incidence and clinical impact of cachexia: facts and numbers—update 2014. J Cachexia Sarcopenia Muscle *5*, 261. 10.1007/S13539-014-0164-8.
13. von Haehling, S., Anker, M.S., and Anker, S.D. (2016). Prevalence and clinical impact of cachexia in chronic illness in Europe, USA, and Japan: facts and numbers update 2016. 10.1002/jcsm.12167.
14. Law, M.L. (2022). Cancer cachexia: Pathophysiology and association with cancer-related pain. Frontiers in Pain Research *3*, 971295. 10.3389/FPAIN.2022.971295/BIBTEX.
15. Vaughan, V.C., Martin, P., and Lewandowski, P.A. (2013). Cancer cachexia: impact, mechanisms and emerging treatments. J Cachexia Sarcopenia Muscle *4*, 95. 10.1007/S13539-012-0087-1.
16. Aguilar-Cazares, D., Chavez-Dominguez, R., Marroquin-Muciño, M., Perez-Medina, M., Benito-Lopez, J.J., Camarena, A., Rumbo-Nava, U., and Lopez-Gonzalez, J.S.

(2022). The systemic-level repercussions of cancer-associated inflammation mediators produced in the tumor microenvironment. Front Endocrinol (Lausanne) *13*. 10.3389/FENDO.2022.929572/FULL.

17. Maccio, A., Sanna, E., Neri, M., Oppi, S., and Madeddu, C. (2021). Molecular Sciences Cachexia as Evidence of the Mechanisms of Resistance and Tolerance during the Evolution of Cancer Disease. 10.3390/ijms22062890.
18. Baracos, V.E., Mazurak, V.C., and Bhullar, A.S. (2019). Cancer cachexia is defined by an ongoing loss of skeletal muscle mass. Ann Palliat Med *8*, 3–12. 10.21037/APM.2018.12.01.
19. Stephens, N.A., Gray, C., MacDonald, A.J., Tan, B.H., Gallagher, I.J., Skipworth, R.J.E., Ross, J.A., Fearon, K.C.H., and Greig, C.A. (2012). Sexual dimorphism modulates the impact of cancer cachexia on lower limb muscle mass and function. Clinical Nutrition *31*, 499–505. 10.1016/J.CLNU.2011.12.008.
20. Wallengren, O., Iresjö, B.M., Lundholm, K., and Bosaeus, I. (2015). Loss of muscle mass in the end of life in patients with advanced cancer. Supportive Care in Cancer *23*, 79–86. 10.1007/S00520-014-2332-Y/TABLES/3.
21. Queiroz, A.L., Dantas, E., Ramsamooj, S., Murthy, A., Ahmed, M., Zunica, E.R.M., Liang, R.J., Murphy, J., Holman, C.D., Bare, C.J., et al. (2022). Blocking ActRIIB and restoring appetite reverses cachexia and improves survival in mice with lung cancer. Nature Communications 2022 13:1 *13*, 1–17. 10.1038/s41467-022-32135-0.
22. Martin, L., Birdsell, L., MacDonald, N., Reiman, T., Clandinin, M.T., McCargar, L.J., Murphy, R., Ghosh, S., Sawyer, M.B., and Baracos, V.E. (2013). Cancer cachexia in the age of obesity: Skeletal muscle depletion is a powerful prognostic factor, independent of body mass index. Journal of Clinical Oncology *31*, 1539–1547. 10.1200/JCO.2012.45.2722.
23. Kleeff, J., Michalski, C., Friess, H., and Büchler, M.W. (2006). Pancreatic cancer: from bench to 5-year survival. Pancreas *33*, 111–118. 10.1097/01.mpa.0000229010.62538.f2.
24. Bachmann, J., Heiligensetzer, M., Krakowski-Roosen, H., Büchler, M.W., Friess, H., and Martignoni, M.E. (2008). Cachexia worsens prognosis in patients with resectable pancreatic cancer. Journal of Gastrointestinal Surgery *12*, 1193–1201. 10.1007/S11605-008-0505-Z/TABLES/6.
25. Farhang-Sardroodi, S., La Croix, M.A., and Wilkie, K.P. (2022). Chemotherapy-induced cachexia and model-informed dosing to preserve lean mass in cancer treatment. PLoS Comput Biol *18*, e1009505. 10.1371/JOURNAL.PCBI.1009505.
26. Garcia, J.M., Cata, J.P., Dougherty, P.M., and Smith, R.G. (2008). Ghrelin Prevents Cisplatin-Induced Mechanical Hyperalgesia and Cachexia. Endocrinology *149*, 455–460. 10.1210/EN.2007-0828.
27. Damrauer, J.S., Stadler, M.E., Acharyya, S., Baldwin, A.S., Couch, M.E., and Guttridge, D.C. (2018). Chemotherapy-induced muscle wasting: association with NF-κB and cancer cachexia. Eur J Transl Myol *28*, 158–166. 10.4081/ejtm.2018.7590.
28. Le Bricon, T., Gugins, S., Cynober, L., and Baracos, V.E. (1995). Negative impact of cancer chemotherapy on protein metabolism in healthy and tumor-bearing rats. Metabolism *44*, 1340–1348. 10.1016/0026-0495(95)90040-3.
29. Setiawan, T., Sari, I.N., Wijaya, Y.T., Julianto, N.M., Muhammad, J.A., Lee, H., Chae, J.H., and Kwon, H.Y. (2023). Cancer cachexia: molecular mechanisms and

treatment strategies. Journal of Hematology & Oncology 2023 16:1 *16*, 1–26. 10.1186/S13045-023-01454-0.
30. Mirza, K.A., and Tisdale, M.J. (2012). Role of Ca2 + in proteolysis-inducing factor (PIF)-induced atrophy of skeletal muscle. Cell Signal *24*, 2118–2122. 10.1016/J.CELLSIG.2012.07.016.
31. Kang, E.A., Park, J.M., Jin, W., Tchahc, H., Kwon, K.A., and Hahm, K.B. (2022). Amelioration of cancer cachexia with preemptive administration of tumor necrosis factor-α blocker. J Clin Biochem Nutr *70*, 117. 10.3164/JCBN.21-21.
32. Busch, K., Kny, M., Huang, N., Klassert, T.E., Stock, M., Hahn, A., Graeger, S., Todiras, M., Schmidt, S., Chamling, B., et al. (2021). Inhibition of the NLRP3/IL-1β axis protects against sepsis-induced cardiomyopathy. J Cachexia Sarcopenia Muscle *12*, 1653–1668. 10.1002/JCSM.12763.
33. Kumar, S., Kishimoto, H., Chua, H.L., Badve, S., Miller, K.D., Bigsby, R.M., and Nakshatri, H. (2003). Interleukin-1 alpha promotes tumor growth and cachexia in MCF-7 xenograft model of breast cancer. Am J Pathol *163*, 2531–2541. 10.1016/S0002-9440(10)63608-5.
34. Barber, M.D., Powell, J.J., Lynch, S.F., Fearon, K.C.H., and Ross, J.A. (2000). A polymorphism of the interleukin-1 β gene influences survival in pancreatic cancer. British Journal of Cancer 2000 83:11 *83*, 1443–1447. 10.1054/bjoc.2000.1479.
35. Laird, B.J., McMillan, D., Skipworth, R.J.E., Fallon, M.T., Paval, D.R., McNeish, I., and Gallagher, I.J. (2021). The Emerging Role of Interleukin 1β (IL-1β) in Cancer Cachexia. Inflammation *44*, 1223. 10.1007/S10753-021-01429-8.
36. Pototschnig, I., Feiler, U., Diwoky, C., Vesely, P.W., Rauchenwald, T., Paar, M., Bakiri, L., Pajed, L., Hofer, P., Kashofer, K., et al. (2023). Interleukin-6 initiates muscle- and adipose tissue wasting in a novel C57BL/6 model of cancer-associated cachexia. J Cachexia Sarcopenia Muscle *14*, 93–107. 10.1002/JCSM.13109.
37. Daou, H.N. (2020). Exercise as an anti-inflammatory therapy for cancer cachexia: a focus on interleukin-6 regulation. Am J Physiol Regul Integr Comp Physiol *318*, R296–R310. 10.1152/AJPREGU.00147.2019.
38. Fan, M., Gu, X., Zhang, W., Shen, Q., Zhang, R., Fang, Q., Wang, Y., Guo, X., Zhang, X., and Liu, X. (2022). Atractylenolide I ameliorates cancer cachexia through inhibiting biogenesis of IL-6 and tumour-derived extracellular vesicles. J Cachexia Sarcopenia Muscle *13*, 2724–2739. 10.1002/JCSM.13079.
39. Fearon, K., Strasser, F., Anker, S.D., Bosaeus, I., Bruera, E., Fainsinger, R.L., Jatoi, A., Loprinzi, C., MacDonald, N., Mantovani, G., et al. (2011). Definition and classification of cancer cachexia: An international consensus. Lancet Oncol *12*, 489–495. 10.1016/S1470-2045(10)70218-7.
40. Heiden, M.G.V., Cantley, L.C., and Thompson, C.B. (2009). Understanding the Warburg Effect: The Metabolic Requirements of Cell Proliferation. Science *324*, 1029. 10.1126/SCIENCE.1160809.
41. Ruan, G.T., Xie, H.L., Hu, C.L., Liu, C.A., Zhang, H.Y., Zhang, Q., Wang, Z.W., Zhang, X., Ge, Y.Z., Lin, S.Q., et al. (2023). Comprehensive prognostic effects of systemic inflammation and Insulin resistance in women with breast cancer with different BMI: a prospective multicenter cohort. Scientific Reports 2023 13:1 *13*, 1–13. 10.1038/s41598-023-31450-w.

42. Djiogue, S., Kamdje, A.H.N., Vecchio, L., Kipanyula, M.J., Farahna, M., Aldebasi, Y., and Etet, P.F.S. (2013). Insulin resistance and cancer: the role of insulin and IGFs. Endocr Relat Cancer *20*, R1–R17. 10.1530/ERC-12-0324.
43. Todorov, P.T., Deacon, M., and Tisdale, M.J. (1997). Structural analysis of a tumor-produced sulfated glycoprotein capable of initiating muscle protein degradation. J Biol Chem *272*, 12279–12288. 10.1074/JBC.272.19.12279.
44. Watchorn, T.M., Waddell, I., and Ross, J.A. (2002). Proteolysis-inducing factor differentially influences transcriptional regulation in endothelial subtypes. Am J Physiol Endocrinol Metab *282*. 10.1152/AJPENDO.00408.2001/ASSET/IMAGES/LARGE/H10420767005.JPEG.
45. Mirza, K.A., and Tisdale, M.J. (2012). Role of Ca2+ in proteolysis-inducing factor (PIF)-induced atrophy of skeletal muscle. Cell Signal *24*, 2118–2122. 10.1016/J.CELLSIG.2012.07.016.
46. Agustsson, T., Rydén, M., Hoffstedt, J., Van Harmelen, V., Dicker, A., Laurencikiene, J., Isaksson, B., Permert, J., and Arner, P. (2007). Mechanism of increased lipolysis in cancer cachexia. Cancer Res *67*, 5531–5537. 10.1158/0008-5472.CAN-06-4585.
47. Oliver, F.J., Mé Nissier-De Murcia, J., Nacci, C., Decker, P., Andriantsitohaina, R., Muller, S., De La Rubia, G., Stoclet, J.C., and De Murcia, G. (1999). Resistance to endotoxic shock as a consequence of defective NF-κB activation in poly (ADP-ribose) polymerase-1 deficient mice. EMBO J *18*, 4446–4454.
48. He, W.A., Berardi, E., Cardillo, V.M., Acharyya, S., Aulino, P., Thomas-Ahner, J., Wang, J., Bloomston, M., Muscarella, P., Nau, P., et al. (2013). NF-κB–mediated Pax7 dysregulation in the muscle microenvironment promotes cancer cachexia. J Clin Invest *123*, 4821. 10.1172/JCI68523.
49. Liu, D., Qiao, X., Ge, Z., Shang, Y., Li, Y., Wang, W., Chen, M., Si, S., and Chen, S.Z. (2019). IMB0901 inhibits muscle atrophy induced by cancer cachexia through MSTN signaling pathway. Skelet Muscle *9*, 1–14. 10.1186/S13395-019-0193-2/FIGURES/7.
50. Fearon, K.C.H., Glass, D.J., and Guttridge, D.C. (2012). Cancer Cachexia: Mediators, Signaling, and Metabolic Pathways. Cell Metab *16*, 153–166. 10.1016/j.cmet.2012.06.011.
51. Evans, W.J., Morley, J.E., and Argilés, J. (2008). UC Irvine UC Irvine Previously Published Works Title Cachexia: a new definition Permalink Publication Date Copyright Information. Clinical Nutrition *27*, 793–799. 10.1016/j.clnu.2008.06.013.
52. Suzuki, T., Ebner, N., Palus, S., Haehling, S. von, and Springer, J. (2020). Progesterone improves survival in hepatoma cachexia rat model. JCSM Rapid Commun *3*, 3–10. 10.1002/RCO2.11.
53. Garcia, J.M., and Shamliyan, T.A. (2017). Nonsteroidal Anti-Inflammatory Drugs in Patients with Anorexia-Cachexia Syndrome Associated with Malignancy and Its Treatments. Am J Med *130*, 1033–1036. 10.1016/j.amjmed.2017.03.037.
54. Ogino, M., and Hanazono, M. (1998). Indomethacin acts as an antitumor and anticachexic agent in colon 26- bearing CDF1 mice. Int J Clin Oncol *3*, 176–181. 10.1007/BF02489912/METRICS.
55. Chen, S.Z., and Qiu, Z.G. (2011). Combined treatment with GH, insulin, and indomethacin alleviates cancer cachexia in a mouse model. J Endocrinol *208*, 131–136. 10.1677/JOE-10-0341.

56. Lonnroth, C., Svaninger, G., Gelin, J., Cahlin, C., Iresjo, B.M., Cvetkovska, E., Edstrom, S., Andersson, M., Svanberg, E., and Lundholm, K. (1995). Effects related to indomethacin prolonged survival and decreased tumor-growth in a mouse-tumor model with cytokine dependent cancer cachexia. Int J Oncol *7*, 1405–1413. 10.3892/IJO.7.6.1405.
57. Graf, S.A., and Garcia, J.M. (2017). Anamorelin hydrochloride in the treatment of cancer anorexia–cachexia syndrome: design, development, and potential place in therapy. Drug Des Devel Ther *11*, 2325–2331. 10.2147/DDDT.S110131.
58. Rezaei, S., de Oliveira, L.C., Ghanavati, M., Shadnoush, M., Akbari, M.E., Akbari, A., Hadizadeh, M., Ardehali, S.H., Wakabayashi, H., Elhelali, A., et al. (2023). The effect of anamorelin (ONO-7643) on cachexia in cancer patients: Systematic review and meta-analysis of randomized controlled trials. https://doi.org/10.1177/10781552231189864. 10.1177/10781552231189864.
59. Currow, D., Temel, J.S., Abernethy, A., Milanowski, J., Friend, J., and Fearon, K.C. (2017). ROMANA 3: A phase 3 safety extension study of anamorelin in advanced non-small-cell lung cancer (NSCLC) patients with cachexia. Annals of Oncology *28*, 1949–1956. 10.1093/annonc/mdx192.
60. Garcia, J.M., Boccia, R. V., Graham, C.D., Yan, Y., Duus, E.M., Allen, S., and Friend, J. (2015). Anamorelin for patients with cancer cachexia: An integrated analysis of two phase 2, randomised, placebo-controlled, double-blind trials. Lancet Oncol *16*, 108–116. 10.1016/S1470-2045(14)71154-4.
61. Takayama, K., Takiguchi, T., Komura, N., and Naito, T. (2023). Efficacy and safety of anamorelin in patients with cancer cachexia: Post-hoc subgroup analyses of a placebo-controlled study. Cancer Med *12*, 2918. 10.1002/CAM4.5206.
62. Nishie, K., Sato, S., and Hanaoka, M. (2022). Anamorelin for cancer cachexia. Drugs Today (Barc) *58*, 97–104. 10.1358/DOT.2022.58.3.3381585.
63. Talbert, E.E., Cuitiño, M.C., Ladner, K.J., Rajasekerea, P. V., Siebert, M., Shakya, R., Leone, G.W., Ostrowski, M.C., Paleo, B., Weisleder, N., et al. (2019). Modeling Human Cancer-induced Cachexia. Cell Rep *28*, 1612. 10.1016/J.CELREP.2019.07.016.
64. Rashidi, B., Yang, M., Jiang, P., Baranov, E., An, Z., Wang, X., Moossa, A.R., and Hoffman, R.M. (2000). A highly metastatic Lewis lung carcinoma orthotopic green fluorescent protein model. Clin Exp Metastasis *18*, 57–60. 10.1023/A:1026596131504/METRICS.
65. Neyroud, D., Nosacka, R.L., Judge, A.R., and Hepple, R.T. (2019). Colon 26 Adenocarcinoma (C26)-Induced Cancer Cachexia Impairs Skeletal Muscle Mitochondrial Function and Content. J Muscle Res Cell Motil *40*, 59. 10.1007/S10974-019-09510-4.
66. Sato, Y., Fu, Y., Liu, H., Lee, M.Y., and Shaw, M.H. (2021). Tumor-immune profiling of CT-26 and Colon 26 syngeneic mouse models reveals mechanism of anti-PD-1 response. BMC Cancer *21*, 1–12. 10.1186/S12885-021-08974-3/FIGURES/5.
67. Bonetto, A., Rupert, J.E., Barreto, R., and Zimmers, T.A. (2016). The Colon-26 Carcinoma Tumor-bearing Mouse as a Model for the Study of Cancer Cachexia. J Vis Exp, 54893. 10.3791/54893.
68. Guigni, B.A., van der Velden, J., Matthew Kinsey, C., Carson, J.A., and Toth, M.J. (2020). Effects of conditioned media from murine lung cancer cells and human tumor

cells on cultured myotubes. Am J Physiol Endocrinol Metab *318*, E22. 10.1152/AJPENDO.00310.2019.
69. Guigni, B.A., van der Velden, J., Matthew Kinsey, C., Carson, J.A., and Toth, M.J. (2020). Effects of conditioned media from murine lung cancer cells and human tumor cells on cultured myotubes. Am J Physiol Endocrinol Metab *318*, E22–E32. 10.1152/AJPENDO.00310.2019.
70. Stankevicius, V., Vasauskas, G., Bulotiene, D., Butkyte, S., Jarmalaite, S., Rotomskis, R., and Suziedelis, K. (2016). Gene and miRNA expression signature of Lewis lung carcinoma LLC1 cells in extracellular matrix enriched microenvironment. BMC Cancer *16*, 1–13. 10.1186/S12885-016-2825-9/FIGURES/3.
71. Bertram, J.S., and Janik, P. (1980). Establishment of a cloned line of Lewis Lung Carcinoma cells adapted to cell culture. Cancer Lett *11*, 63–73. 10.1016/0304-3835(80)90130-5.
72. Mukund, K., and Subramaniam, S. (2020). Skeletal muscle: A review of molecular structure and function, in health and disease. Wiley Interdiscip Rev Syst Biol Med *12*. 10.1002/WSBM.1462.
73. Dumont, N.A., Wang, Y.X., Von Maltzahn, J., Pasut, A., Bentzinger, C.F., Brun, C.E., and Rudnicki, M.A. (2015). Dystrophin expression in muscle stem cells regulates their polarity and asymmetric division. Nature Medicine 2015 21:12 *21*, 1455–1463. 10.1038/nm.3990.
74. Scott, W., Stevens, J., and Binder-Macleod, S.A. (2001). Human Skeletal Muscle Fiber Type Classifications. Phys Ther *81*, 1810–1816. 10.1093/PTJ/81.11.1810.
75. Lieber, R.L., Roberts, T.J., Blemker, S.S., Lee, S.S.M., and Herzog, W. (2017). Skeletal muscle mechanics, energetics and plasticity. Journal of NeuroEngineering and Rehabilitation 2017 14:1 *14*, 1–16. 10.1186/S12984-017-0318-Y.
76. Flück, M., and Hoppeler, H. (2003). Molecular basis of skeletal muscle plasticity--from gene to form and function. Rev Physiol Biochem Pharmacol *146*, 159–216. 10.1007/S10254-002-0004-7.
77. McClelland, G.B., and Scott, G.R. (2002). Muscle Plasticity: Response to training and detraining. Physiotherapy *88*, 398–408. 10.1016/S0031-9406(05)61265-5.
78. Damas, F., Angleri, V., Phillips, S.M., Witard, O.C., Ugrinowitsch, C., Santanielo, N., Soligon, S.D., Costa, L.A.R., Lixandrão, M.E., Conceição, M.S., et al. (2019). Myofibrillar protein synthesis and muscle hypertrophy individualized responses to systematically changing resistance training variables in trained young men. J Appl Physiol (1985) *127*, 806–815. 10.1152/JAPPLPHYSIOL.00350.2019.
79. Hennebry, A., Oldham, J., Shavlakadze, T., Grounds, M.D., Sheard, P., Fiorotto, M.L., Falconer, S., Smith, H.K., Berry, C., Jeanplong, F., et al. (2017). IGF1 stimulates greater muscle hypertrophy in the absence of myostatin in male mice. Journal of Endocrinology *234*, 187–200. 10.1530/JOE-17-0032.
80. Yoshida, T., and Delafontaine, P. (2020). Mechanisms of IGF-1-Mediated Regulation of Skeletal Muscle Hypertrophy and Atrophy. Cells *9*. 10.3390/CELLS9091970.
81. Adams, G.R. (2001). Insulin-like growth factor in muscle growth and its potential abuse by athletes. Western Journal of Medicine *175*, 7.
82. McMillin, S.L., Schmidt, D.L., Kahn, B.B., and Witczak, C.A. (2017). GLUT4 is not necessary for overload-induced glucose uptake or hypertrophic growth in mouse skeletal muscle. Diabetes *66*, 1491–1500. 10.2337/DB16-1075/-/DC1.

83. Richter, E.A., and Hargreaves, M. (2013). Exercise, GLUT4, and skeletal muscle glucose uptake. Physiol Rev *93*, 993–1017. 10.1152/PHYSREV.00038.2012/ASSET/IMAGES/LARGE/Z9J0031326620008.JPEG.
84. Evans, P.L., McMillin, S.L., Weyrauch, L.A., and Witczak, C.A. (2019). Regulation of Skeletal Muscle Glucose Transport and Glucose Metabolism by Exercise Training. Nutrients 2019, Vol. 11, Page 2432 *11*, 2432. 10.3390/NU11102432.
85. Groennebaek, T., and Vissing, K. (2017). Impact of Resistance Training on Skeletal Muscle Mitochondrial Biogenesis, Content, and Function. Front Physiol *8*, 713. 10.3389/FPHYS.2017.00713.
86. Hargreaves, M., and Spriet, L.L. (2020). Skeletal muscle energy metabolism during exercise. Nature Metabolism 2020 2:9 *2*, 817–828. 10.1038/s42255-020-0251-4.
87. Porter, C., Reidy, P.T., Bhattarai, N., Sidossis, L.S., and Rasmussen, B.B. (2015). Resistance Exercise Training Alters Mitochondrial Function in Human Skeletal Muscle. Med Sci Sports Exerc *47*, 1922. 10.1249/MSS.0000000000000605.
88. McKinnell, I.W., and Rudnicki, M.A. (2004). Molecular mechanisms of muscle atrophy. Cell *119*, 907–910. 10.1016/j.cell.2004.12.007.
89. Bonaldo, P., and Sandri, M. (2013). Cellular and molecular mechanisms of muscle atrophy. Dis Model Mech *6*, 25–39. 10.1242/DMM.010389.
90. Sartori, R., Romanello, V., and Sandri, M. (2021). Mechanisms of muscle atrophy and hypertrophy: implications in health and disease. Nature Communications 2021 12:1 *12*, 1–12. 10.1038/s41467-020-20123-1.
91. Bonaldo, P., and Sandri, M. (2013). Cellular and molecular mechanisms of muscle atrophy. Dis Model Mech *6*, 25. 10.1242/DMM.010389.
92. Cohen, S., Brault, J.J., Gygi, S.P., Glass, D.J., Valenzuela, D.M., Gartner, C., Latres, E., and Goldberg, A.L. (2009). During muscle atrophy, thick, but not thin, filament components are degraded by MuRF1-dependent ubiquitylation. J Cell Biol *185*, 1083–1095. 10.1083/JCB.200901052.
93. Fielitz, J., Kim, M.S., Shelton, J.M., Latif, S., Spencer, J.A., Glass, D.J., Richardson, J.A., Bassel-Duby, R., and Olson, E.N. (2007). Myosin accumulation and striated muscle myopathy result from the loss of muscle RING finger 1 and 3. J Clin Invest *117*, 2486–2495. 10.1172/JCI32827.
94. Clarke, B.A., Drujan, D., Willis, M.S., Murphy, L.O., Corpina, R.A., Burova, E., Rakhilin, S. V., Stitt, T.N., Patterson, C., Latres, E., et al. (2007). The E3 Ligase MuRF1 degrades myosin heavy chain protein in dexamethasone-treated skeletal muscle. Cell Metab *6*, 376–385. 10.1016/J.CMET.2007.09.009.
95. Nascimbeni, A.C., Fanin, M., Masiero, E., Angelini, C., and Sandri, M. (2012). Impaired autophagy contributes to muscle atrophy in glycogen storage disease type II patients. Autophagy *8*, 1697. 10.4161/AUTO.21691.
96. Sandri, M. (2013). Protein breakdown in muscle wasting: Role of autophagy-lysosome and ubiquitin-proteasome. Int J Biochem Cell Biol *45*, 2121. 10.1016/J.BIOCEL.2013.04.023.
97. Nakae, J., Kitamura, T., Kitamura, Y., Biggs Iii, W.H., Arden, K.C., and Accili, D. (2003). The Forkhead Transcription Factor Foxo1 Regulates Adipocyte Differentiation growth arrest associated with terminal differentiation. These processes are accompanied by characteristic changes in gene expression. Dev Cell *4*, 119–129.

98. Puig, O., Marr, M.T., Ruhf, M.L., and Tjian, R. (2003). Control of cell number by Drosophila FOXO: downstream and feedback regulation of the insulin receptor pathway. Genes Dev *17*, 2006–2020. 10.1101/GAD.1098703.
99. Tran, H., Brunet, A., Griffith, E.C., and Greenberg, M.E. (2003). The many forks in FOXO's road. Sci STKE *2003*. 10.1126/STKE.2003.172.RE5.
100. Milan, G., Romanello, V., Pescatore, F., Armani, A., Paik, J.H., Frasson, L., Seydel, A., Zhao, J., Abraham, R., Goldberg, A.L., et al. (2015). Regulation of autophagy and the ubiquitin–proteasome system by the FoxO transcriptional network during muscle atrophy. Nature Communications 2015 6:1 *6*, 1–14. 10.1038/ncomms7670.
101. Lecker, S.H., Jagoe, R.T., Gilbert, A., Gomes, M., Baracos, V., Bailey, J., Price, S.R., Mitch, W.E., and Goldberg, A.L. (2004). Multiple types of skeletal muscle atrophy involve a common program of changes in gene expression. FASEB J *18*, 39–51. 10.1096/FJ.03-0610COM.
102. Brown, J.L., Rosa-Caldwell, M.E., Lee, D.E., Blackwell, T.A., Brown, L.A., Perry, R.A., Haynie, W.S., Hardee, J.P., Carson, J.A., Wiggs, M.P., et al. (2017). Mitochondrial degeneration precedes the development of muscle atrophy in progression of cancer cachexia in tumour-bearing mice. J Cachexia Sarcopenia Muscle *8*, 926. 10.1002/JCSM.12232.
103. van der Ende, M., Grefte, S., Plas, R., Meijerink, J., Witkamp, R.F., Keijer, J., and van Norren, K. (2018). Mitochondrial dynamics in cancer-induced cachexia. Biochimica et Biophysica Acta (BBA) - Reviews on Cancer *1870*, 137–150. 10.1016/J.BBCAN.2018.07.008.
104. White, J.P., Puppa, M.J., Sato, S., Gao, S., Price, R.L., Baynes, J.W., Kostek, M.C., Matesic, L.E., and Carson, J.A. (2012). IL-6 regulation on skeletal muscle mitochondrial remodeling during cancer cachexia in the ApcMin/+ mouse. Skelet Muscle *2*. 10.1186/2044-5040-2-14.
105. Barreto, R., Mandili, G., Witzmann, F.A., Novelli, F., Zimmers, T.A., and Bonetto, A. (2016). Cancer and Chemotherapy Contribute to Muscle Loss by Activating Common Signaling Pathways. Front Physiol *7*, 472. 10.3389/FPHYS.2016.00472.
106. Mao, X., Gu, Y., Sui, X., Shen, L., Han, J., Wang, H., Xi, Q., Zhuang, Q., Meng, Q., and Wu, G. (2021). Phosphorylation of Dynamin-Related Protein 1 (DRP1) Regulates Mitochondrial Dynamics and Skeletal Muscle Wasting in Cancer Cachexia. Front Cell Dev Biol *9*. 10.3389/FCELL.2021.673618/FULL.
107. da Silva, F.M., Rosa-Caldwell, M.E., Schrems, E.R., Martinez, L., Amos, M.G., Lim, S., Cabrera, A.R., Brown, J.L., Washington, T.A., and Greene, N.P. (2022). PGC-1α overexpression is not sufficient to mitigate cancer cachexia in either male or female mice. Appl Physiol Nutr Metab *47*, 933. 10.1139/APNM-2022-0086.
108. Julienne, C.M., Dumas, J.F., Goupille, C., Pinault, M., Berri, C., Collin, A., Tesseraud, S., Couet, C., and Servais, S. (2012). Cancer cachexia is associated with a decrease in skeletal muscle mitochondrial oxidative capacities without alteration of ATP production efficiency. J Cachexia Sarcopenia Muscle *3*, 265–275. 10.1007/S13539-012-0071-9.
109. Beltrà, M., Pöllänen, N., Fornelli, C., Tonttila, K., Hsu, M.Y., Zampieri, S., Moletta, L., Corrà, S., Porporato, P.E., Kivelä, R., et al. (2023). NAD+ repletion with niacin counteracts cancer cachexia. Nature Communications 2023 14:1 *14*, 1–14. 10.1038/s41467-023-37595-6.

110. Brown, J.L., Lawrence, M.M., Ahn, B., Kneis, P., Piekarz, K.M., Qaisar, R., Ranjit, R., Bian, J., Pharaoh, G., Brown, C., et al. (2020). Cancer cachexia in a mouse model of oxidative stress. J Cachexia Sarcopenia Muscle *11*, 1688. 10.1002/JCSM.12615.
111. Xu, T., Yang, X., Wu, C., Qiu, J., Fang, Q., Wang, L., Yu, S., and Sun, H. (2018). Pyrroloquinoline quinone attenuates cachexia-induced muscle atrophy via suppression of reactive oxygen species. J Thorac Dis *10*, 2752–2759. 10.21037/JTD.2018.04.112.
112. Shimizu, H., Langenbacher, A.D., Huang, J., Wang, K., Otto, G., Geisler, R., Wang, Y., and Chen, J.N. (2017). The calcineurin-FoxO-MuRF1 signaling pathway regulates myofibril integrity in cardiomyocytes. Elife *6*. 10.7554/ELIFE.27955.
113. Waddell, D.S., Baehr, L.M., Van Den Brandt, J., Johnsen, S.A., Reichardt, H.M., Furlow, J.D., and Bodine, S.C. (2008). The glucocorticoid receptor and FOXO1 synergistically activate the skeletal muscle atrophy-associated MuRF1 gene. Am J Physiol Endocrinol Metab *295*, 785–797. 10.1152/AJPENDO.00646.2007/ASSET/IMAGES/LARGE/ZH10100854250007.JPEG.
114. Sandri, M., Sandri, C., Gilbert, A., Skurk, C., Calabria, E., Picard, A., Walsh, K., Schiaffino, S., Lecker, S.H., and Goldberg, A.L. (2004). Foxo transcription factors induce the atrophy-related ubiquitin ligase atrogin-1 and cause skeletal muscle atrophy. Cell *117*, 399–412. 10.1016/S0092-8674(04)00400-3.
115. Sacheck, J., Ohtsuka, A., McLary, C., and Goldberg, A.L. (2004). IGF-1 stimulates muscle growth by suppressing protein breakdown and expression of atrophy-related ubiquitin-ligases, atrogin-1 and MuRF1. Am. J. Physiol. *in press*.
116. Chubanava, S., and Treebak, J.T. (2023). Regular exercise effectively protects against the aging-associated decline in skeletal muscle NAD content. Exp Gerontol *173*, 112109. 10.1016/J.EXGER.2023.112109.
117. Xie, N., Zhang, L., Gao, W., Huang, C., Huber, P.E., Zhou, X., Li, C., Shen, G., and Zou, B. (2020). NAD+ metabolism: pathophysiologic mechanisms and therapeutic potential. Signal Transduction and Targeted Therapy 2020 5:1 *5*, 1–37. 10.1038/s41392-020-00311-7.
118. Campelj, D., and Philp, A. (2022). NAD+ Therapeutics and Skeletal Muscle Adaptation to Exercise in Humans. Sports Medicine *52*, 91–99. 10.1007/S40279-022-01772-2/FIGURES/2.
119. Ji, L.L., and Yeo, D. (2022). Maintenance of NAD+ Homeostasis in Skeletal Muscle during Aging and Exercise. Cells *11*. 10.3390/CELLS11040710.
120. Goody, M.F., and Henry, C.A. (2018). A need for NAD+ in muscle development, homeostasis, and aging. Skelet Muscle *8*. 10.1186/S13395-018-0154-1.
121. Mehmel, M., Jovanović, N., and Spitz, U. (2020). Nicotinamide Riboside—The Current State of Research and Therapeutic Uses. Nutrients *12*. 10.3390/NU12061616.
122. Covarrubias, A.J., Perrone, R., Grozio, A., and Verdin, E. (2020). NAD+ metabolism and its roles in cellular processes during ageing. Nature Reviews Molecular Cell Biology 2020 22:2 *22*, 119–141. 10.1038/s41580-020-00313-x.
123. Stein, L.R., and Imai, S.I. (2014). Specific ablation of Nampt in adult neural stem cells recapitulates their functional defects during aging. EMBO J *33*, 1321–1340. 10.1002/EMBJ.201386917.
124. Migliavacca, E., Tay, S.K.H., Patel, H.P., Sonntag, T., Civiletto, G., McFarlane, C., Forrester, T., Barton, S.J., Leow, M.K., Antoun, E., et al. (2019). Mitochondrial

oxidative capacity and NAD+ biosynthesis are reduced in human sarcopenia across ethnicities. Nat Commun *10*. 10.1038/S41467-019-13694-1.
125. Cantó, C., Menzies, K.J., and Auwerx, J. (2015). NAD+ Metabolism and the Control of Energy Homeostasis: A Balancing Act between Mitochondria and the Nucleus. Cell Metab *22*, 31–53. 10.1016/J.CMET.2015.05.023.
126. Zhang, H., Ryu, D., Wu, Y., Gariani, K., Wang, X., Luan, P., D'Amico, D., Ropelle, E.R., Lutolf, M.P., Aebersold, R., et al. (2016). NAD+ repletion improves mitochondrial and stem cell function and enhances life span in mice. Science (1979) *352*, 1436–1443. 10.1126/SCIENCE.AAF2693/SUPPL_FILE/ZHANG.SM.PDF.
127. Pirinen, E., Cantó, C., Jo, Y.S., Morato, L., Zhang, H., Menzies, K.J., Williams, E.G., Mouchiroud, L., Moullan, N., Hagberg, C., et al. (2014). Pharmacological Inhibition of poly(ADP-ribose) polymerases improves fitness and mitochondrial function in skeletal muscle. Cell Metab *19*, 1034–1041. 10.1016/J.CMET.2014.04.002.
128. Rose, M., Burgess, J.T., O'Byrne, K., Richard, D.J., and Bolderson, E. (2020). PARP Inhibitors: Clinical Relevance, Mechanisms of Action and Tumor Resistance. Front Cell Dev Biol *8*. 10.3389/FCELL.2020.564601.
129. Faraoni, I., and Graziani, G. (2018). Role of BRCA Mutations in Cancer Treatment with Poly(ADP-ribose) Polymerase (PARP) Inhibitors. Cancers (Basel) *10*. 10.3390/cancers10120487.
130. Harrision, D., Gravells, P., Thompson, R., and Bryant, H.E. (2020). Poly(ADP-Ribose) Glycohydrolase (PARG) vs. Poly(ADP-Ribose) Polymerase (PARP) - Function in Genome Maintenance and Relevance of Inhibitors for Anti-cancer Therapy. Front Mol Biosci *7*, 191. 10.3389/fmolb.2020.00191.
131. Tarragó, M.G., Chini, C.C.S., Kanamori, K.S., Warner, G.M., Caride, A., de Oliveira, G.C., Rud, M., Samani, A., Hein, K.Z., Huang, R., et al. (2018). A potent and specific CD38 inhibitor ameliorates age-related metabolic dysfunction by reversing tissue NAD+ decline. Cell Metab *27*, 1081. 10.1016/J.CMET.2018.03.016.
132. Rajman, L., Chwalek, K., and Sinclair, D.A. (2018). Therapeutic potential of NAD-boosting molecules: the in vivo evidence. Cell Metab *27*, 529. 10.1016/J.CMET.2018.02.011.
133. Cakir-Kiefer, C., Muller-Steffner, H., Oppenheimer, N., and Schuber, F. (2001). Kinetic competence of the cADP-ribose-CD38 complex as an intermediate in the CD38/NAD+ glycohydrolase-catalysed reactions: implication for CD38 signalling. Biochem J *358*, 399–406. 10.1042/0264-6021:3580399.
134. Sauve, A.A., Munshi, C., Lee, H.C., and Schramm, V.L. (1998). The reaction mechanism for CD38. A single intermediate is responsible for cyclization, hydrolysis, and base-exchange chemistries. Biochemistry *37*, 13239–13249. 10.1021/BI981248S.
135. Amé, J.C., Rolli, V., Schreiber, V., Niedergang, C., Apiou, F., Decker, P., Muller, S., Höger, T., Ménissier-de Murcia, J., and De Murcia, G. (1999). PARP-2, A novel mammalian DNA damage-dependent poly(ADP-ribose) polymerase. J Biol Chem *274*, 17860–17868. 10.1074/JBC.274.25.17860.
136. Jiang, H., Kim, J.H., Frizzell, K.M., Kraus, W.L., and Lin, H. (2010). Clickable NAD analogues for labeling substrate proteins of poly(ADP-ribose) polymerases. J Am Chem Soc *132*, 9363–9372. 10.1021/JA101588R.
137. Mendoza-Alvarez, H., and Alvarez-Gonzalez, R. (1993). THE J~URNAL OF BIOLOGICAL CHEXISTRY Poly(ADP-ribose) Polymerase Is a Catalytic Dimer and

the Automodi~catio~ Reaction Is I~termolec~lar*. *268*, 22575–22580. 10.1016/S0021-9258(18)41568-2.
138. Matta, E., Kiribayeva, A., Khassenov, B., Matkarimov, B.T., and Ishchenko, A.A. (2020). Insight into DNA substrate specificity of PARP1-catalysed DNA poly(ADP-ribosyl)ation. Scientific Reports 2020 10:1 *10*, 1–11. 10.1038/s41598-020-60631-0.
139. van Beek, L., McClay, É., Patel, S., Schimpl, M., Spagnolo, L., and Maia de Oliveira, T. (2021). Parp power: A structural perspective on parp1, parp2, and parp3 in dna damage repair and nucleosome remodelling. Int J Mol Sci *22*, 5112. 10.3390/IJMS22105112/S1.
140. Kim, M.K. (2018). Novel insight into the function of Tankyrase (Review). Oncol Lett *16*, 6895–6902. 10.3892/OL.2018.9551/HTML.
141. Todorova, T., Bock, F.J., and Chang, P. (2015). PARP13 and RNA regulation in immunity and cancer. Trends Mol Med *21*, 373. 10.1016/J.MOLMED.2015.03.002.
142. Todorova, T., Bock, F.J., and Chang, P. (2014). PARP13 regulates cellular mRNA post-transcriptionally and functions as a pro-apoptotic factor by destabilizing TRAILR4 transcript. Nature Communications 2014 5:1 *5*, 1–14. 10.1038/ncomms6362.
143. Yang, C., Wierbiłowicz, K., Dworak, N.M., Bae, S.Y., Tengse, S.B., Abianeh, N., Drake, J.M., Abbas, T., Ratan, A., Wotton, D., et al. (2023). Induction of PARP7 Creates a Vulnerability for Growth Inhibition by RBN2397 in Prostate Cancer Cells. Cancer Research Communications *3*, 592. 10.1158/2767-9764.CRC-23-0086.
144. Gozgit, J.M., Vasbinder, M.M., Abo, R.P., Kunii, K., Kuplast-Barr, K.G., Gui, B., Lu, A.Z., Molina, J.R., Minissale, E., Swinger, K.K., et al. (2021). PARP7 negatively regulates the type I interferon response in cancer cells and its inhibition triggers antitumor immunity. Cancer Cell *39*, 1214-1226.e10. 10.1016/J.CCELL.2021.06.018.
145. Shao, C., Qiu, Y., Liu, J., Feng, H., Shen, S., Saiyin, H., Yu, W., Wei, Y., Yu, L., Su, W., et al. (2018). PARP12 (ARTD12) suppresses hepatocellular carcinoma metastasis through interacting with FHL2 and regulating its stability. Cell Death & Disease 2018 9:9 *9*, 1–14. 10.1038/s41419-018-0906-1.
146. Welsby, I., Hutin, D., Gueydan, C., Kruys, V., Rongvaux, A., and Leo, O. (2014). PARP12, an Interferon-stimulated Gene Involved in the Control of Protein Translation and Inflammation. Journal of Biological Chemistry *289*, 26642–26657. 10.1074/JBC.M114.589515.
147. Welsby, I., Hutin, D., Gueydan, C., Kruys, V., Rongvaux, A., and Leo, O. (2014). PARP12, an interferon-stimulated gene involved in the control of protein translation and inflammation. J Biol Chem *289*, 26642–26657. 10.1074/JBC.M114.589515.
148. Gu, H., Yan, W., Wang, Y., Xu, W., Huang, L., Yang, J., Zhai, B., Wang, H., Su, Y., Zhu, Q., et al. (2023). Discovery of the Potent and Highly Selective PARP7 Inhibitor as a Novel Immunotherapeutic Agent for Tumors. J Med Chem *66*, 473–490. 10.1021/ACS.JMEDCHEM.2C01452/SUPPL_FILE/JM2C01452_SI_008.PDB.
149. Hajikhezri, Z., Darweesh, M., Akusjärvi, G., and Punga, T. (2020). Role of CCCH-Type Zinc Finger Proteins in Human Adenovirus Infections. Viruses *12*. 10.3390/V12111322.
150. Iwata, H., Goettsch, C., Sharma, A., Ricchiuto, P., Goh, W.W. Bin, Halu, A., Yamada, I., Yoshida, H., Hara, T., Wei, M., et al. (2016). PARP9 and PARP14 cross-regulate

macrophage activation via STAT1 ADP-ribosylation. Nature Communications 2016 7:1 *7*, 1–19. 10.1038/ncomms12849.
151. Xing, J., Zhang, A., Du, Y., Fang, M., Minze, L.J., Liu, Y.J., Li, X.C., and Zhang, Z. (2021). Identification of poly(ADP-ribose) polymerase 9 (PARP9) as a noncanonical sensor for RNA virus in dendritic cells. Nature Communications 2021 12:1 *12*, 1–17. 10.1038/s41467-021-23003-4.
152. Kang, M., Park, S., Park, S.H., Lee, H.G., and Park, J.H. (2022). A Double-Edged Sword: The Two Faces of PARylation. International Journal of Molecular Sciences 2022, Vol. 23, Page 9826 *23*, 9826. 10.3390/IJMS23179826.
153. Zampieri, M., Bacalini, M.G., Barchetta, I., Scalea, S., Cimini, F.A., Bertoccini, L., Tagliatesta, S., De Matteis, G., Zardo, G., Cavallo, M.G., et al. (2021). Increased PARylation impacts the DNA methylation process in type 2 diabetes mellitus. Clin Epigenetics *13*, 1–13. 10.1186/S13148-021-01099-1/FIGURES/7.
154. Wei, H., and Yu, X. (2016). Functions of PARylation in DNA Damage Repair Pathways. Genomics Proteomics Bioinformatics *14*, 131–139. 10.1016/J.GPB.2016.05.001.
155. Rose, M., Burgess, J.T., O'Byrne, K., Richard, D.J., and Bolderson, E. (2020). PARP Inhibitors: Clinical Relevance, Mechanisms of Action and Tumor Resistance. Front Cell Dev Biol *8*, 564601. 10.3389/FCELL.2020.564601/BIBTEX.
156. Chen, A. (2011). PARP inhibitors: its role in treatment of cancer. Chin J Cancer *30*, 463. 10.5732/CJC.011.10111.
157. Liu, X., Shi, Y., Maag, D.X., Palma, J.P., Patterson, M.J., Ellis, P.A., Surber, B.W., Ready, D.B., Soni, N.B., Ladror, U.S., et al. (2012). Iniparib nonselectively modifies cysteine-containing proteins in tumor cells and is not a Bona Fide PARP inhibitor. Clinical Cancer Research *18*, 510–523. 10.1158/1078-0432.CCR-11-1973/84745/AM/INIPARIB-NON-SELECTIVELY-MODIFIES-CYSTEINE.
158. Graziani, G., and Szabó, C. (2005). Clinical perspectives of PARP inhibitors. Pharmacol Res *52*, 109–118. 10.1016/J.PHRS.2005.02.013.
159. Tattersall, A., Ryan, N., Wiggans, A.J., Rogozińska, E., and Morrison, J. (2022). Poly(ADP-ribose) polymerase (PARP) inhibitors for the treatment of ovarian cancer. Cochrane Database of Systematic Reviews *2022*. 10.1002/14651858.CD007929.PUB4/MEDIA/CDSR/CD007929/IMAGE_N/NCD007929-CMP-008.02.SVG.
160. Bai, P., Canto, C., Brunyánszki, A., Huber, A., Szántó, M., Cen, Y., Yamamoto, H., Houten, S.M., Kiss, B., Oudart, H., et al. (2011). PARP-2 regulates SIRT1 expression and whole-body energy expenditure. Cell Metab *13*, 450–460. 10.1016/J.CMET.2011.03.013.
161. Bai, P., Cantó, C., Oudart, H., Brunyánszki, A., Cen, Y., Thomas, C., Yamamoto, H., Huber, A., Kiss, B., Houtkooper, R.H., et al. (2011). PARP-1 inhibition increases mitochondrial metabolism through SIRT1 activation. Cell Metab *13*, 461–468. 10.1016/J.CMET.2011.03.004.
162. Mao, X., Gu, Y., Sui, X., Shen, L., Han, J., Wang, H., Xi, Q., Zhuang, Q., Meng, Q., and Wu, G. (2021). Phosphorylation of Dynamin-Related Protein 1 (DRP1) Regulates Mitochondrial Dynamics and Skeletal Muscle Wasting in Cancer Cachexia. Front Cell Dev Biol *9*. 10.3389/FCELL.2021.673618/FULL.

163. Pin, F., Huot, J.R., and Bonetto, A. (2022). The Mitochondria-Targeting Agent MitoQ Improves Muscle Atrophy, Weakness and Oxidative Metabolism in C26 Tumor-Bearing Mice. Front Cell Dev Biol *10*, 861622. 10.3389/FCELL.2022.861622/BIBTEX.
164. Blackwell, T.A., Cervenka, I., Khatri, B., Brown, J.L., Rosa-Caldwell, M.E., Lee, D.E., Perry, R.A., Brown, L.A., Haynie, W.S., Wiggs, M.P., et al. (2018). Transcriptomic analysis of the development of skeletal muscle atrophy in cancer-cachexia in tumor-bearing mice. Physiol Genomics *50*, 1071–1082. 10.1152/PHYSIOLGENOMICS.00061.2018/ASSET/IMAGES/LARGE/ZH70111843220009.JPEG.
165. Jang, H.R., Lee, K., Jeon, J., Kim, J.R., Lee, J.E., Kwon, G.Y., Kim, Y.G., Kim, D.J., Ko, J.W., and Huh, W. (2020). Poly (ADP-Ribose) Polymerase Inhibitor Treatment as a Novel Therapy Attenuating Renal Ischemia-Reperfusion Injury. Front Immunol *11*, 564288. 10.3389/FIMMU.2020.564288/BIBTEX.
166. Xu, Y., Wang, B., Liu, X., Deng, Y., Zhu, Y., Zhu, F., Liang, Y., and Li, H. (2021). Sp1 Targeted PARP1 Inhibition Protects Cardiomyocytes From Myocardial Ischemia-Reperfusion Injury via Downregulation of Autophagy. Front Cell Dev Biol *9*. 10.3389/FCELL.2021.621906.
167. Zhou, H.Z., Swanson, R.A., Simonis, U., Ma, X., Cecchini, G., and Gray, M.O. (2006). Poly(ADP-ribose) polymerase-1 hyperactivation and impairment of mitochondrial respiratory chain Complex I function in reperfused mouse hearts. https://doi.org/10.1152/ajpheart.00823.2005 *291*, 714–723. 10.1152/AJPHEART.00823.2005.
168. Zha, S., Li, Z., Cao, Q., Wang, F., and Liu, F. (2018). PARP1 inhibitor (PJ34) improves the function of aging-induced endothelial progenitor cells by preserving intracellular NAD + levels and increasing SIRT1 activity. Stem Cell Res Ther *9*, 1–10. 10.1186/S13287-018-0961-7/FIGURES/7.
169. Hassa, P.O., and Hottiger, M.O. (1999). A role of poly (ADP-ribose) polymerase in NF-kappaB transcriptional activation. Biol Chem *380*, 953–959. 10.1515/BC.1999.118.
170. Vuong, B., Hogan-Cann, A.D.J., Alano, C.C., Stevenson, M., Chan, W.Y., Anderson, C.M., Swanson, R.A., and Kauppinen, T.M. (2015). NF-κB transcriptional activation by TNFaα requires phospholipase C, extracellular signal-regulated kinase 2 and poly(ADP-ribose) polymerase-1. J Neuroinflammation *12*, 1–16. 10.1186/S12974-015-0448-8/FIGURES/10.
171. Doles, J.D., Hogan, K.A., O'Connor, J., Wahner Hendrickson, A.E., Huston, O., and Jatoi, A. (2018). Does the Poly (ADP-Ribose) Polymerase Inhibitor Veliparib Merit Further Study for Cancer-Associated Weight Loss? Observations and Conclusions from Sixty Prospectively Treated Patients. J Palliat Med *21*, 1334. 10.1089/JPM.2018.0023.
172. Tian, Y.N., Chen, H.D., Tian, C.Q., Wang, Y.Q., and Miao, Z.H. (2020). Polymerase independent repression of FoxO1 transcription by sequence-specific PARP1 binding to FoxO1 promoter. Cell Death & Disease 2020 11:1 *11*, 1–12. 10.1038/s41419-020-2265-y.
173. Fouquerel, E., Goellner, E.M., Yu, Z., Gagné, J.P., de Moura, M.B., Feinstein, T., Wheeler, D., Redpath, P., Li, J., Romero, G., et al. (2014). ARTD1/PARP1 Negatively

Regulates Glycolysis by Inhibiting Hexokinase 1 Independent of NAD+ Depletion. Cell Rep *8*, 1819–1831. 10.1016/J.CELREP.2014.08.036.
174. Piskunova, T.S., Yurova, M.N., Ovsyannikov, A.I., Semenchenko, A. V., Zabezhinski, M.A., Popovich, I.G., Wang, Z.-Q., and Anisimov, V.N. (2008). Deficiency in Poly(ADP-ribose) Polymerase-1 (PARP-1) Accelerates Aging and Spontaneous Carcinogenesis in Mice. Curr Gerontol Geriatr Res *2008*, 1–11. 10.1155/2008/754190.
175. Trombold, J.R., Barnes, J.N., Critchley, L., and Coyle, E.F. (2010). Ellagitannin consumption improves strength recovery 2-3 d after eccentric exercise. Med Sci Sports Exerc *42*, 493–498. 10.1249/MSS.0B013E3181B64EDD.
176. James, D.I., Smith, K.M., Jordan, A.M., Fairweather, E.E., Griffiths, L.A., Hamilton, N.S., Hitchin, J.R., Hutton, C.P., Jones, S., Kelly, P., et al. (2016). First-in-Class Chemical Probes against Poly(ADP-ribose) Glycohydrolase (PARG) Inhibit DNA Repair with Differential Pharmacology to Olaparib. ACS Chem Biol *11*, 3179–3190. 10.1021/ACSCHEMBIO.6B00609.
177. McCarthy, J.J., Srikuea, R., Kirby, T.J., Peterson, C.A., and Esser, K.A. (2012). Inducible Cre transgenic mouse strain for skeletal muscle-specific gene targeting. Skelet Muscle *2*, 8. 10.1186/2044-5040-2-8.
178. McCarthy, J.J., Srikuea, R., Kirby, T.J., Peterson, C.A., and Esser, K.A. (2012). Inducible Cre transgenic mouse strain for skeletal muscle-specific gene targeting. Skelet Muscle *2*, 8. 10.1186/2044-5040-2-8.
179. Kunze, F.A., Bauer, M., Komuczki, J., Lanzinger, M., Gunasekera, K., Hopp, A.-K., Lehmann, M., Becher, B., Müller, A., and Hottiger, M.O. (2019). ARTD1 in Myeloid Cells Controls the IL-12/18-IFN-γ Axis in a Model of Sterile Sepsis, Chronic Bacterial Infection, and Cancer. J Immunol *202*, 1406–1416. 10.4049/JIMMUNOL.1801107.
180. Cameron, A.M., Castoldi, A., Sanin, D.E., Flachsmann, L.J., Field, C.S., Puleston, D.J., Kyle, R.L., Patterson, A.E., Hässler, F., Buescher, J.M., et al. (2019). Inflammatory macrophage dependence on NAD+ salvage is a consequence of reactive oxygen species-mediated DNA damage. Nat Immunol *20*, 420–432. 10.1038/S41590-019-0336-Y.
181. Santinelli-Pestana, D. V., Aikawa, E., Singh, S.A., and Aikawa, M. (2023). PARPs and ADP-Ribosylation in Chronic Inflammation: A Focus on Macrophages. Pathogens 2023, Vol. 12, Page 964 *12*, 964. 10.3390/PATHOGENS12070964.
182. Oei, S.L., and Shi, Y. (2001). Poly(ADP-Ribosyl)ation of Transcription Factor Yin Yang 1 under Conditions of DNA Damage. Biochem Biophys Res Commun *285*, 27–31. 10.1006/BBRC.2001.5115.
183. Allinson, S.L., Dianova, I.I., and Dianov, G.L. (2003). Poly(ADP-ribose) polymerase in base excision repair: Always engaged, but not essential for DNA damage processing. Acta Biochim Pol *50*, 169–179. 10.18388/ABP.2003_3724.
184. Páhi, Z.G., Borsos, B.N., Pantazi, V., Ujfaludi, Z., and Pankotai, T. (2020). PARylation During Transcription: Insights into the Fine-Tuning Mechanism and Regulation. Cancers (Basel) *12*. 10.3390/CANCERS12010183.
185. Le May, N., Iltis, I., Amé, J.C., Zhovmer, A., Biard, D., Egly, J.M., Schreiber, V., and Coin, F. (2012). Poly (ADP-ribose) glycohydrolase regulates retinoic acid receptor-mediated gene expression. Mol Cell *48*, 785–798. 10.1016/J.MOLCEL.2012.09.021.

186. Zhang, F., Wang, Y., Wang, L., Luo, X., Huang, K., Wang, C., Du, M., Liu, F., Luo, T., Huang, D., et al. (2013). Poly(ADP-ribose) Polymerase 1 Is a Key Regulator of Estrogen Receptor α-dependent Gene Transcription. J Biol Chem *288*, 11348. 10.1074/JBC.M112.429134.
187. Lai, Y.S., Chang, C.W., Pawlik, K.M., Zhou, D., Renfrow, M.B., and Townes, T.M. (2012). SRY (sex determining region Y)-box2 (Sox2)/poly ADP-ribose polymerase 1 (Parp1) complexes regulate pluripotency. Proc Natl Acad Sci U S A *109*, 3772–3777. 10.1073/PNAS.1108595109/-/DCSUPPLEMENTAL.
188. Lu, H., Wang, X., Li, T., Urvalek, A.M., Yu, L., Li, J., Zhu, J., Lin, Q., Peng, X., and Zhao, J. (2011). Identification of Poly (ADP-ribose) Polymerase-1 (PARP-1) as a Novel Krüppel-like Factor 8-interacting and -regulating Protein. J Biol Chem *286*, 20335. 10.1074/JBC.M110.215632.
189. Nie, J., Sakamoto, S., Song, D., Qu, Z., Ota, K., and Taniguchi, T. (1998). Interaction of Oct-1 and automodification domain of poly(ADP-ribose) synthetase. FEBS Lett *424*, 27–32. 10.1016/S0014-5793(98)00131-8.
190. Cervellera, M.N., and Sala, A. (2000). Poly(ADP-ribose) polymerase is a B-MYB coactivator. J Biol Chem *275*, 10692–10696. 10.1074/JBC.275.14.10692.
191. Tulin, A., and Spradling, A. (2003). Chromatin loosening by poly(ADP)-ribose polymerase (PARP) at Drosophila puff loci. Science *299*, 560–562. 10.1126/SCIENCE.1078764.
192. Hassa, P.O., and Hottiger, M.O. (2002). The functional role of poly(ADP-ribose)polymerase 1 as novel coactivator of NF-kappaB in inflammatory disorders. Cell Mol Life Sci *59*, 1534–1553. 10.1007/S00018-002-8527-2.
193. Matveeva, E.A., Mathbout, L.F., and Fondufe-Mittendorf, Y.N. (2019). PARP1 is a versatile factor in the regulation of mRNA stability and decay. Sci Rep *9*. 10.1038/S41598-019-39969-7.
194. Mashimo, M., Onishi, M., Uno, A., Tanimichi, A., Nobeyama, A., Mori, M., Yamada, S., Negi, S., Bu, X., Kato, J., et al. (2021). The 89-kDa PARP1 cleavage fragment serves as a cytoplasmic PAR carrier to induce AIF-mediated apoptosis. J Biol Chem *296*. 10.1074/JBC.RA120.014479.
195. Matteini, F., Andresini, O., Petrai, S., Battistelli, C., Rossi, M.N., and Maione, R. (123AD). Poly(ADP-ribose) Polymerase 1 (PARP1) restrains MyoD-dependent gene expression during muscle differentiation. 10.1038/s41598-020-72155-8.
196. Hain, B.A., Xu, H., VanCleave, A.M., Gordon, B.S., Kimball, S.R., and Waning, D.L. (2021). REDD1 deletion attenuates cancer cachexia in mice. J Appl Physiol (1985) *131*, 1718–1730. 10.1152/JAPPLPHYSIOL.00536.2021.
197. Gordon, B.S., Williamson, D.L., Lang, C.H., Jefferson, L.S., and Kimball, S.R. (2015). Nutrient-Induced Stimulation of Protein Synthesis in Mouse Skeletal Muscle Is Limited by the mTORC1 Repressor REDD1. J Nutr *145*, 708. 10.3945/JN.114.207621.
198. Harrision, D., Gravells, P., Thompson, R., and Bryant, H.E. (2020). Poly(ADP-Ribose) Glycohydrolase (PARG) vs. Poly(ADP-Ribose) Polymerase (PARP) – Function in Genome Maintenance and Relevance of Inhibitors for Anti-cancer Therapy. Front Mol Biosci *7*. 10.3389/FMOLB.2020.00191.
199. Kir, S., Komaba, H., Garcia, A.P., Economopoulos, K.P., Liu, W., Lanske, B., Hodin, R.A., and Spiegelman, B.M. (2016). PTH/PTHrP receptor mediates cachexia in

models of kidney failure and cancer. Cell Metab *23*, 315–323. 10.1016/j.cmet.2015.11.003.
200. Allison, S.J. (2015). Role of PTH/PTHrP receptor in cachexia. Nature Reviews Nephrology 2015 12:2 *12*, 62–62. 10.1038/nrneph.2015.207.
201. Galland, L., Lecuelle, J., Favier, L., Fraisse, C., Lagrange, A., Kaderbhai, C., Truntzer, C., and Ghiringhelli, F. (2021). Splenic Volume as a Surrogate Marker of Immune Checkpoint Inhibitor Efficacy in Metastatic Non Small Cell Lung Cancer. Cancers (Basel) *13*. 10.3390/CANCERS13123020.
202. Gariani, K., Ryu, D., Menzies, K.J., Yi, H.S., Stein, S., Zhang, H., Perino, A., Lemos, V., Katsyuba, E., Jha, P., et al. (2017). Inhibiting poly ADP-ribosylation increases fatty acid oxidation and protects against fatty liver disease. J Hepatol *66*, 132–141. 10.1016/j.jhep.2016.08.024.
203. Brown, J.L., Rosa-Caldwell, M.E., Lee, D.E., Blackwell, T.A., Brown, L.A., Perry, R.A., Haynie, W.S., Hardee, J.P., Carson, J.A., Wiggs, M.P., et al. (2017). Mitochondrial degeneration precedes the development of muscle atrophy in progression of cancer cachexia in tumour-bearing mice. J Cachexia Sarcopenia Muscle *8*, 926. 10.1002/JCSM.12232.
204. Sha, Z., Zhao, J., and Goldberg, A.L. (2018). Measuring the overall rate of protein breakdown in cells and the contributions of the ubiquitin-proteasome and autophagy-lysosomal pathways. Methods Mol Biol *1844*, 261. 10.1007/978-1-4939-8706-1_17.
205. Zhang, M., Lai, Y., Vasquez, J.L., James, D.I., Smith, K.M., Waddell, I.D., Ogilvie, D.J., Liu, Y., and Agoulnik, I.U. (2020). Androgen Receptor and Poly(ADP-ribose) Glycohydrolase Inhibition Increases Efficiency of Androgen Ablation in Prostate Cancer Cells. Scientific Reports 2020 10:1 *10*, 1–12. 10.1038/s41598-020-60849-y.
206. Tan, A., Younis, A.Z., Evans, A., Creighton, J. V, Coveny, C., Boocock, D.J., Sale, C., Lavery, G.G., Coutts, A.S., and Doig, C.L. PARP1 mediated PARylation contributes to myogenic progression and glucocorticoid transcriptional response. 10.1038/s41420-023-01420-2.
207. Chen, W., E, Q., Sun, B., Zhang, P., Li, N., Fei, S., Wang, Y., Liu, S., Liu, X., and Zhang, X. (2023). PARP1-catalyzed PARylation of YY1 mediates endoplasmic reticulum stress in granulosa cells to determine primordial follicle activation. Cell Death Dis *14*, 524. 10.1038/S41419-023-05984-W.
208. Marchildon, F., Lala, N., Li, G., St.-Louis, C., Lamothe, D., Keller, C., and Wiper-Bergeron, N. (2012). CCAAT/Enhancer Binding Protein Beta is Expressed in Satellite Cells and Controls Myogenesis. Stem Cells *30*, 2619–2630. 10.1002/STEM.1248.
209. Lala-Tabbert, N., AlSudais, H., Marchildon, F., Fu, D., and Wiper-Bergeron, N. (2016). CCAAT/enhancer binding protein β is required for satellite cell self-renewal. Skelet Muscle *6*, 1–11. 10.1186/S13395-016-0112-8/FIGURES/6.
210. Luo, X., Ryu, K.W., Kim, D.S., Nandu, T., Medina, C.J., Gupte, R., Gibson, B.A., Soccio, R.E., Yu, Y., Gupta, R.K., et al. (2017). PARP-1 Controls the Adipogenic Transcriptional Program by PARylating C/EBPβ and Modulating Its Transcriptional Activity. Mol Cell *65*, 260. 10.1016/J.MOLCEL.2016.11.015.

9 Supplementary figures

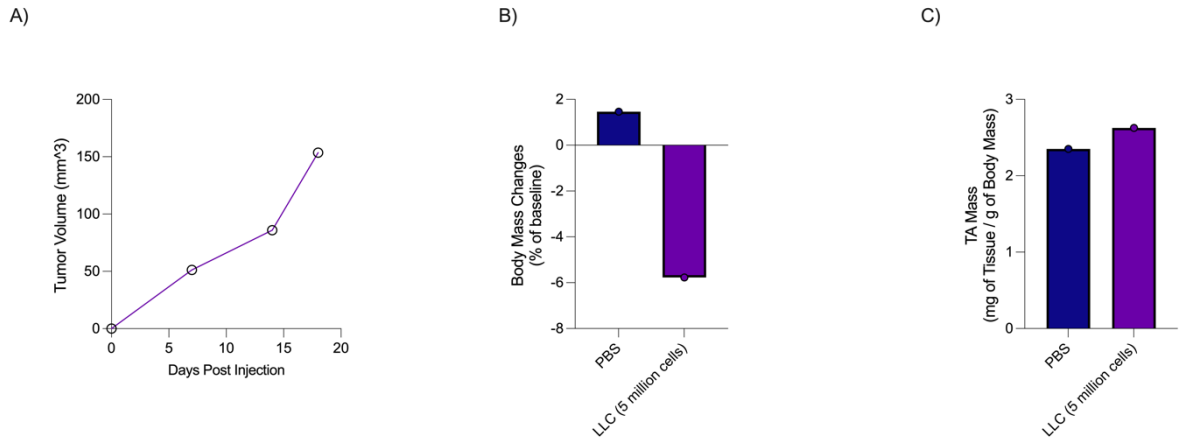

Supplementary Figure 1: Tumor reaches endpoint size prior to cachexia development following injection of 5×10^6 LLC cells.
A) Tumor Volume, B) Percentage change in body mass relative to baseline, and C) TA Mass. (N=1)